The Dissertation Committee for Revathi Ananthakrishnan
certifies that this is the approved version of the following dissertation:

# On the Structural Response of Eukaryotic Cells

Committee:

_____
Josef A. Käs, Supervisor

_____
Tess J. Moon, Supervisor

_____
Linda E. Reichl

_____
Chih-Kang Ken Shih

_____
Michael P. Marder

_____
Rebecca Richards-Kortum

# On the Structural Response of Eukaryotic Cells

**by**

**Revathi Ananthakrishnan, B.Sc., M.Sc.**

**DISSERTATION**

Presented to the Faculty of the Graduate School of

The University of Texas at Austin

in Partial Fulfillment

of the Requirements

for the Degree of

**DOCTOR OF PHILOSOPHY**

THE UNIVERSITY OF TEXAS AT AUSTIN

May 2003

Dedicated to Amma, Appa and Malu

# Acknowledgments

From Bombay, India, to Austin, TX, then to Leipzig, Germany, the Ph.D., like life itself, has been a journey and an experience. Along the way, I have met and interacted with many interesting people, who have all played a role in my completing the Ph.D. Before I started, I had always heard that any Ph.D. is a collaborative effort, containing the contribution of many people. Little did I realize till I was into my own, that in my case, it would be approximately half the world.........

I would like to begin by thanking my advisors Professors Josef Kas and Tess Moon for their guidance, support and encouragement throughout the PhD. I had many joint meetings with them both and greatly benefitted from these discussions. I thank Josef for his great efforts to make me and his other students feel welcome and settled in his country, when we made the transatlantic move to Germany in May 2002. I thank Tess for all the trips she made to Europe after the move, inspite of her many commitments.

I thank all the graduate students and colleagues with whom I have worked closely on this project, escpecially Jochen with whom I have worked for 4 years now. And the others in the stretcher group - past and present - Benton, Bryan, Chieze, Coley, Christian, Dave Stoker, Falk, Frank, Hamid, Karla, Maren, Sam, Stefan, Suzi, Vanessa. I would also like to thank Dave Humphrey, Doug, Martin and Rachel for all the discussions and help and all the other students in Josef's group for the support. I also thank everyone at Evacyte Inc., especially Syd and Jean for the collaboration and interaction. I thank Timo and Jochen a lot for helping me get

settled in Leipzig.

I would like to thank every Professor, student and member of the Center for Nonlinear Dynamics, UT Austin, where I did my work for 4 years. I would like to specially thank Professor Michael Marder for all his help and continued interest in my work. I would like to thank Eric Gerde and Dan Goldman for always being ready to answer my questions and helping me immensely. I also thank Robert Deegan for all the discussions and help. I thank my office mates Pax, Erin, Eric, Andy, Allen and Bjoern for putting up with me in the office. I would like to thank all the students who help maintain the computers at CNLD. I would also like to thank all the Professors and members of the Institute of Soft Matter Physics, Leipzig, especially Elke, Bernd, Undine and Carsten. I would like to specially thank Professors Dirk Drasdo and Angela Stevens of MPI, Leipzig for the collaboration, discussions and their interest in my work.

I gained most of my continuum mechanics and finite element modeling knowledge from Eric Gerde and Sebnem Ozupek. Their willingness to help me at all times and their continuing friendship with me is greatly appreciated. I learnt about the buckling of microtubules via email from Prof Karolyi in summer 2001 and I thank him very much for his help. I also thank all the technical support staff at ABAQUS in US and Germany who have answered my many questions patiently although I was working with an academic license, which comes with very limited technical support - especially David Gray and Suresh Krishnan at ABAQUS South Central, Flower Mound, TX and the staff at the ABAQUS branch in Aachen, Germany.

I thank all the other Professors at UT Austin and outside who have helped

me complete this work. These include my committee members, Professors Reichl, Shih, Marder and Richards-Kortum. I took many classes in engineering mechanics from Professors Becker, Leichti and Mear. Their help in starting me off in these subject areas was invaluable and is gratefully acknowledged. Other Professors outside UT with whom discussions were very useful include Professors Goldbart, Janmey, Morse, MacKintosh, Mogilner, Pollard, Stossel, Xu and I thank them all for answering my emails with many questions so patiently.

I would like to say a special thank you to the Physics and Life Science librarians at UT Austin, Molly and Nancy, for all their help and friendship through these years. I would also like to say a big thank you to Norma, the graduate secretary, for always helping me out with a smile. At CNLD, I thank all the administrative staff - Dorothy, Caryn, Olga and Rosie (also for her candies) for helping me out constantly.

Life as a graduate student would not have been much fun without the numerous friends I made and the many enjoyable times I spent with them all. It would be difficult to describe here the uniqueness and importance of each of these friendships to me and how each one helped me academically or otherwise so I will just mention names. Also, I apologize at the beginning to anyone, whose name I have not included - this is certainly not intentional. My friends in Austin, whom I would like to thank include Agapi, Anil, Amit, Aya, Beth, Bua, Chethan, Dan, Evistati, Eric, Erin, Eyal, Frank, Gelsy, Jinhee, Jori, Julie, Karl, Katya, Ketaki, Kirti, Kort, Kumi, Leah, Linda, Lisa, Melike, Nikola, Nisha, Rafael, Reid, Reza, Roman, Tara, Thomas, Tira. I would also like to thank my german friends Amaya, Axel, Beri, Conny, Frank, Katja, Kathryn, Uma, Wilfred for making me feel less lonely in a new land. I thank my roommates over the past 5 years for putting up

# On the Structural Response of Eukaryotic Cells

Publication No. _____

Revathi Ananthakrishnan, Ph.D.
The University of Texas at Austin, 2003

Supervisors:   Josef A. K$äs$
Tess J. Moon

The actin, microtubule and intermediate filament cytoskeletal polymer assemblies, along with their accessory proteins, govern the mechanical or structural response of an eukaryotic cell to an external stress. Using statistical mechanics tools, this dissertation investigates the molecular properties, such as mesh size, persistence length and filament length, that determine the structural strength of the *in vivo* polymer networks, with an emphasis on the actin network or the cortex of cells. Our study of actin shows how the wide range of shear moduli from 1 Pa to 1 kPa that spans the viscous sol-like state to the elastic gel-like state witnessed in eukaryotic cells can be achieved through transient crosslinking and the spatial distribution of actin and actin crosslinking proteins alone. Thus, this gel-sol transition is achieved without the action of any severing or capping proteins that depolymerize the actin network.

In order to understand how the microscopic quantities controlling the structural properties of these *in vivo* polymers are related to the deformation of a cell observed experimentally, a cell model is created by us. It starts with modeling the

ix

actin cortex as a thick shell and increases in complexity to include microtubules and the nucleus. Our cell model predicts that the structural response of the cell amplifies changes in molecular properties such as the *in vivo* actin concentration. Hence, the sensitivity of the structural response to cytoskeletal changes can be used to distinguish between different cells such as normal and cancer cells and can serve as an indicator of disease.

# Table of Contents

# List of Tables

# List of Figures

# Chapter 1

# Introduction

## 1.1 Composition of the Cytoskeleton

A eukaryotic cell is a complex, compound material, consisting of many structures made of proteins, lipids, carbohydrates and nucleic acids. One main structure in the cell that spans its interior and accounts for most of the protein found *in vivo* is the cytoskeleton - a polymer network of protein fibers. As the scaffold on which the cell is built, the cytoskeleton provides a pathway for organelle transport and signal transduction and is vital for cell motility and cell division [16], [111]. Not surprisingly, it also determines the structural response of the cell. This physics dissertation focuses on the polymer physics of the cytoskeleton, with the aim of understanding how the structural response of the cell to an arbitrary, external stress is governed by the cytoskeleton's microscopic polymer properties. Fundamental polymer quantities such as persistence length (the distance over which the filament can bend in two independent directions), mesh size (a measure of the polymer concentration) and filament length, which describe the structural strength of the network, are related to macroscopic, observable quantities such as the deformation measured experimentally. With this understanding, the study intends to quantitatively explain applied stress versus deformation curves observed from our cell deformation experiment. Another related aspect of this study is the correlation between cell structure and cell function, which means a quantitative understanding of how changes in the

1

cell's structural response can be related to cytoskeletal changes. In cancer cells, the cytoskeleton is altered, due to malignant transformations [66], [154], [12] and consequently so are their mechanical properties. Hence, this study investigates the validity of using the cell's structural response as a marker of malignant changes.

The uniqueness of this work lies in its breadth - bringing together many varied fields to gain an understanding of the mechanical properties of biological cells. Our study begins with geometrical optics to calculate the stresses on a cell placed between two laser beams. The structural response of the cell to such a stress is obtained from continuum mechanics - by solving the differential equations of deformation analytically or numerically (using finite element methods). The observed deformation is a reflection of the unique structural properties of cellular biopolymer networks, which are unrivaled by any synthetic polymer. Polymer physics lends us thermodynamics and statistical mechanics to calculate the structural strength of static polymer networks. But, some of these biopolymer networks, far from being static, are dynamically (transiently) crosslinked and this effect, on strength, is understood with chemical rate kinetics. A knowledge of all these fields combined with experimental data enables us to create a much more complete structural model of a cell than before. This makes it possible to extract structural parameters such as the shear modulus, which can be unique to cell types, and enables us to validate our models and differentiate between different cells - for example, normal and cancerous cells.

In order to pursue the above research goals, a thorough understanding of the key players of cellular mechanics - the cytoskeletal polymers and the accessory proteins within - is required and I start by describing their salient features [16], [111]. The cytoskeleton is made of three types of polymer filaments, called actin, micro-

tubules and intermediate filaments (Figure 1.1). Eukaryotic cells have an actin network just beneath the cell membrane, and microtubules and intermediate filaments in the interior (Figure 1.2). Actin, a semiflexible biopolymer (persistence length $l_p$ = 17 $\mu$m), is made of actin protein monomers 7-9 nm in diameter. The three dimensional network beneath the cell membrane, called the actin cortex, has a mesh size ranging from 50 nm to 300 nm. Microtubules are rod-like polymers ($l_p$ = 5.2 mm) made of tubulin protein subunits, which are 25 nm in diameter. They radiate like spokes from the centrosome or microtubule organizing center, located close to the nucleus, and extend towards the cell membrane. Intermediate filaments have a diameter of 8 to 12 nm, which is in between that of microtubules and actin. They are flexible polymers in the interior of the cell. In cells such as fibroblasts, they are colocalized with the nucleus. Intermediate filaments are made of subunits of either keratin, vimentin, desmin ($l_p$ = 0.1-1 $\mu$m) or neurofilament protein. In addition to these three *in vivo* assemblies, actin bundles called stress fibers are present only in attached cells between focal adhesion points.

The cytoskeletal filaments are crosslinked *in vivo* by various proteins. Actin filaments can assemble into two main forms - a network (cortex) or bundle (stress fibers and focal adhesion points), depending on the size of the crosslinking or bundling protein. The main proteins which transiently crosslink actin filaments (with a certain binding time) are $\alpha$-actinin, filamin and fascin (Figure 1.3). $\alpha$-actinin and filamin have at least two binding sites and crosslink different F-actin filaments to form a 3D actin network as in Figure 1.4 (instead of a bundle as in Figure 1.5), due to their large size. $\alpha$-actinin, found in a wide variety of cells, is an antiparallel, rod-shaped homodimer. It is 3-4 nm wide, 30-40 nm long, and 100 KD in weight (each subunit). Non-muscle filamin or ABP-280(KD) is a homod-

3
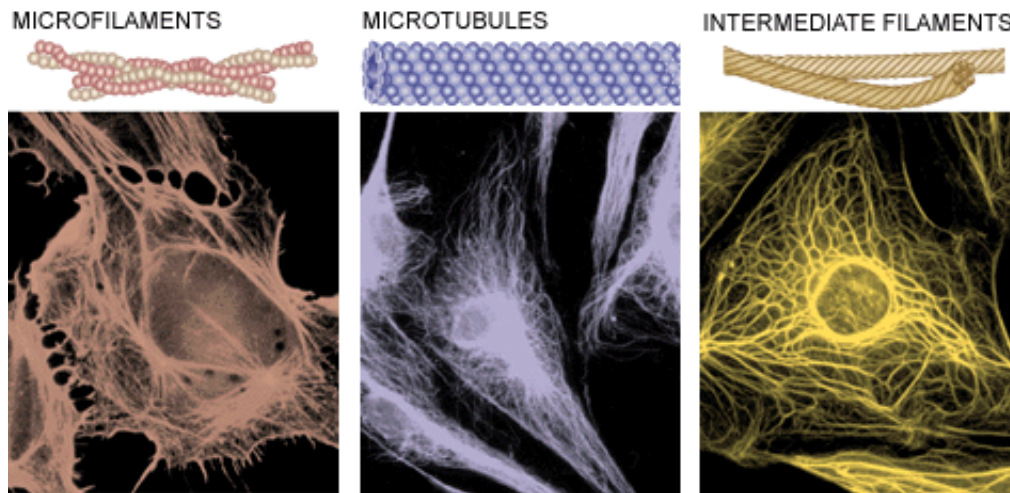
Figure 1.1: The three cytoskeletal polymers - actin (left), microtubules (center) and intermediate filaments (right) - taken from [89]. The cytoskeletal filaments interact to create a composite network that spans the interior of the cell and performs crucial cell functions such as organelle transport, signal transduction, cell motility and cell division.

imeric, actin-binding protein, 160 nm in length. Fascin is a small 55 KD molecule, with a 3.2 nm hydrodynamic radius, that binds actin filaments into bundles. Arp proteins (actin related proteins), which crosslink actin filaments and form branched networks at a fixed angle of $70^o$, are found only at the leading edge of motile cells [134]. Microtubules bind to one another and to actin filaments through proteins called MAPS (microtubule associated proteins) or MIPS (microtubule interacting proteins). Some MAPS also connect microtubules and intermediate filaments [145]. Intermediate filaments bind to one another and to actin and microtubules with the help of IFAPs (intermediate filament-associated proteins). Without the crosslinking and binding proteins *in vivo*, the network would be fluid-like [228].

In addition to the crosslinking proteins in the cell, there are also actin motor
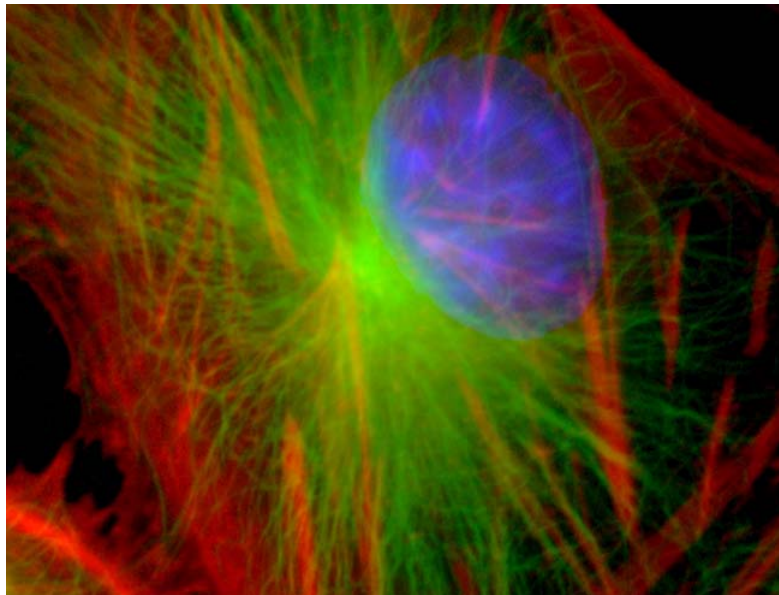
Figure 1.2: In this image of an attached cell, taken from [42], different fluorescent markers have been used as tags for different cellular components. The main structural components of the cell include the actin cytoskeleton (red) seen beneath the cell membrane, the microtubules (green) - observed to radiate outward from the microtubule organizing center towards the cell periphery - and the cell nucleus (stained in blue). There is no staining for intermediate filaments in this image.

proteins such as the myosin family and microtubule motor proteins such as dynein and kinesin. Myosin is involved in cell contraction and motility by the movement of a myosin molecule along an actin filament. Dynein and kinesin are involved in the movement of microtubules. While some investigations conclude that myosin strengthens actin networks [16], others conclude that it fluidizes the actin network (Figure 1.6 [86]). Although these studies do not agree in their conclusions, they clearly show that the motor proteins influence the mechanical properties of cells. Other important proteins *in vivo* are the actin sequestering proteins like thymosine-beta 4 and profilin and severing proteins and capping proteins, which control length, like Cap Z, severin and gelsolin (Table 1.1).
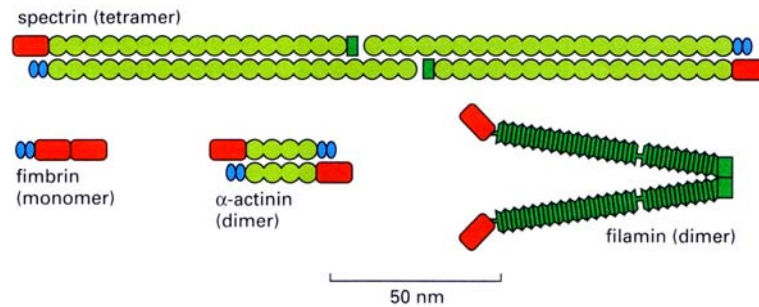
Figure 1.3: The structure of four actin crosslinking proteins, taken from [2]. Each crosslinker shown has two binding sites (red), in order to couple two actin filaments. The distance between these binding sites determines whether the crosslinkers form tight actin bundles, loosely packed bundles or actin networks.

The composite cytoskeletal polymers, including the accessory proteins, determine the structural response of a eukaryotic cell. In this dissertation, I have constructed a model of a eukaryotic cell, by taking into account the geometry of the cell, the architecture of the cytoskeleton (seen from micrographs taken in our group and other groups studying the cytoskeleton) as well as the polymer properties of the cytoskeleton. Before describing my model and the cell deformation experiment that motivated it, I discuss the existing deformation experiments, their models and the missing piece in these models.

## 1.2   Some Cell Elasticity Experiments, Their Model Adjuncts and the Missing Piece

Many ingenious experiments have been devised to apply a known force or stress to a eukaryotic cell and measure its deformation - these include the cell poker [232], atomic force microscopy (AFM) [117], microplate manipulation [196], magnetic bead microrheometry [10], [11] and micropipette aspiration [96]. While some
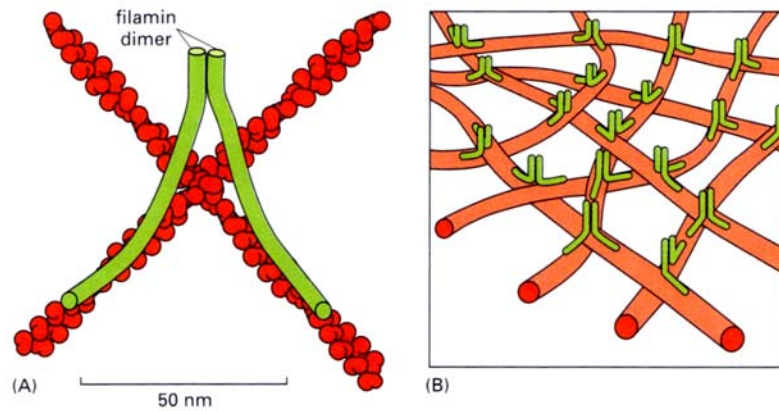
Figure 1.4: The structure of the three dimensional gel-like network formed by the actin crosslinking protein filamin, taken from [2]. a) Filamin is a homodimeric protein, 160 nm in length. Hence, it is very flexible and can tether two actin filaments even at large angles. b) An actin mesh or network crosslinked by filamin is structurally strong.

of these techniques deform local regions of the cell (local deformation techniques) and extract structural properties, others deform the whole cell (global deformation techniques). The cell poker and AFM are similar deformation techniques on attached cells, where a hard indentor is used to apply a local force to probe the cell and measure its deformation. In the whole cell deformation technique of microplate manipulation, a spherical cell is seized between a rigid glass plate at the bottom and a flexible glass plate at the top, which acts as a force sensor. The deformation of the cell is then measured by subjecting it to various controlled forces, such as a step force or a sinusoidal force of a certain frequency. The viscoelastic properties of cells can be obtained in the magnetic bead microrheometry technique from the local deformation response of attached magnetic beads to force pulses. The micropipette aspiration of cells involves applying a known local pressure to suck a cell into a pipette and measuring the resulting extension into the pipette.
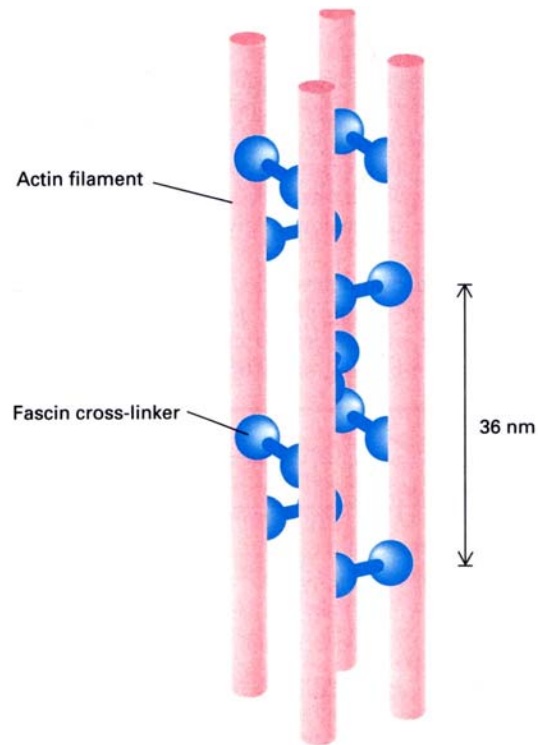
Figure 1.5: The structure of actin filaments bridged by the actin crosslinking protein fascin, taken from [111]. Fascin is a short, stiff crosslinker that binds actin filaments into a parallel alignment - a tightly packed bundle.

Suitable accompanying models have been created to analyze the experimental deformation of eukaryotic cells and extract structural parameters, such as the shear modulus and viscosity (Table 1.2 and Appendix B.4). The table also includes models for red blood cells (which are not eukaryotic cells, as they have only a peripheral 2D spectrin cytoskeleton and no interior structure or nucleus), since the next chapter discusses and compares our simple red blood cell model with these other models. However, our interest lies in eukaryotic cells and their models. These range from a simple continuum mechanics model for the micropipette aspiration of neutrophils [28] to open-cell foam networks and prestressed cable net models
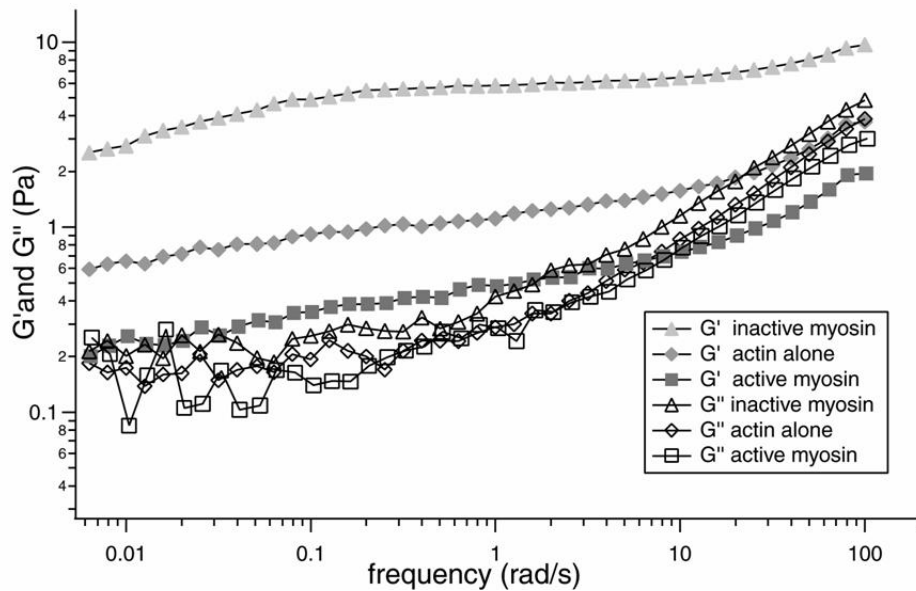
Figure 1.6: Rheology results from actin and actin-myosin networks (36 $\mu$M actin, 0.14 $\mu$M myosin), taken from [86]. G', the storage modulus, measures the elastic strength of the network, while G", the loss modulus, measures the viscous component. The modulus G' is lower for the myosin-actin network than for the actin network alone. Hence, the addition of myosin fluidizes the actin network.

[182], which explore the connection between deformability and internal cellular structure (Appendix B.4 explains how some of these models link the two properties). The cell poker experiment mentioned earlier relates the structural properties of the cytoskeleton (modulus and viscosity) to its leukocyte data with a model of a hyperelastic sphere deformed by a rigid indentor [232], while the AFM experiment on fibroblasts uses a variation of the Hertz model [117] to analyze its data. The shear modulus and viscosity of a fibroblast deformed in the microplate experiment are obtained from a 3-element micromechanical model [196]. In the magnetic microrheometry experiment of Bausch et al. [10], the displacement of the magnetic beads, along with the model of the fibroblast cell as an elastic plate coupled to a

fixed viscoelastic layer, yields a bulk shear modulus. The micropipette experiment models a chondrocyte as an elastic, homogeneous half space, subjected to an axisymmetric force by the micropipette, in order to associate Young's modulus and aspirated length [96].

The shear modulus and viscosity extracted from the different experiments vary due to the assumptions inherent in the model, to suit the experimental conditions. Also, the continuum models used are macroscopic in nature - they extract one shear modulus for the whole cell from experiment and hence do not consider the underlying microscopic polymer physics of the cytoskeleton. This is precisely the missing piece or gap this thesis aims to bridge - to explain how the strength of the cell extracted from the models can be accounted for by strength of the individual cytoskeletal polymer assemblies and then their interactions. Before discussing our structural model based on the polymer networks, I discuss what is already known about the strength of these polymer networks.

## 1.3   Polymer Networks

There have been *in vitro* experimental studies [92], [214] on the structural response of the individual cytoskeletal polymer networks, which compare the stress-strain relations and the strain and frequency dependence of the shear modulus of the different polymer networks. Rheology, a common experimental technique to study the structural properties of *in vitro* reconstituted polymer networks, is the easiest and first way to understanding cellular mechanics - the strength of *in vivo* networks is hard to measure experimentally. The rheology experiments on the different cytoskeletal networks, shown in Figure 1.7, reveal that the structural prop-

10

erties of the individual networks seem well suited to their function and location in the cell. Crucial cell functions that actin and microtubules are involved in include cell motility and cell division respectively, while intermediate filaments maintain cell shape. The peripheral actin cortex has a high shear modulus, which enables it to withstand stresses from the outside, while the interior intermediate filament network has a lower shear modulus at low strains [92]. Microtubules are stiff and have a much higher shear modulus than actin, due to their large persistence length. These *in vitro* studies on the individual cytoskeletal networks have also determined that a composite network possesses structural properties that cannot be achieved by the individual polymers alone [92]. Therefore, a higher level of complexity in modeling is attained by studying cytoskeletal interactions and the role and contribution of individual cytoskeletal components in determining the overall structural response of the cell. Classical concepts in polymer physics do not elucidate how all these filaments, together with various proteins, give the cell its structural strength [113] - the deformation results from the whole cell experiments have not been related to the polymer properties of the cytoskeleton.

The rheology experiments yield a value for the structural strength of the polymer networks, which is now discussed. Rheology can be performed by either a stress relaxation or an oscillatory shear experiment. A stress relaxation experiment consists of subjecting the polymer sample to a constant initial strain and observing the stress relax as a function of time. From this data, the shear modulus of the polymer as a function of time, $G(t)$, is obtained. In an oscillatory shear experiment, the sample is subjected to a constant amplitude sinusoidal shear, which yields data to calculate the complex shear modulus as a function of frequency, $G(\omega)$. The two shear moduli $G(t)$ and $G(\omega)$ are Fourier transforms of each other. Further, $G(\omega)$ can be decomposed into an elastic component $G'$ (storage modulus) and a

11
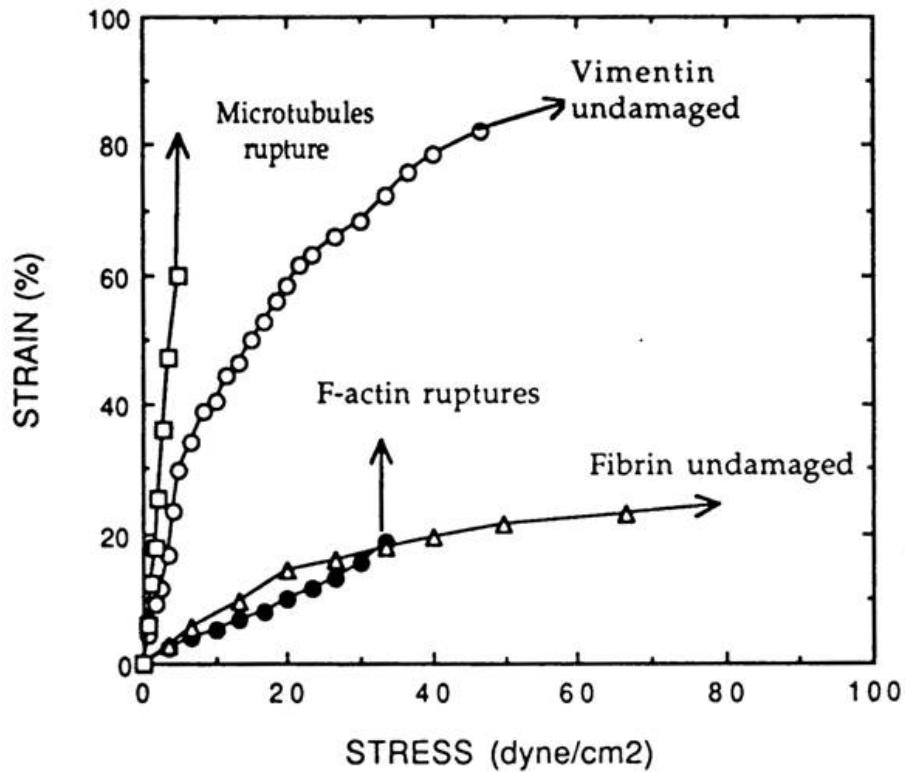
Figure 1.7: Stress-strain characteristics for the different cytoskeletal elements (actin, microtubules and vimentin) from rheology experiments, taken from [92]. Actin has a high shear modulus at low strains, while intermediate filaments play a structural role only at much higher strains.

viscous component $G''$ (loss modulus). Whether represented as a function of time or frequency, the shear modulus $G$ of a polymer network is not constant. It displays a viscoelastic behavior instead of a simple elastic behavior, which means that the shear stress $\sigma_{shear}$ applied to the network is related to the shear strain $\epsilon_{shear}$ by the relation

12

$$\sigma_{shear} = \int_0^t G(t-t')\frac{d\epsilon_{shear}(t')}{dt'}dt' \ (valid \ for \ linear \ viscoelasticity). \ (1.1)$$

However, a network may display a constant shear modulus (plateau shear modulus) or elastic characteristics over a certain time or frequency range. An *in vitro* actin network behaves elastically at low frequencies (between 0.02 and 100 Hz) and our further studies that assume the actin network is elastic are carried out in such a regime.

Rheology experiments have been performed on both uncrosslinked as well as crosslinked actin networks [90], [91], [92], [93], [94], [98], [86], [164], [81], [133], [193], [171], [236], [55], [114], [140], [141], [163], [204], [225], [227], [229], [121], [54]; theories have also been developed to explain the structural properties of *in vitro* tightly entangled, uncrosslinked and crosslinked actin networks [116], [128], [129], [113], [114]. Actin rheology experiments have yielded a plateau shear modulus (low frequency behavior between 0.02 and 100 Hz) ranging from 0.1-0.2 $N/m^2$ (or Pa) [133] to 0.2-2 Pa [209] for a 1 mg/ml uncrosslinked solution. Joint rheology experiments on uncrosslinked networks from the labs of Janmey and Pollard [224] have shown that a 1 mg/ml solution of freshly purified actin, 6 $\mu m$ in mean length, has a plateau modulus of $\sim$ 0.5 Pa, as shown in Figure 1.8. The corresponding theoretical prediction for a 1 mg/ml uncrosslinked network, 4.25 $\mu m$ in length, is 0.1 Pa [129]. While both experiment and theory predict a high frequency behavior ($>$ 200 Hz) of $G(\omega) \propto (i\omega)^{3/4}$, they differ in magnitude by a factor of 4 [129], [114]. Rheology experiments have also been performed on an actin network crosslinked with $\alpha$-actinin or filamin, and the modulus value measured is higher than that of an actin network alone and depends strongly on the crosslinker

13

concentration used (Table 1.3). Microtubule and intermediate filament rheology experiments [165], [214] have been performed, although much less extensively than actin rheology.
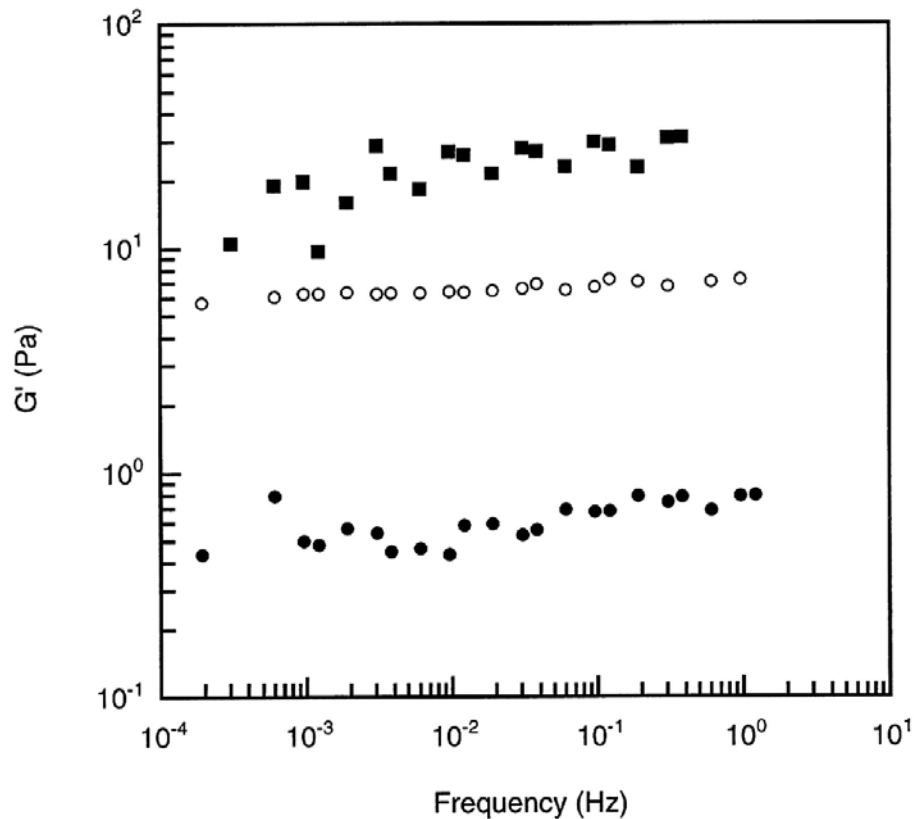


Figure 1.8: Rheology to find the shear modulus G' of a freshly prepared actin solution (black circle), taken from [224]. The rheological properties change with an increase in the storage time of the actin solution (open circles and black squares)

Although, the rheology of *in vitro* polymer networks is the first step to understanding cellular mechanics, there are important differences between them and *in vivo* networks. For example, the filaments in actin rheology are typically polydis-

perse in length - between 2-70 $\mu m$ [113], 1 mg/ml in concentration and immersed in an artificial cytosol-like environment. The *in vivo* cortex, in contrast, is made of short filaments - between 0.1 and 3 $\mu m$, 5-10 mg/ml in concentration and is a transiently crosslinked, dynamic actin network. One example of dynamic behavior observed *in vivo* is treadmilling - the process by which actin filaments polymerize at the positive end and depolymerize at the negative end, at a constant rate. Also, the reconstituted actin networks show a phase transition, at physiological concentrations, to the nematic phase, while the *in vivo* actin cortex of suspended cells seems to be fairly isotropic. However, the extent of the plateau shear modulus (in frequency space) and its transition to a frequency dependent behavior in the high frequency internal dynamics regime are observed to be the same in *in vitro* actin networks, artificial cells (actin coated vesicles) [79] and eukaryotic cells (fibroblasts) [117], which demonstrates the importance of actin in cytoskeletal response.

A way to study the strength of *in vivo* networks, although not quantitatively precise, is the use of cytoskeletal drugs. Drugs that affect individual cytoskeletal components are employed, to get an insight into each network's contribution to the cell's structural response. The use of cytochalasins and latraculin, to disrupt the actin network, results in a marked decrease in cell strength [162], [213], [230] which again indicates that actin is a key player in cytoskeletal mechanics. Disrupting microtubules with depolymerizing drugs seems to have a much smaller effect on the structural response [162], [213]. Recently, an *in vivo* experimental estimate for the shear modulus has been obtained in the perinuclear and lamellar regions of COS7 epithelial cells, by analyzing the Brownian motion of endogenous particles in these areas [230]. This study shows that the strength of the *in vivo* actin network is necessary but not sufficient to explain lamellar mechanics.

Since actin is considered to be the main player [187], [166], [35] out of the three *in vivo* polymers, our cell model, described below, starts with incorporating the actin network. However, we use models of increasing complexity, by starting with actin and successively adding the other cytoskeletal polymers, whose strengths are based on theoretical estimates. Our final model includes the actin cortex, the rod-like microtubules and the nucleus.

## 1.4  Our Structural Model for a Eukaryotic Cell

Our structural model for a cell, motivated by our cell deformation technique called the optical stretcher - explained in detail in Chapter 2, is developed to study and utilize the differences in the cytoskeletal polymers of normal and cancer cells, to detect malignant changes. Initially, a thick (hollow) shell model has been constructed for a cell with a predominant actin cortex. The spoke-like microtubules are then included in our model, to observe how they strengthen the structure and affect the structural response. Intermediate filaments play a role at large deformations [214] and have not been considered in our model. The nucleus of the cell, a fairly spherical object of Young's modulus $\sim 1000$ Pa [72], has also been finally included in our structural model. A preliminary understanding of the strength of stress fibers or actin bundles is gained by modeling an isotropic network of actin filaments and bundles and estimating its strength. The contribution of different cytoskeletal filament interactions to structural strength has not been studied in this thesis.

Our study of actin estimates the structural strength of the cortex by using isotropic actin network models with physiologically relevant parameters, such as

actin and crosslinker concentrations and filament length. This is an approximation to the cortex, which can show local inhomogeneity and anisotropy, but since there is no direct method to determine the cortex's strength, this is our starting point to quantify it. To find the contribution of actin to cell strength, the shear modulus of cells is compared with our calculated shear modulus of a permanently crosslinked actin network of cellular concentration. For a homogeneous, actin network through the entire cell, the modulus obtained is much lower than the shear modulus of fibroblasts, epithelial cells, macrophages etc. (Table 1.2). Soft cells such as neutrophils have a much smaller shear modulus and may be explained by this calculation. However, if a high 'effective' concentration of both the *in vivo* actin and crosslinking proteins is achieved due to localization into a cortex, the calculated shear modulus of the network is high even for a transiently crosslinked network, and can explain the observed *in vivo* moduli of fibroblasts and other cells. Thus, our theoretical study shows that the spatial distribution and transient crosslinking of actin crosslinking proteins enable cells to change the structural strength of actin networks over a wide range, from fluid-like to solid behavior, without using capping or severing proteins to depolymerize actin.

Our cell model has been used to investigate how the sensitivity of structural parameters to changes in the cytoskeletal networks' properties can be used as an indicator of disease. The cytoskeleton is a dynamic material, whose architecture and structural composition reflect cell function. The cytoskeleton of cancer cells indicates their state of malignancy - cancer cells have a much lower actin content than normal cells ($\sim$ 35 percent lower) [66], [9], [185]. Polymer models of crosslinked actin networks have shown that the network's shear modulus has a nonlinear dependence on the actin concentration (shear modulus $\sim (concentration)^{2.2}$) [113]. By assuming the same concentration-modulus relation for the *in vivo* cortex, our

model predicts that the deformation of the cell will show the same sensitive dependence on the cortex's actin concentration - hence, the structural response can be used to distinguish non-cancerous and cancerous cells. There has been previous experimental evidence for differentiating cell types from the micropipette aspiration of non-cancerous and cancerous white blood cells [144] as well as the micropipette aspiration of a panel of nontransformed and malignantly transformed rat fibroblasts [216]. The experiments and model by Paulitschke et al. [144] find that the elastic rigidity of white blood cells in the resting phase from chronic myeloid leukemic patients is much lower than that from healthy donors. Ward et al. [216] report that the structural parameters extracted from their transformed cell data are approximately fifty percent lower than those extracted from their nontransformed cell data and conclude that there exists a direct correlation between an increase in deformability and the progression of tumorigenecity. Recent experiments have been performed to deform normal and cancerous fibroblasts with the optical stretcher [169], [221] and the viscoelastic parameters extracted from the data point to a difference in the structural response of normal and cancerous fibroblasts. In summary, our model and experiments suggest that the structural response of cancer cells is a good parameter to characterize them.

Table 1.1: Concentration of Key Actin Proteins in Certain Cells, taken from [151]. Only a part of the total actin in the cell is in the polymerized form due to the action of sequestering proteins such as Thymosin $\beta$-4 and Profilin

| Protein concentration ($\mu$M) | Acanth-amoeba | Dictyo-stellium | Neutro-phil[1] | Xeno-pus egg extract | Plate-let[1] | S. cerevisiae |
|---|---|---|---|---|---|---|
| Polymerized actin | 100 | 90 | 100 | 4 | 330 | 2 |
| Unpoly-merized actin | 100 | 160 | 300 | 12 | 220 | 0.01 |
| Profilin | 100 | | | 5 | | present |
| Thymosin $\beta$-4 | absent | absent | | 20 | 550 | absent |
| ADF/Cofilin | 20 | <100 | | 3 | 30 | present |
| Arp2/3 Complex | 2-4 | present | 10 | | 9 | present |
| Capping protein | 1 | 1 | 1-2 | | 5 | 1 |
| Gelsolin | absent | | | | 5 | |
| $\alpha$-actinin | 4 | 3 | | | | |
| Filamin | absent | | | | 6 | |
| ABP 120 | absent | 6 | | | | |

[1] The data for the neutrophil and platelet cells are reported for the unactivated state.

2. The actin concentration in fibroblasts is estimated to be 8.4-11.3 mg/ml. This range is obtained with a knowledge of the concentration of unpolymerized actin in fibroblasts [135] and the ratio of unpolymerized to polymerized actin in these cells [23].

Table 1.2: Cell Deformation Techniques, Structural Parameters Extracted and the Model Adjunct. The structural parameters extracted depend on the experimental technique, cell type and the model adjunct

| Technique | Cell Type | Rheological Constant | Model Adjunct | Refe-rence |
|---|---|---|---|---|
| AFM | Fibroblast | G'=300 G"=200 | Hertz | [117] |
| | Fibroblast | E=1.2 $10^4$ stable edge | Hertz | [161] |
| | | E<(3000-5000) leading edge | | |
| | Platelet | E=$(1-50)$ $10^3$ | Hertz | [152] |
| | Epithelial | E=7500-9700 Normal cell | Hertz | [109] |
| | | E=300-1000 Cancer cell | | |
| | Endothelial | E=1300-7200 | Hertz | [122] |
| | Rat liver Macrophage | E=100-1000 | Hertz | [160] |

1. E=Young's Modulus, V= Viscosity, G= Shear Modulus, K1 = Bulk Modulus, K = Bending modulus G', G"= Storage and Loss modulus. $G = \frac{E}{2(1+\nu)}$, where $\nu$ is Poisson's ratio.

2. E, G, G' and G" are in $N/m^2$ or Pa, and V is in Pa.s unless specified.

Table 1.2 Continued

| Technique | Cell Type | Rheological Constant | Model Adjunct | Reference |
|---|---|---|---|---|
| Micropipette Aspiration | Chondrocyte | E=650 | Finite Element | [96] |
| | Endothelial | E=400 | Infinite Homogeneous Half Space | [194] |
| | Platelet | E=170 V=1000 | Endothelial Type | [73] |
| | Leukocyte | E=0.75-23.8 | 3 Element Mechanical | [190] |
| | Hair Cell | E=15.4 $10^{-3}$ | Elastic Shell Theory | [177] |
| | Neutrophil | G=36 $\mu N/m$ V=150 Ns/m | Liquid Drop | [110] |
| | Red blood Cell | G=5 $10^{-3}$ mN/m K1=500 mN/m K = $10^{-19}$ Nm | Shell Theory | [37] |
| Whole Cell Rheometry | Dictyostellium | G'=200 G"=20 Wild type | Direct Measurement | [34] |
| | | G'=100 No $\alpha$-actinin | | |
| Magnetic Bead Micro - Rheometry | Fibroblast | G=$10^4$ V = $10^3$ | 4 Element Mechanical | [10] |
| | Macrophage | G=343 V=210 | 4 Element Mechanical | [11] |
| Bead Microrheology | Fibroblast | E=1700 V=4 $10^5$ | Kelvin-Voigt | [153] |

1. E=Young's Modulus, V= Viscosity, G= Shear Modulus, K1 = Bulk Modulus, K = Bending modulus G', G"= Storage and Loss modulus. $G = \frac{E}{2(1+\nu)}$, where $\nu$ is Poisson's ratio.

2. E, G, G' and G" are in $N/m^2$ or Pa, and V is in Pa.s unless specified.

Table 1.2 Continued

| Technique | Cell Type | Rheological Constant | Model Adjunct | Reference |
|---|---|---|---|---|
| Laser Tracking Microrheology | Epithelial Cell | G'=72 G"=38.2 | Direct Measurement | [230] |
| Microplates | Fibroblast | E=1000 V=$10^4$ | 3 Element Mechanical | [196] |
| Cell Poker | Neutrophil | G=118 | Secant | [232] |
| | Lymphocyte | G=291 | | |
| Tensegrity Model | Adhered Cell | E=18-92 | Six Strut Tensegrity | [87] [182] |
| Electric Field Deformation | Red Blood Cell | G=4 $10^{-6}$ N/m V=4 $10^{-7}$ Ns/m | Elastic Theory of Shells | [97] |
| | Red Blood Cell | G=6.1 $10^{-6}$ N/m V=3.4 $10^{-7}$ Ns/m | Elastic Theory of Shells | [36] |
| Optical Stretcher | Red Blood Cell | G=1.3 $10^{-5}$ N/m | Thin Shell Theory | [68] |
| Optical Tweezer | Red Blood Cell | G=2.5 $10^{-6}$ N/m | Elastic Shell Theory | [80] |
| | Red Blood Cell | G=2 $10^{-4}$ N/m | Elastic Shell Theory | [178] |
| Flicker Spectroscopy | Red Blood Cell | K=4 $10^{-19}$ Nm | Flicker Eigenmode Decomposition | [189] |
| | Red Blood Cell | K=2 $10^{-30}$ Nm | Flicker Eigenmode Decomposition | [238] |
| | Red Blood Cell | K=5 $10^{-20}$ Nm | Flicker Eigenmode Decomposition | [14] |

1. E=Young's Modulus, V= Viscosity, G= Shear Modulus, K1 = Bulk Modulus, K = Bending modulus G', G"= Storage and Loss modulus. $G = \frac{E}{2(1+\nu)}$, where $\nu$ is Poisson's ratio.

2. E, G, G' and G" are in $N/m^2$ or Pa, and V is in Pa.s unless specified.

Table 1.3: Rheological Data from Crosslinked Actin Networks. The rheological constants measured depend on both the actin and crosslinker concentrations and the filament length

Crosslinker(CL): Amoeba-$\alpha$-actinin

| $\rho_{actin}$ $\mu M$ | Actin Length $\mu m$ | $\rho_{CL}$ $\mu M$ | Rheological Constant $N/m^2$ | Frequency Hz | Temp $^oC$ | Reference |
|---|---|---|---|---|---|---|
| 15 | | 0.1 | $G^*$=0.15 | 3  $10^{-4}$ | 25 | [208] |
| | | | $G^*$=0.3 | 1.9  $10^{-1}$ | 25 | |
| 15 | | 0.3 | $G^*$=10 | $10^{-1}$ | 25 | [209] |
| | | | $G^*$=30 | 1 | 25 | |
| 24 | | 1.6 | G'=4.7-100 G"=0.06284-0.1987 | $10^{-3} - 1$ | 25 | [137] |
| 24 | 20 | 1.8 | $G^*$=4 | $1.6\ 10^{-4} - 1.6$ | 23 | [140] |
| | | 2.4 | $G^*$=6-20 | $1.6\ 10^{-3} - 1.6$ | 23 | |

Crosslinker(CL): Chicken-$\alpha$-actinin

| $\rho_{actin}$ $\mu M$ | Actin Length $\mu m$ | $\rho_{CL}$ $\mu M$ | Rheological Constant $N/m^2$ | Frequency Hz | Temp $^oC$ | Reference |
|---|---|---|---|---|---|---|
| 15 | | 0.1 | $G^*$=5 | 3  $10^{-4}$ | 25 | [208] |
| | | | $G^*$= 4.5 | 1.9  $10^{-1}$ | 25 | |
| 15 | | 0.3 | $G^*$=3 | $10^{-1}$ | 25 | [209] |
| | | | $G^*$=3 | 1 | 25 | |
| 15 | | 0.03 | $G^*$=2-3 | $10^{-4} - 1$ | 25 | [225] |
| | | | $G^*$=4-5 | $10^{-4} - 1$ | 15 | |
| 24 | 10-15 | 0.48 | G(t)=2-10 | t=0.01-10 sec | 25 | [229] |
| | | | G(t)=4-10 | t=0.1-100 sec 1-3 % strain | 15 | |

1. G(t)= Relaxational Shear Modulus, G', G"=Storage and Loss modulus, $G^* = \sqrt{(G'^2 + G''^2)}$

2. 1 mg/ml of actin = 24 $\mu$M

Table 1.3 continued

Crosslinker(CL) Actin Binding Protein (ABP)

| $\rho_{actin}$ $\mu M$ | Actin Length $\mu m$ | $\rho_{CL}$ $\mu M$ | Rheological Constant $N/m^2$ | Frequency Hz | Temp $^oC$ | Refe-rence |
|---|---|---|---|---|---|---|
| 96 | 1.5-2.5 | 0.768 | G'=2.5 | $3\ 10^{-2}$ | | [233] |
| 38.4 | | 0.28 | G'=20 G"=0.7-5 | $10^{-2} - 10^2$ | 20 | [137] |
| 10 | 5-6 | 0.033 | G'=0.3 G"=1 | 1 | | [64] |
| | | 0.1 | G'=0.6 G"= 1.2 | 1 | | |
| | | 0.2 | G'= 1.0 G"= 1.5 | 1 | | |

1. G(t)= Relaxational Shear Modulus, G', G"=Storage and Loss modulus, $G^* = \sqrt{(G'^2 + G''^2)}$

2. 1 mg/ml of actin = 24 $\mu$M

24

# Chapter 2

# Red Blood Cells in the Optical Stretcher

## 2.1 Models for Red Blood Cells

Our initial modeling and experimental work on cells has been carried out on red blood cells, due to the simplicity of their structure. This chapter details the experimental technique and accompanying model developed by us to study the structural properties of red blood cells. Their mechanical properties have been characterized extensively in the literature, both theoretically and experimentally. The main experimental techniques that have been developed to study these properties are osmotic swelling [48], fluid shear deformation [82], micropipette suction [156], electric field deformation [36] and optical tweezers [80], [178].

All the above experiments involve applying a force or stress to the cell and using the resulting deformation of the cell to obtain information on its structural properties. The easiest method to apply stress on a red blood cell without any instrument is by osmotically swelling it in a hypotonic solution [48]. A balance is then established between the osmotic pressure, elastic stresses in the cell membrane and surface tension. Another way is to stretch cells by adhering them to the surface of a flow channel and applying a fluid shear stress [82]. A simple and ingenious instrument to deform cells, devised a long time ago but still in standard use, is the micropipette [156]. Micropipette aspiration involves applying a pressure

differential across the pipette, to suck a part of the cell into it. More recently, a high frequency electric field has also be used to deform red blood cells [36]. A much more recent development to study red blood cells is the optical tweezer [80], [178]. The optical tweezer set up to stretch a red blood cell uses a double beam trap (two focused laser beams) to hold and deform the cell by applying forces to silica beads attached to its membrane. Finally, there is a technique to characterize red blood cells structurally without the application of a stress, which is based on a phenomenon detected in them quite some time ago [14]. Red blood cells exhibit a flicker (brownian motion), whose measurement at a minimum of two points on the cell membrane is correlated to calculate structural properties.

To analyze the data and extract structural parameters such as the shear modulus, these experiments have been accompanied by theoretical and modeling work. Simple continuum models - where the cell is modeled as a continuum structure as opposed to a discrete structure with various components - exist to interpret the deformation of blood cells using the micropipette technique [37]; Evans [37] has developed equations to describe the local deformation of the cell, as it gets aspirated into the circular head of the pipette. The models used to extract structural parameters from other techniques are discussed in detail in Appendix A.1.

Many of the deformation techniques discussed above are invasive - the very act of measurement could change the observed response and structural parameters extracted. For instance, both the micropipette and the tweezer apply high local stresses on the cell to deform it, and this affects the linear modulus extracted from data. Also, the widely accepted micropipette technique and the tweezer method, which stretch a single cell at a time, are slow measurement processes. So, a new method of deforming red blood cells and other cells has been developed by us, and

a different accompanying model created to analyze the structural properties of a cell subjected to a radiation force on the entire cell. Our set up called the optical stretcher (Figure 2.1) uses two counter-propagating divergent laser beams to trap and stretch individual suspended cells placed between them [68], [69]. This is a non-invasive technique, where a large number of cells can be deformed per hour by flowing them at a constant rate through a microfluidic channel placed between the two laser beams. Also, due to the low energy density of the unfocused beams, cells can be deformed without damage even at high laser powers (200 mW for red blood cells). Hence, the stretcher is a versatile tool to study the mechanical properties of cells.

## 2.2   Modeling Red Blood Cells in the Optical Stretcher

At first, the fact that a cell gets stretched, and not squeezed, in the optical stretcher set up seems counter-intuitive. However, the phenomenon of stretching can be understood once the cell surface stress is determined using geometrical optics. This is done by employing the principle of momentum conservation and calculating the momentum transfer to the cell at each point on its surface, due to a light ray hitting it from each of the two laser beams (the rays from the laser are considered parallel and only a single reflection at each surface is taken into account). This calculation, shown in detail in Appendix A.2, proves that the total force on the cell at every point is outward and normal to the surface [68], [69].

With the aim of validating the calculated stress profile, a model for red blood cells deforming in the stretcher has been created. Red blood cells lack a complex internal structure such as a 3-D cytoskeleton and a nucleus, unlike eukaryotic cells.

27
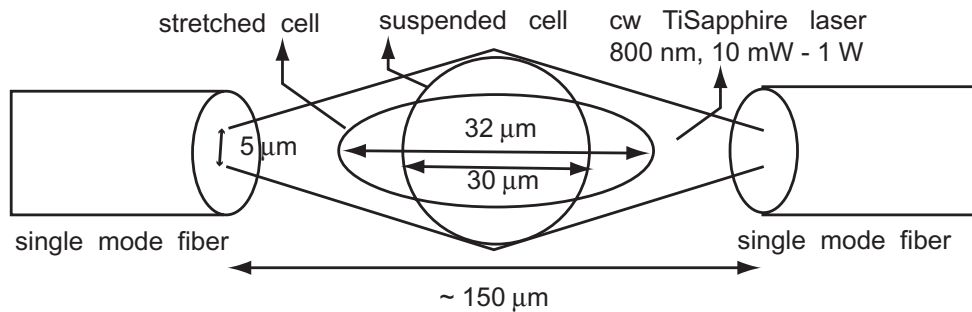
Figure 2.1: Schematic figure of the optical stretcher set up, showing a cell being deformed by two counter propagating and divergent laser beams

They have a simple structure of a homogeneous liquid interior surrounded by a thin 2-D cytoskeletal network beneath the plasma membrane. This network, called spectrin, is the main structural element of red blood cells. The ratio of the cell radius to membrane thickness of a red blood cell is approximately 100. The red blood cells are swollen osmotically into a perfect spherical shape for the experimental study. Due to the above properties, the red blood cell has been modeled by us as a thin shell (spherical membrane). The linear membrane theory of shells [124] applies to a thin isotropic shell with Young's modulus $E$, Poisson's ratio $\nu$ and thickness to radius ratio smaller than $\frac{1}{20}$. Also, in a thin shell, there are no normal stresses and the bending forces are negligible compared to the stretching (membrane) forces (Appendix A.3). With these assumptions, membrane theory can be used to calculate the stresses and displacements in a spherical shell under a given state of loading. Linear theory is used to analyze the structural response of red blood cells, as high stress levels are not reached in the experiment ($\frac{\sigma_0}{E} \leq 2.5 \cdot 10^{-3} \leq 10^{-2}$ [102]).

The stress acting on the cell, deforming in the stretcher, is rotationally symmetric about the laser axis and is perpendicular to the surface of the cell. Figure

28
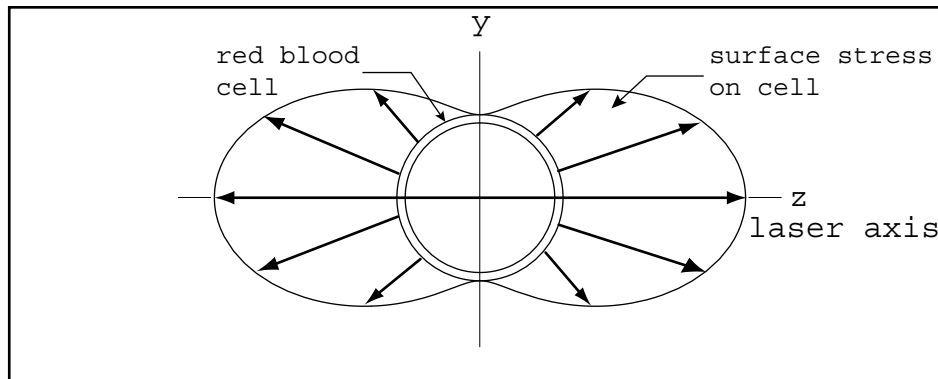
Figure 2.2: Typical stress profile for a red blood cell in the stretcher (laser beams along $z$ axis) when the half-width of the laser beam at the cell and the cell radius are approximately equal. The calculated surface stress on the cell (arrows) is outward and normal

2.2 shows a typical surface stress profile for a red blood cell. This polar plot is the functional form closest to our calculation from ray optics - $\sigma_r = \sigma_0 \, cos^2(\phi)$, where $\sigma_r$ is the radial stress, $\sigma_0$, the peak stress along the z-axis and $\phi$ is the polar angle ([68], Figure 3). Figure 2.3 shows a blood cell deforming in the optical stretcher beam geometry. The radial displacement resulting in the cell due to the stress is measured as the laser power is increased. Cell stretching is observed using a microscope; the images of the unstretched and stretched cell are stored in a computer and the stretching of the membrane can be calculated using a fit program on the images [68]. This experimental result for deformation is then compared with the prediction from membrane theory, which is described below. Figure 2.4 is a graphical depiction for $\approx 50$ cells of the correlation between the experimental and calculated values of the relative radial displacement in the cell along the beam axis and perpendicular to it, as a function of the peak stress (which is related to the laser power). The deformations are plotted for $E.h = 3.9 \, . \, 10^{-5} \, Nm^{-1}$ (Young's mod-

29
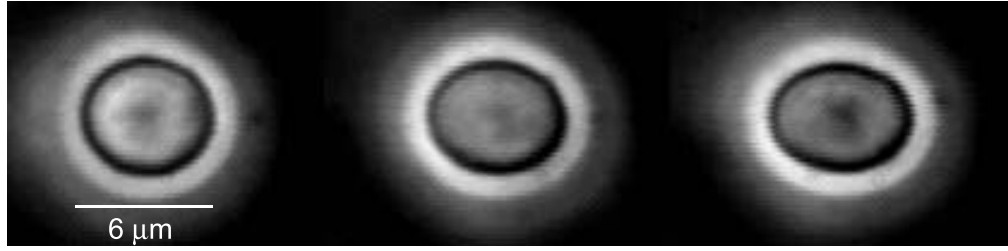
Figure 2.3: A red blood cell deforming in the optical stretcher beam geometry at laser powers of 49, 78.5 and 112.5 mW (Courtesy J. Guck). The deformed cell shape is elliptical

ulus.Thickness of membrane) and a Poisson's ratio of 0.5 (the spectrin network is assumed to be incompressible). The good correlation between experiment and theory suggests that the red blood cell satisfies the assumptions of a thin shell and can be modeled as a spherical membrane.

The problem of modeling red blood cells as a membrane and calculating deformations, which can be compared to experiment, lends itself naturally to spherical coordinates - any point on the spherical membrane is characterized by $r$, the distance to the point from the center, $\phi$, the polar angle and $\theta$, the azimuthal angle (Figure A.7, Appendix A.4.). In the case of an non-axisymmetric load on a spherical membrane, there are three displacements: the radial displacement $w$ along the radial direction, the meridional displacement $v$ along the polar direction and the hoop displacement $u$, along the azimuthal direction. However, for an axisymmetric loading (about the z axis), only the meridional and radial displacements exist and they depend on the polar angle $\phi$ only. From membrane theory, $v$ and $w$ are shown to be as follows (Appendix A.4).

$$v(\phi) = \frac{\rho}{E\ h}(v_p + A)sin\phi \qquad (2.1)$$
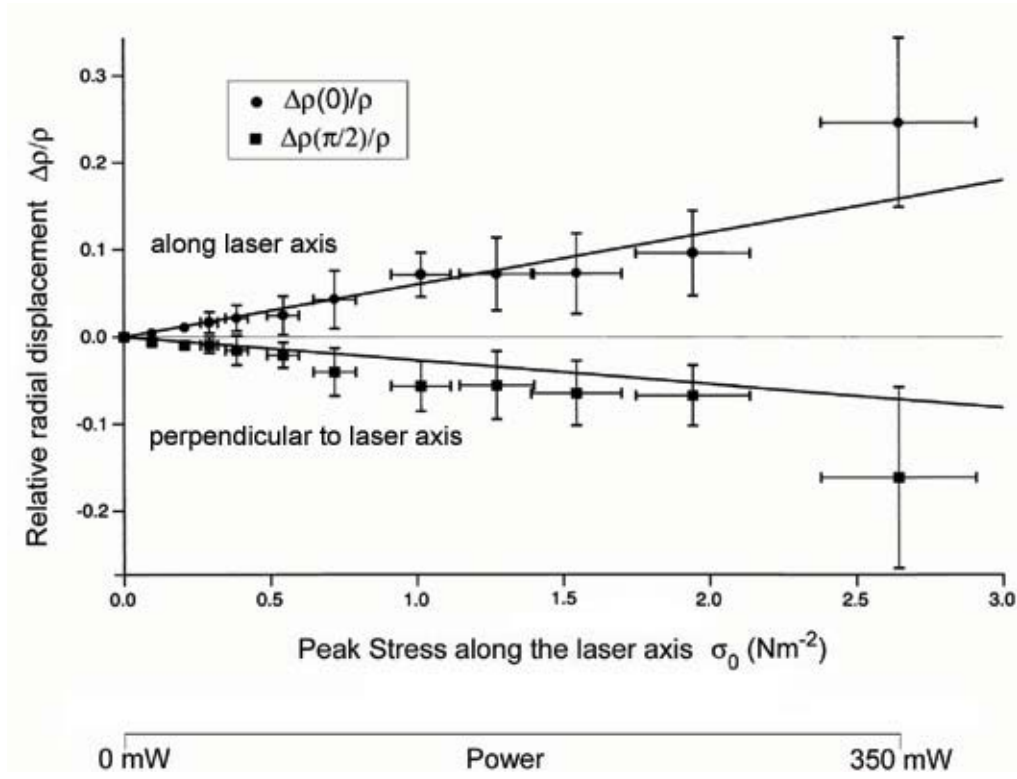
Figure 2.4: Correlation in radial displacement between experiment and theory of a cell in the stretcher. The dark lines are the prediction for radial displacement from linear membrane theory while the dots and squares are experimental data points [68]. At high laser powers (350 mW), linear membrane theory does not explain the data

$$w(\phi) = \frac{\rho}{E\ h}[v_p\ cos\phi - (1 + \nu)\frac{P_1}{sin^2\phi} + \rho\ \sigma_r + A\ cos\phi] \qquad (2.2)$$

where

$$v_p = \int \frac{1}{sin\phi}[(1 + \nu)(\rho\ \sigma_r - \frac{2\ P_1}{sin^2\phi})]d\phi \qquad (2.3)$$

31

$$P_1 = \int_0^\phi \sigma_r \; sin\psi \; cos\psi \; d\psi \tag{2.4}$$

and $\sigma_r$ is the radial stress, $\rho$, the radius of the membrane, $h$, the shell thickness, $E$, Young's modulus and $\nu$ is the Poisson's ratio.

For the stress distribution , $\sigma_r = \sigma_0 \; cos^2\phi$, acting on a red blood cell trapped in the stretcher,

$$v(\phi) = \frac{\rho^2 \sigma_0}{E \; h}[(\frac{1+\nu}{2}) \; cos\phi \; sin\phi] \tag{2.5}$$

and

$$w(\phi) = \frac{\rho^2 \sigma_0}{E \; h}[(\frac{1+\nu}{4} + 1)cos^2\phi - \frac{1+\nu}{4}] \tag{2.6}$$

The constant $A$ in the equations for meridional and radial displacement is evaluated by using the appropriate boundary conditions: $v = 0$ at $\phi = \frac{\pi}{2}$ for rotationally symmetric loading. The equations for the radial and meridional deformation are now complete. However, only the radial deformation observed experimentally is compared with membrane theory calculations. The meridional displacement cannot be measured experimentally in any easy way.

## 2.3 Shear Modulus Values Extracted from Different Red Blood Cell Experiments

The shear modulus extracted for red blood cells from the optical stretcher experiment is $1.3 \; . \; 10^{-5}$ N/m. The commonly used micropipette technique mea-

sures shear moduli values in the range $6 - 9 \cdot 10^{-6}$ N/m [83]. Two different experiments on red blood cells with tweezers obtain very different values for modulus. Henon et al. [80] report a value in the range of $2.1 - 2.9 \cdot 10^{-6}$ N/m for both discotic and osmotically-swollen cells, while Sleep et al. [178] report $2 \cdot 10^{-4}$ N/m, which is a factor of hundred higher than Henon's value. Electric field deformation of cells yields a shear modulus of $4 \cdot 10^{-6}$ N/m [97]. Possible reasons for the variation in the values measured from different experiments are discussed in the next section.

## 2.4  Summary and Implications

This chapter has discussed modeling red blood cells in the optical stretcher - as a thin shell. The thin shell model has been used to calibrate the stretcher and extract the shear modulus of red blood cells from experiment. The shear modulus extracted by us for red blood cells is compared with that from other experiments and is especially close to the highest value extracted from micropipette experiments [83], the accepted standard in cell deformation. However, there is a variation in the modulus values extracted from different red blood cell experiments [5]. This may be partly due to the different stress state of the cell in each experiment, from a high local stress in the micropipette experiment and a point force in the tweezer experiment to a more uniform stress in the optical stretcher experiment. Although a point force is applied at the poles in the tweezer experiment by Henon et al. [80], their data are taken at polar angle $90^o$, where the deformations are small and likely to be in the linear regime. Hence, they suggest that the shear modulus from micropipette experiments is higher than their value because high local stresses applied by the micropipette could place the cell in the nonlinear regime. However, the modulus from the tweezer experiment by Sleep et al. [178] is ten times higher than that

from micropipette experiments. This result is ascribed by them to the fact that the micropipette can pull hard enough on the cell to decouple the red blood cell membrane - a measurement of the modulus of the membrane can yield a very low value, as compared to that of the spectrin polymer network below. From strain hardening arguments and the stress state of the cell, it may be concluded that the modulus from the stretcher experiment should be the lowest, followed by the tweezer and then the micropipette. Since the data do not show this trend, simple arguments such as strain hardening alone cannot be used to explain the variation in modulus extracted from different experiments. Other factors such as dynamic cross-linking, complex non-linearity, internal architecture adaptation, and additional internal "support", such as from actomyosin complexes in network repair, may also play an important role [26]. For instance, recent atomic force microscopy results for the force-extension curve of a single spectrin chain reveal its complex nonlinear behavior - the curve shows an axisymmetric saw tooth pattern, due to the periodic occurrence of a peak and then a drop in the extension force as the chain elongates. These molecular effects, including the unfolding of spectrin and the role of the myosin motor proteins in the spectrin cytoskeleton, are yet to be incorporated in a mechanical model for red blood cell elasticity [26].

The next chapter deals with modeling eukaryotic cells which have a much more complex internal cytoskeletal structure than red blood cells - they too exhibit a variation in the modulus extracted from different experimental techniques for the same cell type (Table 1.2). However, our experience gained in modeling red blood cells is used to create as comprehensive and complete a model as possible for eukaryotic cells.

# Chapter 3

# Thick Shell Model for a Eukaryotic Cell Deforming in the Stretcher

## 3.1  Modeling Eukaryotic Cells

The cytoskeleton of eukaryotic cells spans their whole interior and determines their structural response. The aim of our study is to understand how the cell's structural response can be related to the microscopic polymer properties of the cytoskeleton. This will enable a quantitative explanation of the stress applied versus deformation curves observed from our cell deformation experiment.

A modeling framework has been created by us, in order to probe the structural properties of eukaryotic cells in depth. The previous chapter discusses a simple thin shell or membrane model created by us for red blood cells [68], [69]. However, a different model is required to account for the extensive 3D cytoskeleton of eukaryotic cells. So, this chapter discusses a more complex 3D thick shell continuum mechanics model for spherical eukaryotic cells in suspension, suitable for cells deformed in the optical stretcher set up. The present study is concerned with the structural response of a cell only to an external stress (passive elasticity or viscoelasticity) and not to any intracellularly generated force (active response) as discussed in [196].

The main assumption of this chapter is that the semiflexible actin polymer network beneath the cell membrane plays a key role in determining the structural response of the cell [187], [166], [35], [162], [213]. Therefore, our model is designed for the deformation of a cell in which the actin cortex predominates. This has been observed in fluorescence images of cancer cells where the actin cortex is seen as a much thinner ring than in normal cells (Figure 3.1), while the interior seems to be negligible. The actin cytoskeleton in cancer cells is altered [154], [12] and the total actin content is lower than in normal cells [66], [9], [185], [99]. So, these cells present us with an opportunity to study the actin network in isolation and to estimate the effect of malignant changes on the structural response of cells. By modeling the actin cortex as a shell, this chapter performs a parameter study, to understand the effect of a variation in shell thickness and in actin concentration of the cortex on the deformation of the shell. Our shell model predicts that the structural response of the cell amplifies changes in the actin concentration and is a sensitive parameter to distinguish normal and cancerous cells.

## 3.2   Modeling a Eukaryotic Cell with a Predominant Actin Cortex Deforming in the Stretcher

Our model for a eukaryotic cell in the stretcher combines the geometry of the cell with a knowledge of polymer properties from theoretical and experimental studies, to understand how the structure and properties of cellular polymer networks, at a molecular level, relate to macroscopic observable quantities. Therefore, fundamental polymer quantities such as persistence length, mesh size and filament length are related to the observed deformation.
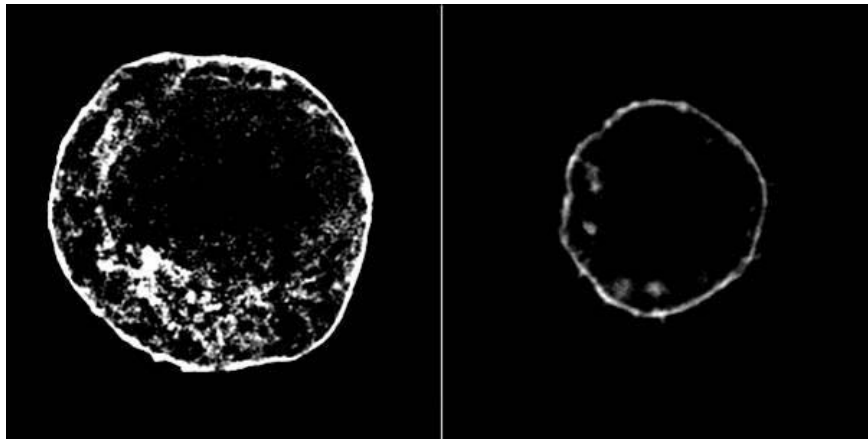
Figure 3.1: Fluorescence image of the actin cortex of a normal (left) and cancerous fibroblast (right) (Courtesy J. Guck). Image size is 15 $\mu$m in both cases. The actin cytoskeleton in cancer cells is altered and the total actin content is lower than in normal cells

Initially, our model makes this connection by considering only one cytoskeletal polymer network - actin - and starts with a eukaryotic cell in which the actin cortex is the main component and the interior is assumed negligible. A thick shell (hollow inside) continuum model is used to model such a cell and to study its deformation to an arbitrary surface stress. The thickness of the actin cortex varies from five percent to twenty percent of the radius of the cell (as seen in fluorescence images taken in our group).

While the present chapter considers only the actin cortex, the interior network of microtubules and intermediate filaments is present in most cells and needs to be considered in our further models (Chapter 5). Experimental evidence [78] suggests that such cells can be modeled structurally as a three layered solid, with the three layers being the outermost actin cortex, the interior network of microtubules and intermediate filaments and finally the nucleus. The structural analysis

37

of the thick shell model and the three layered solid model can be carried out by reducing these problems to the deformation of a solid sphere and a spherical cavity, both of which are analytically tractable. The radial deformation of a thick shell (Figure B.1, Appendix B.1.) with a hollow interior is a superposition of the radial displacement of a solid sphere (radius $r_0$) and that of a spherical cavity (radius $r_1$, which is less than $r_0$) [112]. The principle of superposition can be applied, since linear elastic theory is used throughout the analysis. The radial deformation for any axisymmetric stress on the shell is calculated by the method described in Appendix B.1. and is of the form

$$\frac{\Delta r_0}{r_0} = \frac{F_G(r_0, r_1, \phi, \nu)}{G},$$
(3.1)

where $G$ is the shear modulus of the shell material and $F_G$ is the geometric factor that arises from the spherical geometry of the cell and the effect of the applied stress on it. So, $F_G$ depends on the shell thickness $h$ ($h = r_0 - r_1$, where $r_0$ and $r_1$ are the inner and outer shell radii respectively), the Poisson's ratio $\nu$ of the shell material and $\phi$, the polar angle where it is measured. Hence, the radial deformation is the product of a factor that contains only the material property ($G$) and a factor that contains only the geometry of the cell ($F_G$). The exact deformation for a given stress is obtained by evaluating the boundary conditions of the problem, namely the radial and meridional stresses at the outer surface $r_0$ and inner surface $r_1$ of the shell (equations shown in Appendix B.1.).

Before this section describes a parameter study of the radial deformation $\frac{\Delta r_0}{r_0}$ as a function of variables that the geometric factor $F_G$ and the shear modulus $G$ depend on (such as the shell thickness $\frac{h}{r_0}$ and the actin concentration $\rho$ respectively),

38

it discusses $F_G$ and the calculation of $G$. To calculate the effect of cell geometry ($F_G$) on the deformation of a thick shell, the surface stress acting on a cell needs to be specified. Our calculations consider the stress acting on a cell in the optical stretcher set up, which is rotationally symmetric about the laser axis and is perpendicular to the surface of the cell [68]. The surface stress profile depends on the ratio of $\omega$, the half width of the laser beam at the cell, to $\rho$, the radius of the cell ($\frac{\omega}{\rho}$). In this chapter, a structural analysis has been performed for the functional forms closest to our calculations from ray optics for two typical stress profiles, shown in Figure 3.2 - $\sigma_r = \sigma_0 \, cos^2\phi$ ($\frac{\omega}{\rho} = 1.1$) and $\sigma_r = \sigma_0 \, |cos\phi|^{0.5}$ ($\frac{\omega}{\rho} = 1.5$), where $\sigma_r$ is the radial stress, $\sigma_0$ is the peak stress along the $z$ (laser) axis and $\phi$ is the polar angle. In order to demonstrate the generality of our model, calculations are also performed for a point load acting on the cell (example, tweezer experiment on red blood cells by Henon et al. [80]) by using the stress profile $\sigma_r = \sigma_0 \, cos^{100}\phi$, shown in Figure 3.2. The functional form $cos^n\phi$ is used to fit the stress profiles from ray optics calculations, due to the assumed spherical geometry of the cell and the applied axisymmetric stress. Given any of the above surface stress profiles, the geometric factor $F_G$ of a shell can be calculated from equations B.2 to B.4 in Appendix B.1. by setting $G = 1$.

In order to calculate the structural response of an elastic, actin shell (hollow inside) of variable thickness, subjected to the different external stresses, an understanding of the material property of the actin cortex ($G$) is also required. The cortex, however, displays a time dependent behavior or a viscoelastic modulus $G(t)$. The elastic-viscoelastic correspondence principle allows us, though, to use the deformation solution of the elastic shell to calculate the structural response of a viscoelastic shell (Appendix B.2). If $w(t)$, the time dependent radial displacement, is known from the optical stretcher experiment, the shear modulus $G(t)$ of the actin cortex

39
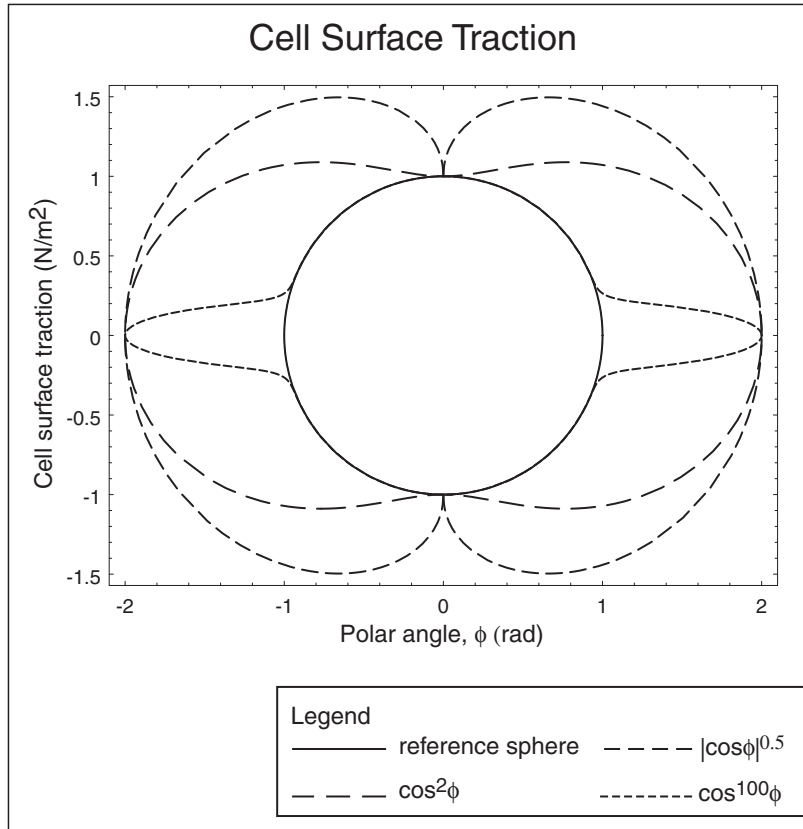
Figure 3.2: Different surface stress profiles on a cell in the stretcher set up depending on the ratio of half width of the laser beam at the cell, $\omega$, to the radius of the cell, $\rho$. The stress on the cell is localized when $\frac{\omega}{\rho} < 1$ and its mathematical form is approximated by high powers of $cos\phi$ ($cos^{100}\phi$ for example)

can be extracted (Appendix B.3). Our approach here is the opposite - to estimate $G(t)$ from theoretical studies of the polymer physics of actin networks and then predict $w(t)$. A knowledge of the linear viscoelastic properties of permanently crosslinked [113] and uncrosslinked actin networks [128], [129] enables us to estimate $G(t)$ and study the sensitivity of $w(t)$ to a variation in the concentration ($mesh\ size = (concentration)^{-1/2}$) of the actin cortex. Applying isotropic actin network models to the cortex is an approximation, but a starting point to quantify the cortex's strength. The implications that this assumption leads to regarding the cortex's strength are discussed in the next chapter.

The cortex's strength is estimated using two models or theories, as limits to the partially (transiently) crosslinked cortex: a tightly entangled permanently crosslinked actin network [113] and an uncrosslinked actin network [128], [129]. The strength of a permanently crosslinked network is first considered here - it has been determined that even a small number of crosslinks in this network leads to a broad and high elastic plateau in the shear modulus $G^*(\omega)$ at low frequencies. In the plateau region (<100 Hz), the shear modulus (plateau modulus $G_p$) is time independent and the network behaves exactly as an elastic solid does. Our analysis below is concerned with the plateau regime. At frequencies greater than the plateau region (at frequencies > 200 Hz) is the internal dynamics regime. In the internal dynamics regime, the shear modulus is time dependent and obeys a scaling law. At high frequencies (> 1000 Hz), the network's structural behavior displays a viscous or loss modulus that is much greater than the elastic or storage modulus.

The plateau modulus is calculated using parameters that closely match physiological conditions. This polymer physics calculation shows from thermodynamic and scaling laws that the plateau modulus depends on the concentration of the net-
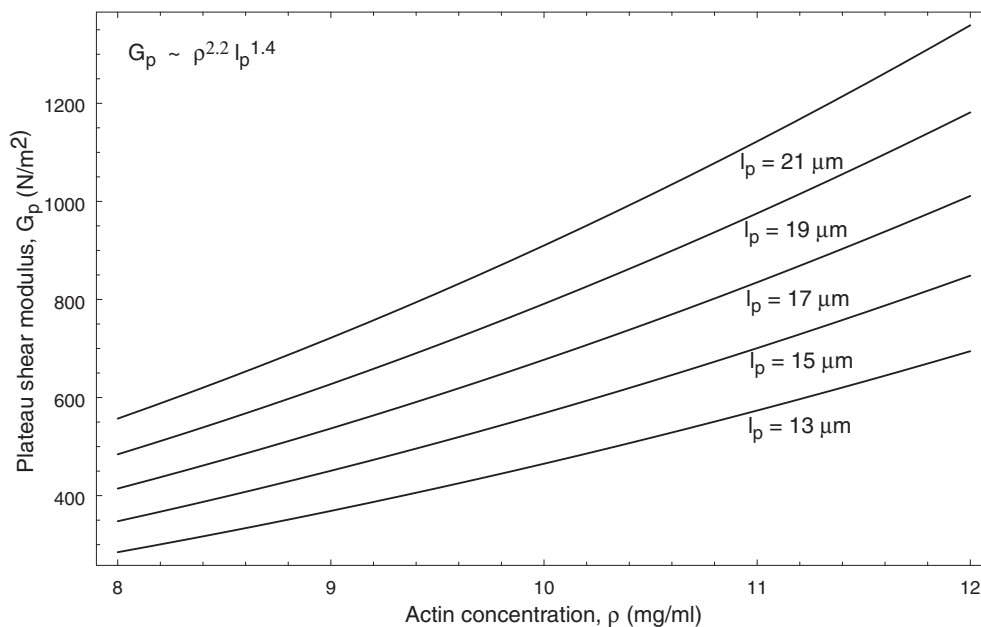
Figure 3.3: Plateau shear modulus, $G_p$, of a tightly entangled, crosslinked actin network [113] as a function of the two parameters it depends on - persistence length, $l_p$, and actin concentration $\rho$. Due to the nonlinear dependence of $G_p$ on $\rho$, even a small change in $\rho$ results in a significant change in $G_p$, which is reflected in the deformation of an actin shell

work and the persistence length of actin filaments (see Figure 3.3) and is given by $G_p = \frac{k_b T l_p^2}{\rho^{-1} l_e^3}$ [113], where $k_b$ is Boltzmann's constant and $T$ is temperature. Assuming 10 mg/ml concentration of crosslinked actin, persistence length $l_p = 17\ \mu m$ (typical *in vivo* values), entanglement length $l_e = 0.875\ \mu m$ (calculated using $l_p$ and $\rho$), $G_p$ is $\sim 670\ N/m^2$.

With an estimate of $G_p$ for an actin network (and a knowledge of $F_G$ for a given stress profile), the radial displacement of a thick actin shell can now be determined for any axisymmetric stress - the deformation is of the form $\frac{w(t)}{r_0} = \frac{\Delta r_0}{r_0} = \frac{\sigma_0 F_G}{G_p}$. A parameter study is, then, performed to observe the effect and relative importance of cell geometry ($F_G$ which depends on the shell or cortex thickness and the Poisson's ratio of the shell material) and of material property ($G_p$ which depends on the actin concentration and the persistence length) on the radial deformation, for different stress profiles. Figures 3.4 and 3.5 depict the variation in the geometric factor $F_G$ with shell thickness and Poisson's ratio respectively - for a thin shell and a $cos^2\phi$ stress, $F_G$ depends inversely on shell thickness - $F_G \sim \left(\frac{h}{r_0}\right)^{-1}$, and weakly on the Poisson's ratio of the material - $F_G \sim \nu^{-0.25}$. The change in deformation with shell thickness is shown as a polar plot in Figure 3.6 for the same surface stress, while Figures 3.7 and 3.8 depict the dependence of deformation on the concentration and persistence length respectively. These calculations help us understand the relative contributions of the concentration $\rho$, shell thickness $\frac{h}{r_0}$ and persistence length $l_p$ in determining the deformation of the shell. Our study shows that, in the parameter range studied, changing the concentration by a factor of two ($\frac{\Delta r_0}{r_0} \sim \rho^{-2.2}$) is equivalent to changing the shell thickness by a factor of four ($\frac{\Delta r_0}{r_0} \sim \left(\frac{h}{r_0}\right)^{-1}$ for a thin shell). Varying the persistence length affects the deformation as $l_p^{-1.4}$. However, the persistence length of actin has been measured accurately *in vitro* ($l_p$=17 $\mu$m) and may not be significantly different *in vivo*. Hence, of the

43

given parameters, the actin concentration is the most sensitive parameter control-ling the deformation, and varying it appears to be an important way for a cell to regulate its structural response. The range of concentration used is determined by the conditions for the network to be in the tightly entangled regime, bounded by the loosely entangled and nematic regimes [128], [27]. The effect of various applied stresses on the cell is now analyzed in Figure 3.9, which shows the deformation for the three stress profiles on the same plot, using typical values. For example, a shell thickness of 5 percent, Poisson's ratio 0.45, stress profile $\sigma = 1\, cos^2\phi$ yields a relative radial deformation of 1 percent along the laser axis. For the same total force (on one hemisphere), the stress profile $\sigma = cos^{100}\phi$ yields a deformation of 6.5 percent.

At frequencies higher than the plateau regime (internal dynamics regime), if the form of the time dependent shear modulus $G(t)$ of a crosslinked actin network is known, the elastic-viscoelastic correspondence principle can be used to find the viscoelastic deformation of a cell with mainly the actin cortex (Appendix B.2).

An uncrosslinked actin network is our next model for the cortex. The plateau modulus of such a network (between 0.02 and 100 Hz) is determined by the curvature and orientational stresses in the deformed network and is given by $G_p = \frac{7\rho k_b T}{5l_e} + \frac{3\rho k_b T}{5l}$ [128], [129], where $l$ is the filament length. Figure 3.10 shows the variation of the plateau modulus with persistence length and actin concentra-tion. With the same parameters used for crosslinked networks, a plateau modulus calculated for an uncrosslinked network is two magnitudes lower. For such a small value of the plateau modulus, the linear thick shell theory predicts a very large de-formation (30 percent relative deformation for a thick shell of 20 percent thickness subjected to a stress $\sigma = cos^2\phi$). These large deformations are not observed in
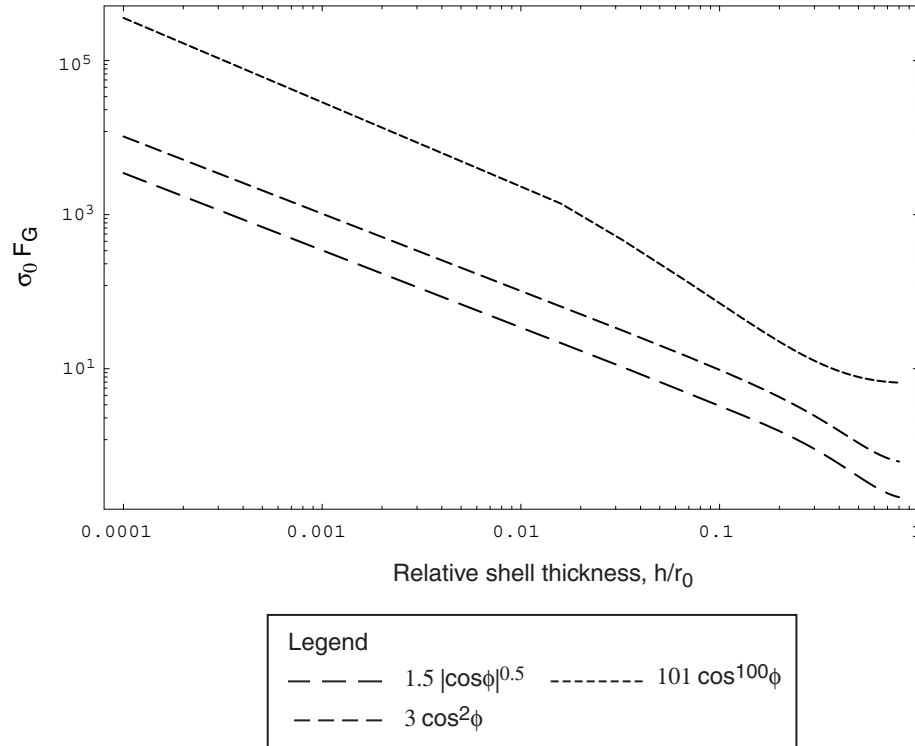
Figure 3.4: Geometric factor $F_G$ for the relative radial displacement multiplied by the peak surface stress $\sigma_0$ along the laser (z) axis at $\phi = 0$, $\sigma_0 F_G$ (for $\sigma = \sigma_0 \, cos^n(\phi)$), as a function of relative shell thickness, $\frac{h}{r_0}$, and Poisson's ratio, $\nu = 0.45$. The geometric factor becomes significant, as the shell thickness decreases.

45
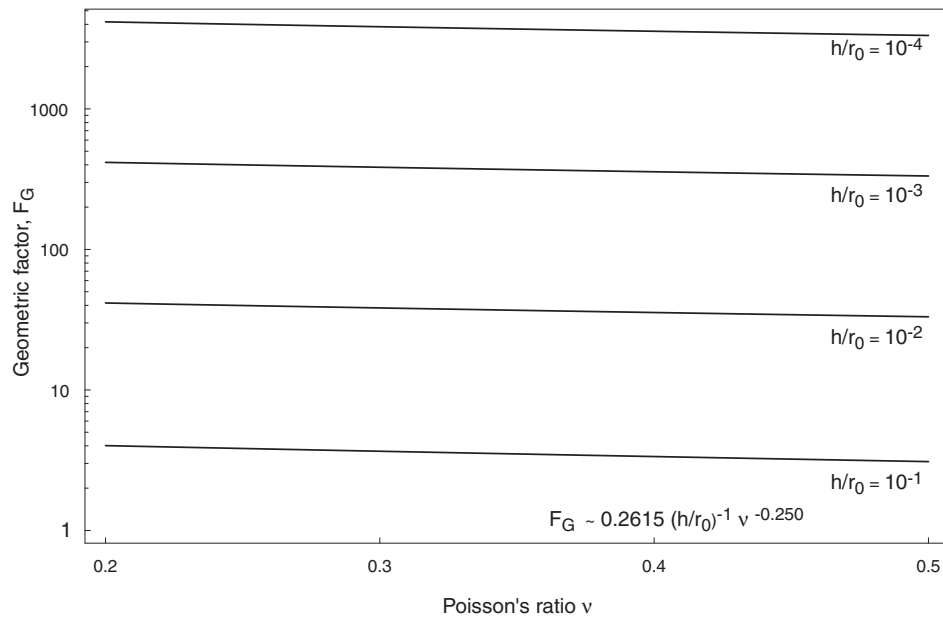
Figure 3.5: Geometric factor, $F_G$, for the relative radial displacement along laser (z) axis at $\phi = 0$ for $\sigma = 3 \, cos^2(\phi)$ as a function of relative shell thickness, $\frac{h}{r_0}$, and Poisson's ratio, $\nu$, for a thin shell. The geometric factor depends weakly on the Poisson's ratio of the material in the thin shell - $F_G \sim \nu^{-0.25}$, and inversely on shell thickness - $F_G \sim \left(\frac{h}{r_0}\right)^{-1}$.
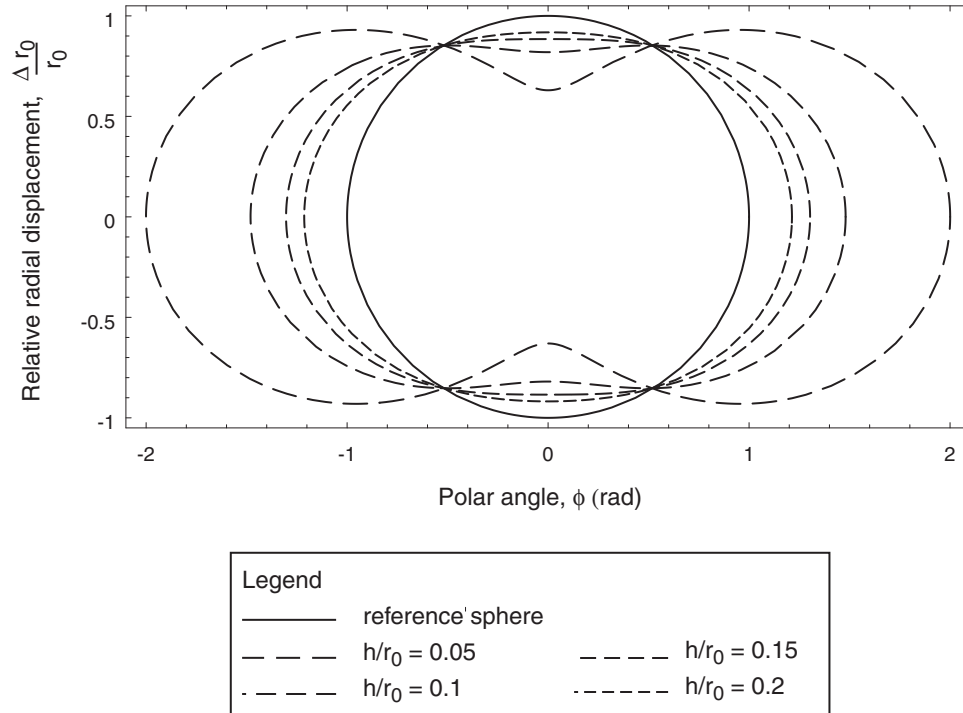
Figure 3.6: Relative radial displacement, $\frac{\Delta r_0}{r_0}$, magnified by $100/\sigma_0$ imposed on a unit reference sphere, for $\sigma = \sigma_0 \, cos^2(\phi)$ on a tightly entangled actin shell, as a function of relative shell thickness, $\frac{h}{r_0}$ and polar angle, $\phi$, for $\sigma_0 = 3$, $\nu = 0.45$, $\rho = 10$ mg/ml and $l_p = 17 \, \mu m$. The radial displacement of an actin shell and shell thickness are inversely related ($\frac{\Delta r_0}{r_0} \sim (\frac{h}{r_0})^{-1}$ for a thin shell).
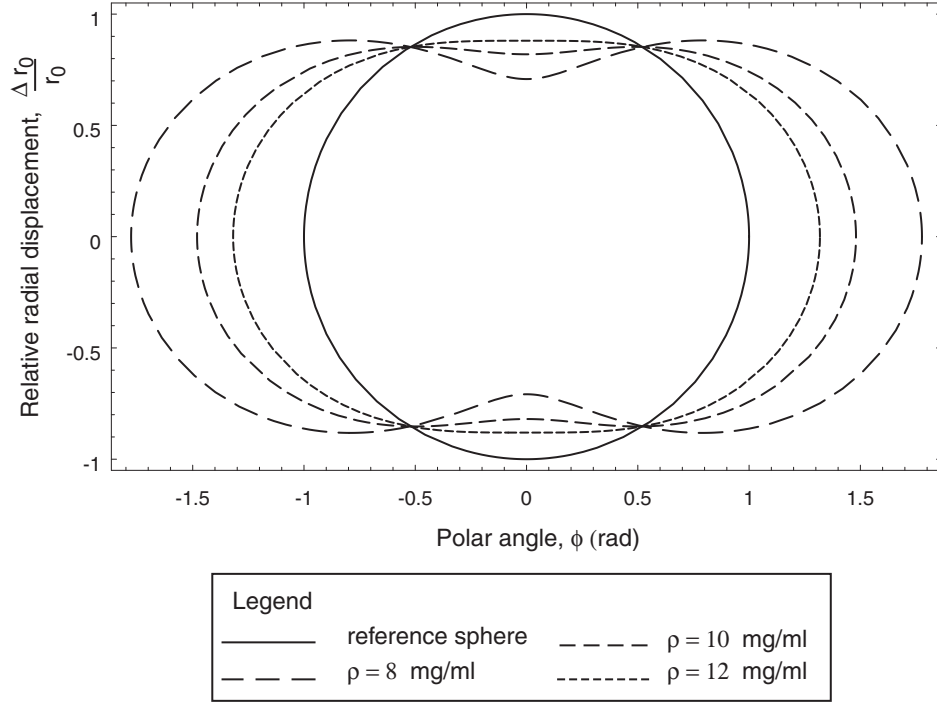
Figure 3.7: Relative radial displacement, $\frac{\Delta r_0}{r_0}$, magnified by $100/\sigma_0$ imposed on a unit reference sphere, for $\sigma = \sigma_0 \, cos^2(\phi)$, as a function of polar angle, $\phi$ and a tightly entangled, crosslinked actin concentration, $\rho$, for a persistence length, $l_p = 17 \, \mu m$, $\sigma_0 = 3$, $\frac{h}{r_0} = 0.1$ and $\nu = 0.45$. The radial displacement has a sensitive dependence on actin concentration, $\rho$, in the shell and is given by $\frac{\Delta r_0}{r_0} \sim \rho^{-2.2}$.
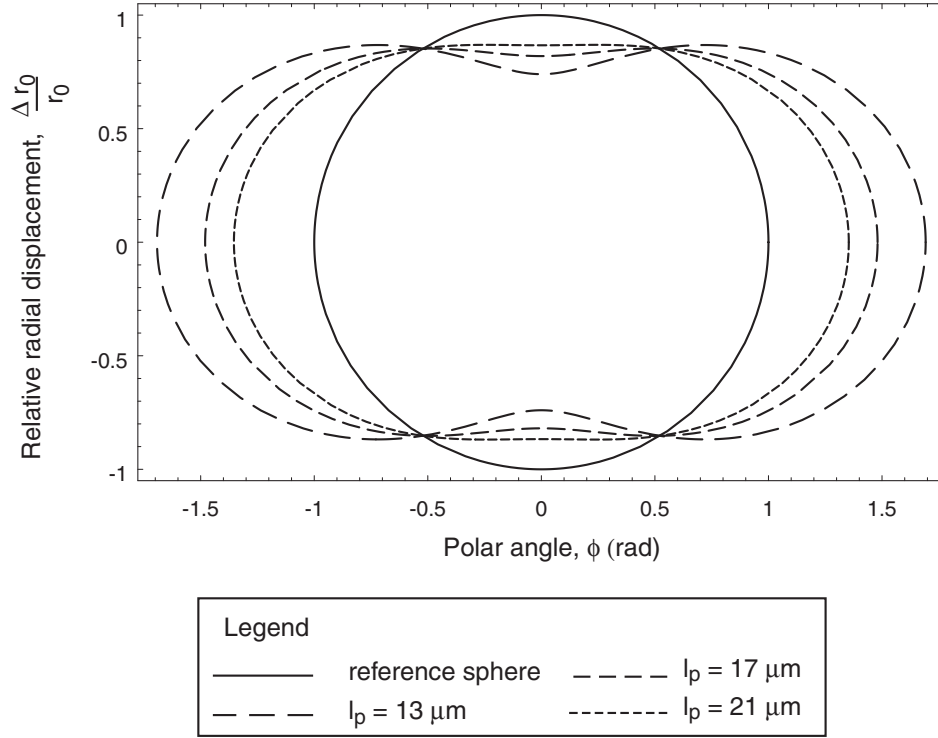
Figure 3.8: Relative radial displacement, $\frac{\Delta r_0}{r_0}$, magnified by $100/\sigma_0$ imposed on a unit reference sphere, for $\sigma = \sigma_0 \, cos^2(\phi)$, as a function of polar angle, $\phi$ and persistence length, $l_p$, for a tightly entangled crosslinked actin concentration, $\rho = 10$ mg/ml, $\sigma_0 = 3$, $\frac{h}{r_0} = 0.1$ and $\nu = 0.45$. The radial displacement is related to the persistence length, $l_p$, of actin filaments in the shell by $\frac{\Delta r_0}{r_0} \sim l_p^{-1.4}$.
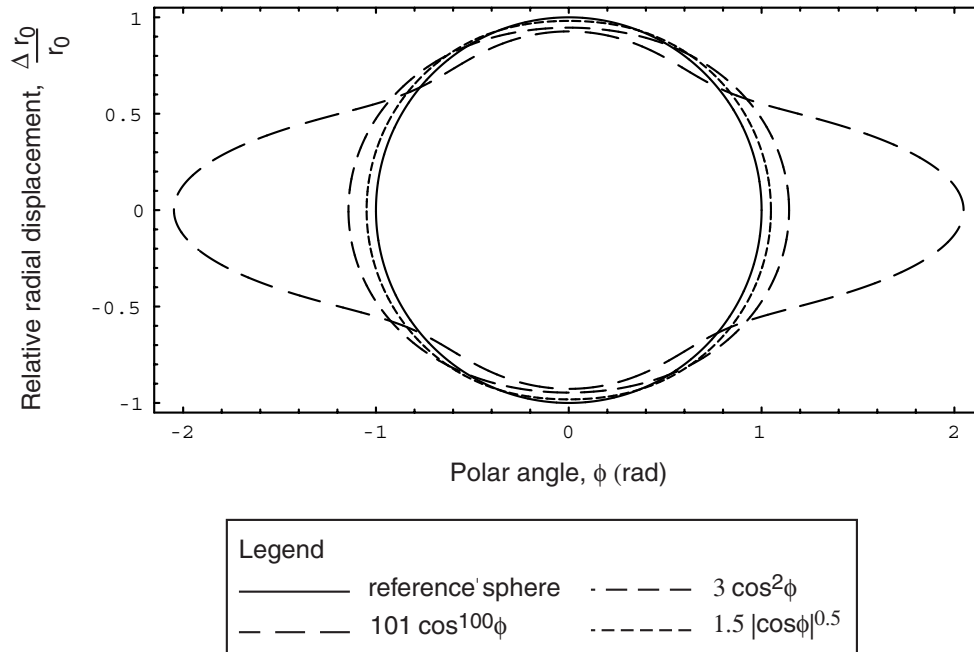
Figure 3.9: Relative radial displacement, $\frac{\Delta r_0}{r_0}$, magnified by 10 imposed on a unit reference sphere, for $\sigma = \sigma_0 \, cos^n(\phi)$ on a tightly entangled, crosslinked actin shell, as a function of polar angle, $\phi$, for $\frac{h}{r_0} = 0.1$, $\nu = 0.45$, $\rho = 10$ mg/ml and $l_p = 17$ $\mu$m. For each stress profile, the total force on one hemisphere is the same, and the effect of a local versus global stress on the actin shell can be observed.
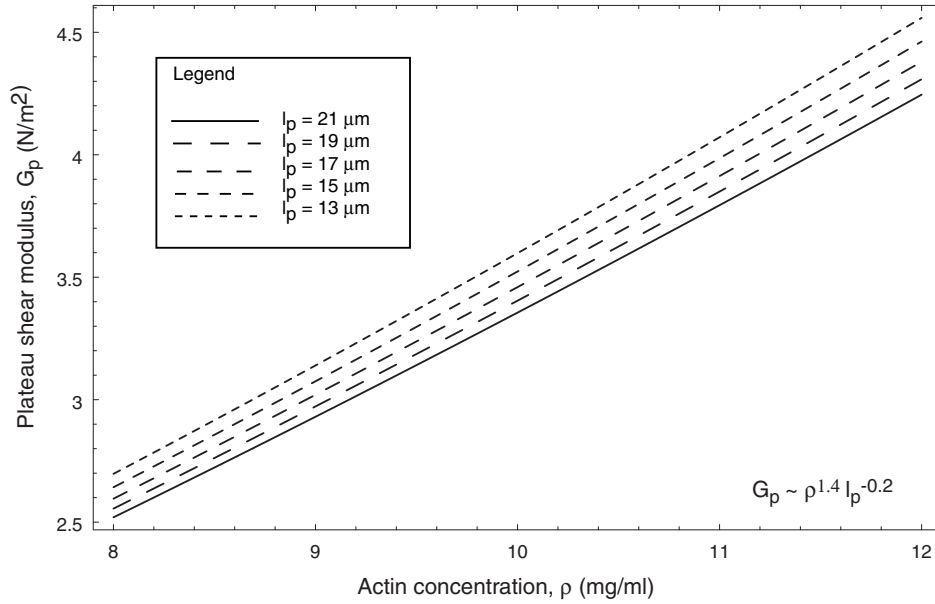
Figure 3.10: Plateau shear modulus, $G_p$, of a tightly entangled, uncrosslinked actin network [128], [129] as a function of persistence length, $l_p$, and actin concentration $\rho$. The modulus of the uncrosslinked network depends on actin concentration as $G_p \sim \rho^{1.4}$ - a much less sensitive dependence than that of a crosslinked network ($G_p \sim \rho^{2.2}$).

experiments which apply similar stresses on cells and suggest that an uncrosslinked actin network has too low a shear modulus to describe cellular mechanics [24]. However, it is also to be noted that linear elasticity does not hold for such large deformations.

## 3.3   Predictions of the Shell Model

Our study relating the structural response to the geometry of the cell as well as polymer properties clearly indicates that the concentration of the actin network

51

$(\frac{\Delta r_0}{r_0} \sim \rho^{-2.2})$ plays a more important role than the thickness of the actin cortex $(\frac{\Delta r_0}{r_0} \sim (\frac{h}{r_0})^{-1}$ for a thin shell), in determining the response. It has been observed in cancer cells that both the thickness of the cortex and amount of actin are reduced [106], [192], [12]. The total actin content in cancer cells can be 35 percent lower than in their non-cancerous counterparts [66], [185], [9]. Our model predicts that even a small change in the actin concentration of cells results in a large change in their structural properties - hence, the structural response is a good parameter to characterize normal and cancerous cells.

The above observation is in agreement with previous experimental studies on cancerous and non-cancerous cells [144], [216]. The micropipette experiments and work by Paulitschke et al. [144] compare the mechanical properties of white blood cells from healthy and chronic myeloid leukemic patients. The structural parameter used in this study is elastic rigidity, defined as $\frac{\Delta P R_p}{L_p / R_p}$, where $\Delta P$ is the step aspiration pressure, $R_p$, the inner radius of the micropipette tip and $L_p$, the aspirated portion of the white blood cell after one minute. It is found that the elastic rigidity of white blood cells in the resting phase from chronic myeloid leukemic patients is much lower than that from healthy donors ($\sim 60\%$ decrease in rigidity for lymphocytes and $\sim 30\%$ for granulocytes) . Ward et al. [216] have performed experiments on a panel of nontransformed and malignantly transformed rat fibroblasts and have analyzed their data using a standard solid model. The study reports that the viscoelastic parameters extracted from their transformed cell data using a standard solid viscoelastic model are $\sim 50\%$ percent lower than those extracted from their nontransformed cell data and concludes that there exists a direct correlation between an increase in deformability and the progression of tumorigenecity (metastasis). Recent experiments have been performed to deform normal and cancerous fibroblasts with the optical stretcher [169], [221], as discussed further in

Chapter 5. The data show distinct time regimes in the structural behavior - when these cells are stretched for approximately a second, they behave elastically at short time scales ($<= 0.2$ seconds) and viscoelastic beyond this time. The viscoelastic parameters extracted from the data using a simple 3 element mechanical model as well as a thick shell model (which incorporates cell geometry) point to a difference in the structural response of normal and cancerous fibroblasts. In summary, our model and these experiments suggest that the structural response of cancer cells reflects the molecular changes in their actin cytoskeleton, such as the concentration and distribution of actin, and can be used to distinguish normal and cancer cells.

## 3.4  Summary

Cell deformation experiments require an appropriate accompanying model to extract and study structural properties. Here, a 3D thick shell model has been created for a spherical eukaryotic cell, with mainly the actin cortex, for the optical stretcher experiment. The approach followed has been to calculate the shear modulus from the polymer physics of isotropic actin networks and to then predict the mechanical response of the shell to an arbitrary surface stress. Therefore, our model relates microscopic quantities such as persistence length and mesh size of the actin polymer network to macroscopic quantities such as the observed deformation. Our structural analysis studies the individual effect of the geometry of the cell and the constitutive properties of the actin polymer network on cell deformation. Applied to cancer cells, it predicts that the sensitivity of the structural response to changes in their actin cortex, particularly the actin concentration, can be used to differentiate them from normal cells.

Our model indicates that the actin cortex may be able to explain the qua-

sistatic structural properties of cells only under the tight localization of actin and the actin crosslinking proteins into a thin shell (Chapter 4). Also, the simple model does not capture features such as nonlinear structural responses, the withstanding of much higher stresses by osmotically swollen cells and other effects. In order to explain these effects, the structural contribution of microtubules and intermediate filaments [214] in the interior of the cell needs to be considered. Also, the effect of interactions among the various cytoskeletal polymers that are considered important, for example the actin-microtubule interaction [176], may need to be included.

# Chapter 4

# The Role of Isotropic Actin Networks in Cells

## 4.1  Isotropic Actin Networks

The actin cortex, along with its accessory proteins, has long known to be an important contributor to cytoskeletal structural response [187], [166], [35], [162], [213]. This *in vivo* (inside the cell) network's ability to change its structural strength by transitioning from a gel-like (solid) state to a sol-like (liquid) state is also crucial for cell motility [92]. There are many possible mechanisms by which the dynamic *in vivo* network can achieve this transition. One way is to depolymerize actin using severing, fragmenting and capping proteins such as severin, gelsolin and CapZ. To better understand these complex processes that govern the structural strength of the *in vivo* actin network, there have been experimental and theoretical estimates of the strength of *in vitro* actin networks. However, there is no direct estimate of the cortex's strength, using *in vivo* values. This chapter predicts the cortex's strength using theories of uncrosslinked, fully crosslinked and partially (transiently) crosslinked actin networks with *in vivo* parameter values, as an approximation to the cortex and a starting point to quantify its strength. This is done by calculating bounds for the plateau shear modulus of the transiently crosslinked cortex, using the above theories. The cortex's contribution to the structural strength of the whole cell is found here by comparing the calculated plateau shear modulus values to the elastic shear modulus commonly extracted from whole cell deformation experiments. With these assumptions for the cortex, our study, using values from the acanthamoeba cell,

shows that the calculated plateau shear modulus values of a partially crosslinked actin network can vary from 1 Pa (viscous network) to 1 kPa (solid network) depending on the spatial distribution of actin and the crosslinker protein - the modulus value is close to that of cells under the condition of tight localization of the *in vivo* actin into a cortex of 13 percent thickness and the crosslinking proteins into a cortex of 5 percent thickness. Hence, our work reveals that transient crosslinking - a different mechanism which does not involve depolymerizing the actin network - can also achieve the dynamic range of shear moduli observed in eukaryotic cells [3].

The actin cortex is a transiently - crosslinked polymer network and is composed of short, rod-like actin filaments, $0.1 < l < 3.0$ $\mu$m in length (Table 4.1). It lies just beneath the cell membrane, as a thick shell-like structure, whose radius can vary from 5 to 20 percent of the cell radius. Actin is a semiflexible polymer, whose persistence length (distance over which the filament can bend in two independent directions) is 17 $\mu$m and whose concentration in various cells differs from 4 mg/ml to 14 mg/ml [151] (Table 4.2). Inside a single cell, the mesh size ( = (concentration)$^{-1/2}$) of the crosslinked cortex increases from 50 nm at the edge of the cell to 300 nm towards the end of the cortex. The transient crosslinking of the short filaments *in vivo* is achieved by various crosslinking proteins such as $\alpha$-actinin and filamin. Both $\alpha$-actinin and filamin form a 3D actin network, instead of a bundle, due to their large size.

The first step towards understanding the structural strength of this *in vivo* actin network (actin cortex) is to study the strength of an *in vitro* actin network through rheology, where the network's strength can be determined by a stress relaxation or oscillatory shear experiment. Rheology has been performed on both uncrosslinked as well as crosslinked actin networks, to obtain values for structural

strength. Theories have also been developed to understand the structural properties of tightly entangled, uncrosslinked and crosslinked isotropic *in vitro* actin networks [128], [129], [113]. The filaments in rheology are typically 2-70 $\mu$m in length and 1 mg/ml in concentration, immersed in an artificial cytosol-like environment. Joint rheology experiments on uncrosslinked networks from the labs of Janmey and Pollard [224] have shown that a 1 mg/ml solution of actin, 6 $\mu$m in mean length, has a plateau shear modulus $G'$ (low frequency behavior between 0.02 and 100 Hz) of 0.5 Pa ($N/m^2$). The corresponding theoretical prediction for $G'$ of a 1 mg/ml, 4.25 $\mu$m network is 0.1 Pa [128], [129]. While both experiment and theory predict a high frequency dependent behavior (> 200 Hz) of $G(\omega) \propto (i\omega)^{3/4}$, they differ in magnitude by a factor of 4 [129], [114]. Rheology experiments have also been performed on actin networks crosslinked with $\alpha$-actinin or filamin, and the modulus measured is higher than that of actin networks alone (Table 4.3). However, even for a high concentration of actin and short filament lengths (96 $\mu$M actin concentration and 1.5-2.5 $\mu$m filament length [233]), the shear modulus is only 2.5 Pa [233]. The theoretical prediction of the strength of a 1 mg/ml crosslinked actin network is $\sim$5 Pa [113].

The extent of the plateau shear modulus (in frequency space) and its transition to a frequency dependent behavior in the high frequency internal dynamics regime are observed to be the same in *in vitro* actin networks and in cells [117]. However, the homogeneous and isotropic networks of rheology differ from the transiently crosslinked dynamic actin cortex, which can change its properties quickly. Nevertheless, interpreting the results obtained by using isotropic actin network theories for the cortex, with *in vivo* parameters, is a start to quantify the cortex's structural strength, which is important for the following reasons. The ability of the cell to perform its normal functions is closely interlinked to the state of its cytoskeleton.

Hence, cell functioning also reflects the state of the actin cortex and its strength via crosslinking. For example, cells lacking actin crosslinker proteins are found to display impaired cortical stability and motility [24], and reduced strength [34]. Also, tumorigenicity has been correlated to and controlled with the amount of actin [66] and actin crosslinker protein [59] in the cell. Another *in vivo* structural property yet to be understood is the actin cortex's high modulus of 30,000 Pa at the leading edge of motile cells such as fibroblasts, which is thirty times the cortex's strength in the cell body [118].

## 4.2   Quantifying the Strength of the Actin Cortex

Our structural study of the cortex considers three static actin networks as approximations to the cortex, and estimates the plateau shear modulus of each network with *in vivo* values, to establish bounds for cortex strength. The three networks are: 1. a tightly entangled, uncrosslinked actin network 2. a tightly entangled, fully crosslinked actin network and 3. a tightly entangled, partially crosslinked network [4]. The partially crosslinked network is our most realistic approximation to the cortex and our calculated results presented here for the numerical range of its shear modulus use *in vivo* values of actin, $\alpha$-actinin concentrations and other parameters from the acanthamoeba cell. Before studying the strengths of these tightly entangled networks, the phase diagram of an actin network is discussed.

The phase diagram in Figure 4.1 depicts the existence of different phases of actin depending on its concentration and filament length - the loosely entangled, tightly entangled, nematic phases and the tightly entangled-nematic coexistence phase. Our interest lies in the tightly entangled isotropic regime, since the actin cortex is believed to be isotropic and not nematic [98]. Also, a loosely entangled
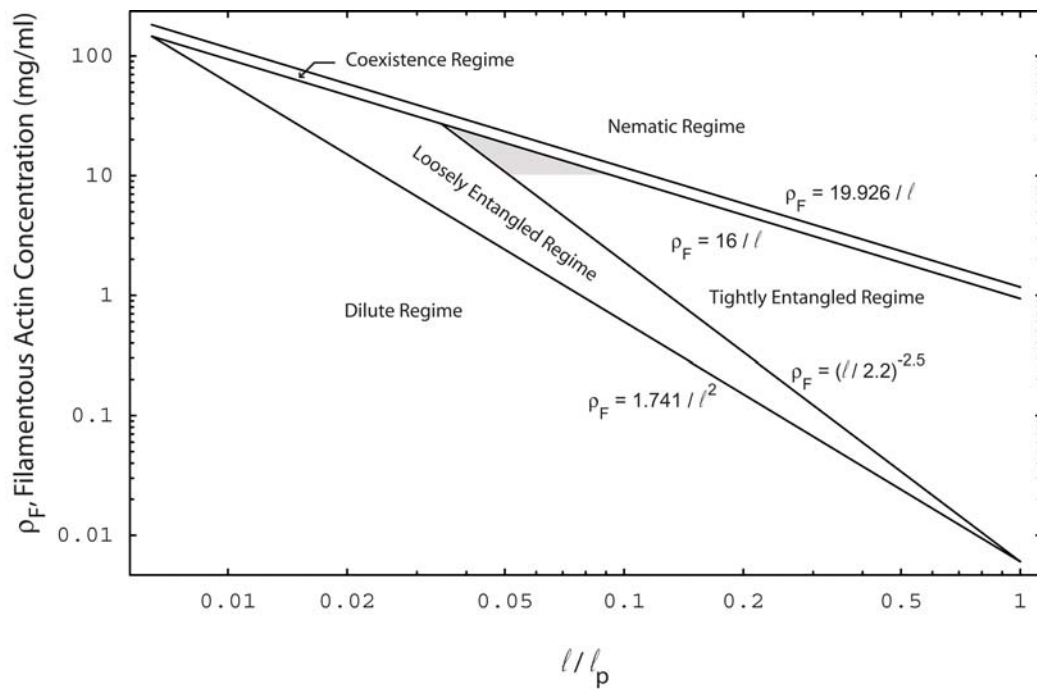
Figure 4.1: Phase diagram for an actin network, showing the loosely entangled regime, tightly entangled regime [128], nematic regime and coexistence regime of tightly entangled and nematic phases [27]. The shaded region shows the range of filament length possible for *in vivo* concentrations greater than 10 mg/ml

network provides negligible structural strength. In the tightly entangled regime, the filament length range becomes narrower and almost monodisperse as the actin concentration increases till this phase disappears at $\sim$ 27 mg/ml, as seen in the shaded region for *in vivo* concentrations higher than 10 mg/ml. Our results for the strength of the actin network assume that the filament length lies in the entangled regime for the concentration considered. However, our numerical results which require a specific actin filament length use 1 $\mu$m - in this case, it is assumed that there is length control of filaments *in vivo* due to the action of severing and capping proteins.

### 4.2.1  Uncrosslinked Actin Network

At frequencies $\omega$ between 0.02 and 100 Hz, an uncrosslinked, tightly entangled actin network has a low shear modulus (called plateau shear modulus), independent of time and behaves like a solid. At frequencies $\omega > 200$ Hz, the shear modulus increases with a power law dependence $\omega^{3/4}$. This chapter focuses only on the elastic low frequency plateau regime. For an uncrosslinked network, the plateau shear modulus is determined by the curvature and orientational stresses. It is given by $G' = G_{curve}(0) + G_{orient}(0) = \frac{7\rho_T k_b T}{5l_e} + \frac{3\rho_T k_b T}{5l}$ [129], where $k_b$ is Boltzmann's constant, $T$ is temperature, $\rho_T$ is the concentration of the actin network, $l_e$, the entanglement length ($l_e = 2^{4/3} l_p^{1/3} D_e^{2/3}$, with $l_p$ the persistence length of actin and $D_e$ its tube diameter) and $l$, the actin filament length (assumed 1 $\mu$m) (Figure 4.2). Figure 4.2 shows that even at actin concentrations similar to those found *in vivo* - for example at 4.16 mg/ml (100 $\mu$M), which is the concentration of polymerized (filamentous) actin in both an acanthamoeba and neutrophil cell (Table 4.2) - an uncrosslinked actin network has too low a plateau shear modulus to describe cellular mechanics: as mentioned earlier, crosslinkers are crucial for cell stability and
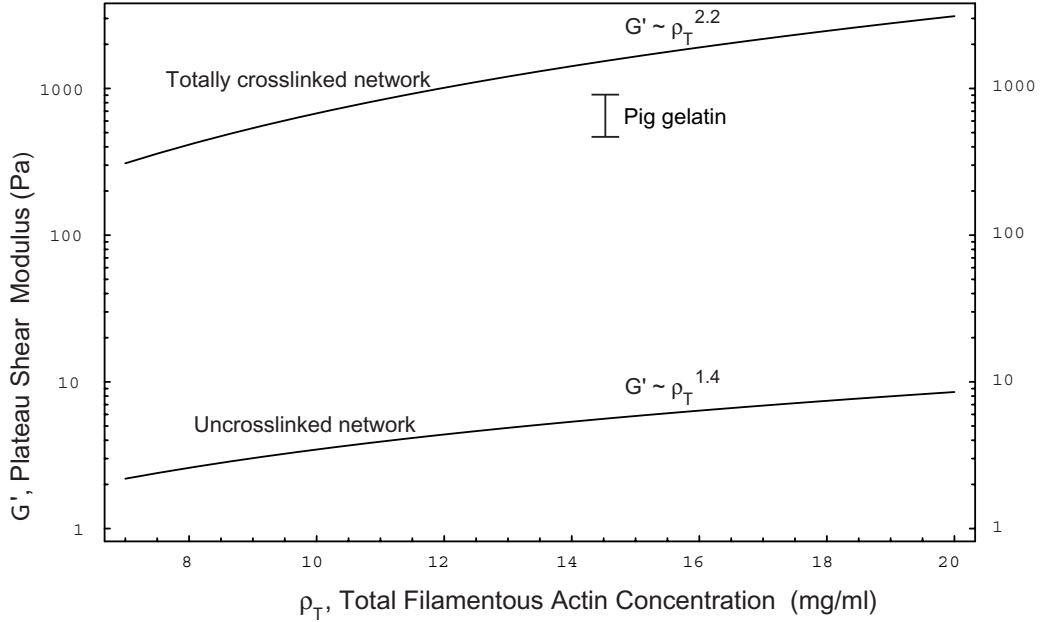
Figure 4.2: Plateau shear modulus, $G$, for uncrosslinked [128], [129] and fully crosslinked [113], tightly entangled actin networks ($l_p = 17$ $\mu$m, $\omega = 1$ Hz), as a function of filamentous actin concentration

motility [24].

### 4.2.2 Fully Crosslinked Actin Network

A fully crosslinked, tightly entangled actin network has a high plateau shear modulus at low frequencies < 100 Hz). Here, $G'$ is given by $G' = \frac{k_b T l_p^2 \rho_T}{l_x^3}$, where $l_x$ is the typical distance between crosslinks, which is $l_e$ in this case [113]. Since $l_e \sim l_p^{1/5} \rho_T^{-2/5}$ [128], [129], $G'$ ultimately depends only on the concentration of the network and the persistence length of actin filaments as $G' = k_b T l_p^{1.4} \rho_T^{2.2}$. Figure 4.2 shows the range of shear moduli calculated for a crosslinked network using *in vivo* values for concentration and other parameters - 17 $\mu$m is used for the persistence

61

length $l_p$ while the filament length is considered to be in the entangled regime for the corresponding concentration (the formula does not have any explicit dependence on filament length). At an *in vivo* concentration of 4.16 mg/ml, the shear modulus of a crosslinked network is $\sim 100$ Pa - this value is compared in the following section to the moduli extracted for various cells.

### 4.2.3   Partially Crosslinked Actin Network

The transition between an uncrosslinked and a fully crosslinked network is a partially crosslinked, percolated network [61]. An uncrosslinked polymer network, which is fluid-like, undergoes a transition to a solid-like network at a critical crosslink density equal to the number of filaments in the system. Such a network is a percolated network. For an *in vivo* actin concentration of 4.16 mg/ml, the number density is $1.6 \times 10^{14}$ filaments/$cm^3$. Therefore, the number of crosslinkers needed to achieve the liquid-solid phase transition is $1.6 \times 10^{14}$ crosslinkers/$cm^3$. According to percolation theory, the ratio of crosslinkers to filaments needed for the transition to occur is one [61]. Our calculations for the partially crosslinked network discussed later in the section are based on the actin crosslinking theory developed by Spiros et al. [180], which is valid above the percolation threshold.

Before obtaining a quantitative estimate of the structural strength of a partially (transiently) crosslinked actin network, this study considers, in Figure 4.3, the qualitative difference in the structural response of a fully crosslinked and a partially crosslinked actin network of the same concentration - Figure 4.3 a) shows the relaxational shear modulus $G(t)$ versus time $t$ and Figure 4.3 b) shows the shear modulus $G(w)$ versus frequency $w$ of the two networks. At very short time scales, less than the average binding time of the crosslinker, a fully crosslinked and par-
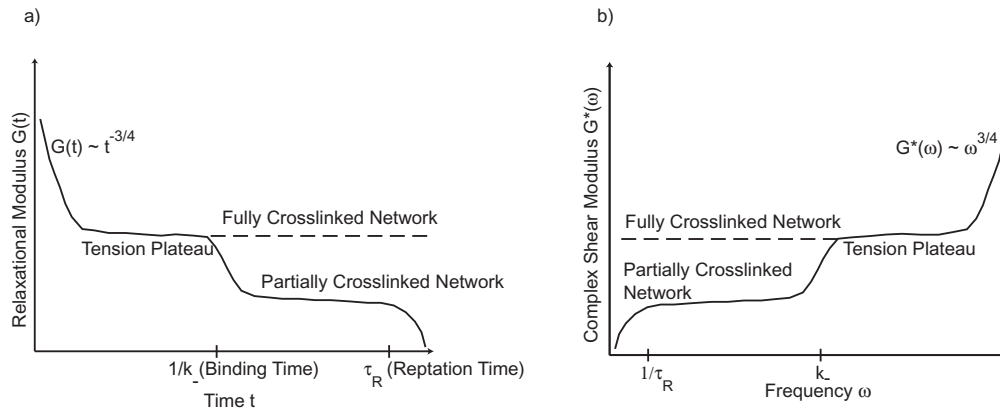
Figure 4.3: Qualitative behavior of the shear modulus of a fully and a partially (transiently) crosslinked, tightly entangled actin network as a function of time (Figure a) and a function of frequency (Figure b)

tially crosslinked network show the same structural behavior with a high plateau modulus after an initial relaxation. However, even beyond the binding time of the crosslinker, the fully crosslinked network cannot relax its stress, since its crosslinks are permanent, while the partially crosslinked network begins to display the transient nature of its crosslinks. It, then, behaves structurally like an uncrosslinked network and displays another plateau, due to the presence of entanglements. This plateau has a low modulus value and is difficult to measure experimentally. At time scales beyond the reptation time $\tau_R$ (the time it takes for a filament to diffuse a distance equal to its own length), the partially crosslinked network behaves like a fluid. Figure 4.3 b) shows the structural behavior of the two networks in frequency space.

In order to finally quantify or calculate the strength of a partially (transiently) crosslinked actin network in acanthamoeba, a tightly entangled, crosslinked actin network and the number of crosslinking points need to be considered now in

greater detail. Firstly, from the phase diagram of Figure 4.1, if an actin network whose filaments are 1 $\mu$m in length is to be tightly entangled, its concentration must lie between 7.2 and 12 mg/ml. So, for an *in vivo* network of 4.16 mg/ml to be tightly entangled, it has to be concentrated in a much smaller volume of the cell (into the cortex), to achieve an effective concentration between 7.2 and 12 mg/ml ($\rho_{eff} = \frac{(\rho_T)_0}{(1-\chi^3)}$, where $(\rho_T)_0$ is the original concentration and $\chi$ is the ratio of the inner radius to outer radius of the shell in which the actin network is concentrated). The plateau modulus of the crosslinked network increases, in this case, by a factor of $(\frac{1}{(1-\chi^3)})^{2.2}$.

Secondly, a rough estimate of the number of crosslinking proteins per filament can be computed from experimental data on both *in vivo* crosslinker and actin concentrations. This experimental estimate can be compared with the maximum number of crosslinks per filament from theory [129], which gives us an idea of whether there is enough crosslinker protein *in vivo* to achieve the maximum crosslinking predicted theoretically. From theory, the number of entanglement points per filament is Round[l/$l_e$] + 1. The number of entanglement points calculated per filament of length 1 $\mu$m for an actin concentration of 7.2 - 12 mg/ml is two. Therefore, the maximum number of crosslinking points per filament is two for this concentration range. The experimental estimate for the number of crosslinkers per filament is obtained in Table 4.2 for acanthamoeba and other cells by dividing the total crosslinker number density *in vivo* by the total number density of actin filaments *in vivo* (1 mg/ml = 3.8 $10^{13}$ actin filaments/$cm^3$). To account for the fact that two filaments are connected by one crosslinker, the calculated crosslinker/filament ratio can be multiplied by two. The calculation does not consider the probability for a specific crosslinker to be in the right position and orientation, to connect two filaments. This estimate is, therefore, an upper bound. The estimate also assumes

that all the crosslinker protein present is bound, which is not true.

So, the number of bound crosslinkers per filament is now calculated, using the following formula in terms of the number densities of actin and the crosslinker [180].

$$\frac{bound\ crosslinker}{total\ actin} = \frac{\alpha}{K_d + \alpha} \tag{4.1}$$

where $\alpha$ is the number density of free crosslinker and $K_d$, the equilibrium dissociation constant of the crosslinker is $\frac{k_-}{k_+}$, where $k_-$ is the dissociation rate constant and $k_+$ is the association rate constant of the crosslinker. Using the number density of actin and $\alpha$-actinin in acanthamoeba and $K_d$ for acanthamoeba $\alpha$-actinin, an estimate of $\sim 1$ is obtained for the ratio of bound crosslinker to polymerized actin. This value suggests that unless the *in vivo* actin crosslinking protein is localized in the cell, there is not enough crosslinker protein to achieve maximum crosslinking (from theory).

However, following Spiros et al. [180], a further improvement in the calculation can be made, by estimating the amount of actin in the filamentous form and in the network form [3]. This allows us not only to calculate the ratio of bound crosslinker to networked actin, but also to finally estimate the plateau modulus of a partially crosslinked network (only the amount of networked actin contributes to strength). The following calculation to obtain $N$, the number density of actin in network form, takes into consideration, in a simple manner, the position and orientation allowed for two filaments to connect, and solves the following coupled equations numerically.

65

$$dN/dt = \beta_1 T(\nu_{x\theta} F^2 + \nu_{x\theta} \delta F N - \gamma_1 N) \qquad (4.2)$$

$$dF/dt = -dN/dt \qquad (4.3)$$

where $N$ is the number density of actin in network form, while $F$ is the number density in filamentous form, $T$ is the total actin density, $\gamma_1 = \frac{\gamma}{\beta_1 T}$, $\gamma$ is the dissociation constant, $\beta_1 = \frac{k_+ \alpha}{K_d}$, $\delta$ is a constant $= 0.25$ and $\nu_{x\theta}$ is the volume fraction of crosslinkers in the right position and orientation to bind. Note that both F*(K convolved with N) and N*(F convolved with K), a measure of crosslinkers in the right position and orientation to bind [180], are written by us as $\nu_{x\theta} N F$. The dimensionless diffusion coefficients of translation and rotation $\epsilon_1$ and $\epsilon_2$ in Spiros et al. have been estimated by us with *in vivo* parameters and are neglected, since $\epsilon_1 \sim 10^{-4}$. Using data from acanthamoeba, Figure 4.4 depicts the volume fraction of networked actin ($\nu_N = \frac{N}{T}$) for different values of $\nu_{x\theta}$ and actin concentration, $\rho_T$ and crosslinker concentration $\rho_{CL}$. The data from Figure 4.4 can be used to find the ratio of bound crosslinker to networked actin, which is a factor $\frac{1}{\nu_N}$ higher than the ratio of bound crosslinker to total polymerized actin. $\nu_N$ can also be used to estimate the modulus, as discussed below.

The objective of the above calculations is to understand actin's contribution to structural strength quantitatively. An upper bound for the cortex's strength is the plateau shear modulus of a fully crosslinked network ($G' = \frac{k_b T l_p^2 \rho_T}{l_x^3}$, where $l_x$, the typical length between crosslinks, is $l_e$), which can be compared to the shear modulus of cells. Table 4.4 shows the shear modulus of a typical cell (fibroblast, which

66
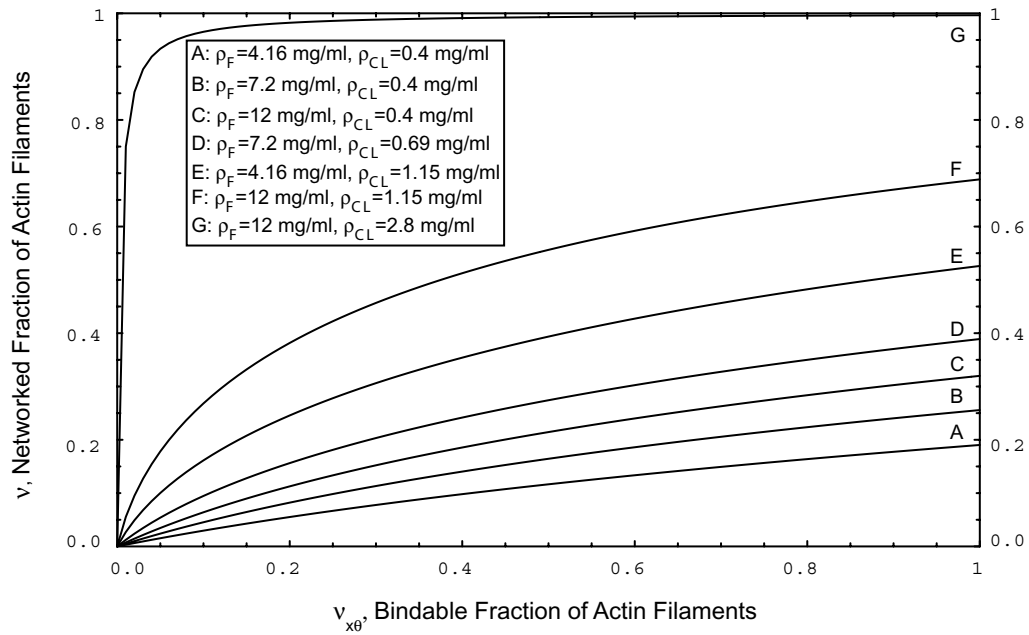
Figure 4.4: The fraction of networked actin filaments (in an Acanthamoeba cell) as a function of the fraction of actin filaments with the appropriate position and orientation to bind to the network. For a homogeneous distribution of actin and crosslinking proteins throughout the cell, the maximum networked fraction of actin filaments is $\sim 19\%$

has a thick actin cortex) as well as the modulus of an epithelial cell, macrophage and neutrophil. For 4.16 mg/ml of polymerized actin as in the acanthameoba and neutrophil cells, the value obtained from a fully crosslinked actin network distributed homogeneously throughout the cell is $\sim 100$ Pa. While the shear modulus of an acanthamoeba cell does not seem to be reported in literature, our calculated value is close to the shear modulus of a neutrophil of 118 Pa [232]. 100 Pa is, however, much lower than the shear modulus extracted from cell deformation experiments on fibroblasts. Furthermore, if a partially crosslinked network is considered, the fraction of networked actin can be used to estimate the effective distance $l_x$ between crosslinks, which increases by a factor of $\nu_N$   ($l_x = \frac{l_e}{\nu_N}$). The modulus of the partially crosslinked network, consequently, decreases from that of a fully crosslinked network, since $G'_{partially\ crosslinked} = \nu_N^3 * G'_{fully\ crosslinked}$, as shown in Figure 4.5. If both the effective concentration ($\rho_{eff} = \frac{(\rho_T)_0}{(1-\chi^3)}$, due to the spatial distribution of actin into a cortex) and the fraction of networked actin are considered, then $G'_{partially\ crosslinked} = (\frac{1}{1-\chi^3})^{2.2} * \nu_N^3 * G'_{fully\ crosslinked}$ (in this case, there is a change in the modulus from the $\rho_T$ dependence as well as from $l_x$). Figure 4.5 shows that a value of 1000 Pa, close to that extracted for fibroblasts, is reached in acanthamoeba only when all the *in vivo* actin is localized into an actin cortex of 13 percent thickness and the crosslinking proteins into a cortex of 5 percent thickness.

Finally, the time scale of transient crosslinking of $\alpha$-actinin $= k_-^{-1}$ (where $k_-$ is the dissociation rate constant) is compared in Table 4.5 to other processes mentioned earlier that can depolymerize the actin network and change its structural properties, namely the association of an actin filament with gelsolin, capping protein or ADF/Cofilin. The dissociation rate $k_-$ is obtained from *in vitro* networks and is assumed to be the same *in vivo*. Beyond the time scale, $k_-^{-1}$, the network behaves like an uncrosslinked network (Xu et al., 2000). For $\alpha$-actinin, $k_-^{-1}$ at 25 degrees is

68
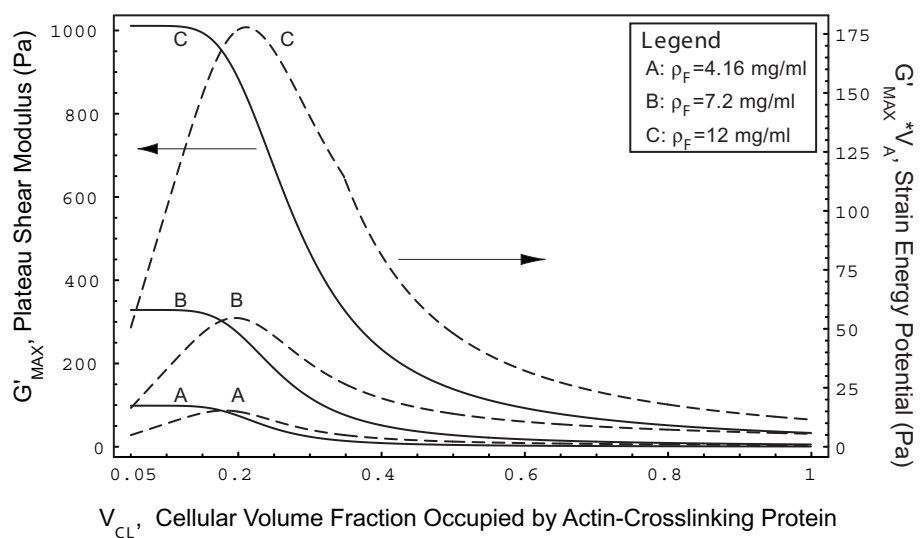
Figure 4.5: The plateau shear modulus and strain energy potential of an Acanthamoeba cell as a function of the volume fraction of actin crosslinking protein. High values for the plateau shear modulus (1000 Pa) are reached in Acanthamoeba only at nearly nematic actin and crosslinking protein concentrations

0.37 secs. The time scales of association of an actin filament with gelsolin, capping protein or ADF/Cofilin can be found approximately by calculating $\frac{1}{k_+ * conc}$ and are 0.4, 0.286 and 0.27 secs for gelsolin capping protein, ADF/cofilin respectively. As can be seen, transient crosslinking occurs on the same time scale as these other phenomena. Since it is just as fast, it may be an alternative or competing mechanism which can control the dynamic structural response of cells - it is likely that the cell has redundant pathways or processes to restructure its actin cytoskeleton.

## 4.3   Results and Discussion

In this work, our knowledge of isotropic actin network models has been applied to cells, to study their implications to cell strength. Our theoretical calculations, with *in vivo* parameter values, suggest that an uncrosslinked network has too low a plateau shear modulus to explain cellular mechanics. Our calculated plateau shear modulus value for a homogeneous, fully crosslinked actin network of 4.16 mg/ml, as found in acanthamoeba and neutrophils, may be able to explain the modulus value of a neutrophil. However, this calculation for a fully crosslinked network, while already an upper bound, is much lower than the shear modulus of cells such as fibroblasts, epithelial cells and macrophages - experimental results from rheology on *in vitro* crosslinked actin networks, even at a high actin concentration and short lengths (96 $\mu$M, 1.5-2.5 $\mu$m), also yield shear modulus values much lower than those of cells. When the spatial distribution of the actin network into a cortex or shell is considered though (which results in a high effective concentration of the actin and crosslinker protein), the theoretical values from both fully and partially crosslinked actin networks are closer to the shear modulus of cells. Thus, our calculations show that the spatial distribution and transient crosslinking of actin and crosslinking proteins enable cells to change the elastic strength of actin

70

networks over a wide range (1 Pa to 1 kPa), from a fluid-like to solid behavior, without using any capping or severing proteins like severin or gelsolin to depolymerize actin. Our results are supported by experiments on gelsolin-null fibroblasts [220] and severin-lacking dictyostelium mutants [6] that show cell motility and other normal cell functions. However, the range of values obtained still cannot explain the 30,000 Pa measured at the leading edge of motile fibroblasts [118]. This observation and our calculations are in agreement with findings by Yamada et al. [230], that actin alone is unable to explain lamellar mechanics.

## 4.4 Summary

Out of the three cytoskeletal elements, actin is considered to be the most important contributor to cellular mechanics [187], [164], [35]. Experiments with cytoskeletal poisons which selectively kill a certain *in vivo* polymer network lend evidence that depolymerizing the actin cytoskeleton leads to a drastic reduction in the structural strength of the cell, while disrupting the microtubule network does not alter it significantly [162], [213]. Also, the viscoelastic response of *in vitro* actin networks, artificial cells [79] and eukaryotic cells (fibroblasts) [117] exhibits similar characteristics in the plateau regime and in the transition to the internal dynamics regime. To quantitatively understand the role and contribution of the *in vivo* actin network to cell strength, this study uses isotropic actin network models with *in vivo* values to calculate actin's shear modulus. Our calculations show that the localization and reconfiguration of actin and actin crosslinking proteins, along with transient crosslinking, can explain the wide range of shear moduli and viscoelastic behavior witnessed in eukaryotic cells - actin does play an important role in cell dynamics. However, the high shear moduli measurements at the leading edge or lamellipodium of fibroblasts cannot be explained by actin alone [118] and the

effect of other structural elements, from stress fibers in the lamellipodium to microtubules and intermediate filaments in the interior, on the cell's dynamic response needs to be investigated. Actin's contribution is undoubtedly crucial but may still not be sufficient to explain all of cellular mechanics.

Table 4.1: Actin Filament Length in Different Cells

| Cell Type | *In vivo* Actin Filament Length ($\mu$m) | Reference |
|---|---|---|
| Resting Human Platelet | 2000 actin filaments 1 $\mu$m length | [77] |
| Dictyostelium Discoideum | 0.2 $\mu$m mean length | [148] |
| | 71 % F-actin mass and 96 % pointed ends 0.22 $\mu$m mean length | |
| | 14 % F-actin mass and 3 % filaments 1.3 $\mu$m mean length | |
| | 15 % F-actin mass and 0.3 % filaments 13 $\mu$m mean length | |
| Polymorpho-nuclear Leukocytes | $4 \; 10^5$ actin filaments 0.27 $\mu$m mean length | [17] |
| Bovine Arterial Endothelial Cells | 3 $\mu$m for confluent cells | [125] |
| | 0.5 $\mu$m for subconfluent cells | |
| Melanophores | 0.2 - 3 $\mu$m | [159] |
| Macrophages | 0.1 $\mu$m | [75] |
| Cells | $\leq 1 \; \mu$m | [188] |

Table 4.2: Concentrations of Actin and Actin Crosslinking Proteins in Certain Cells

| Cell | $\rho_{actin}$ $\mu$M | $\rho_{F-actin}$ $\mu$M | $\rho_{Actinin}$ $\mu$M | $\rho_{Arp2/3}$ $\mu$M | $\rho_{ABP}$ $\mu$M | Cross-linking sites per filament | Reference |
|---|---|---|---|---|---|---|---|
| Human Melanoma | | 120[1] | | | 1 | 2 | [24] |
| Acanth-amoeba | 200 | 100 | 4 | 2-4 | - | 7 | [151] |
| Dictyo-stellium | 250 | 90 | 3 | | 6[3] | 19 | [151] |
| Platelet | 550 | 330 | | 9 | 6 | 3 | [151] |
| Neutro-phil | 400 | 100 | | 10 | | | [151] |
| Macro-phage | 300[2] | | | | 43 | | [186] |

[1] The actin and ABP(280) concentrations in the melanoma cell [24] is reported not in absolute values but as $\rho_{ABP}$:$\rho_{actin}$ = 1:120

[2] The total actin concentration in the macrophage [186] is reported in absolute values and the ratio of $\rho_{ABP}$:$\rho_{actin}$ = 1:7 is also included.

[3] Dictyostellium has only ABP(120) [151].

Table 4.3: Rheological Data from Crosslinked Actin Networks. The rheological constants measured depend on both the actin and crosslinker concentrations and actin filament length

<div align="center">Crosslinker(CL): Amoeba-$\alpha$-actinin</div>

| $\rho_{actin}$ $\mu M$ | Actin Length $\mu m$ | $\rho_{CL}$ $\mu M$ | Rheological Constant $N/m^2$ | Frequency Hz | Temp $^oC$ | Refe-rence |
|---|---|---|---|---|---|---|
| 15 | | 0.1 | $G^*$=0.15 | $3\ 10^{-4}$ | 25 | [208] |
| | | | $G^*$=0.3 | $1.9\ 10^{-1}$ | 25 | |
| 15 | | 0.3 | $G^*$=10 | $10^{-1}$ | 25 | [209] |
| | | | $G^*$=30 | 1 | 25 | |
| 24 | | 1.6 | G'=4.7-100 G"=0.06284-0.1987 | $10^{-3}-1$ | 25 | [137] |
| 24 | 20 | 1.8 | $G^*$=4 | $1.6\ 10^{-4}-1.6$ | 23 | [140] |
| | | 2.4 | $G^*$=6-20 | $1.6\ 10^{-3}-1.6$ | 23 | |

<div align="center">Crosslinker(CL): Chicken-$\alpha$-actinin</div>

| $\rho_{actin}$ $\mu M$ | Actin Length $\mu m$ | $\rho_{CL}$ $\mu M$ | Rheological Constant $N/m^2$ | Frequency Hz | Temp $^oC$ | Refe-rence |
|---|---|---|---|---|---|---|
| 15 | | 0.1 | $G^*$=5 | $3\ 10^{-4}$ | 25 | [208] |
| | | | $G^*$= 4.5 | $1.9\ 10^{-1}$ | 25 | |
| 15 | | 0.3 | $G^*$=3 | $10^{-1}$ | 25 | [209] |
| | | | $G^*$=3 | 1 | 25 | |
| 15 | | 0.03 | $G^*$=2-3 | $10^{-4}-1$ | 25 | [225] |
| | | | $G^*$=4-5 | $10^{-4}-1$ | 15 | |
| 24 | 10-15 | 0.48 | G(t)=2-10 | t=0.01-10 sec | 25 | [229] |
| | | | G(t)=4-10 | t=0.1-100 sec 1-3 % strain | 15 | |

1. G(t)= Relaxational Shear Modulus, G', G"=Storage and Loss modulus, $G^* = \sqrt{(G'^2 + G''^2)}$

2. 1 mg/ml of actin = 24 $\mu$M

Table 4.3 continued

Crosslinker(CL) Actin Binding Protein (ABP)

| $\rho_{actin}$ $\mu M$ | Actin Length $\mu m$ | $\rho_{CL}$ $\mu M$ | Rheological Constant $N/m^2$ | Frequency Hz | Temp $^oC$ | Refe-rence |
|---|---|---|---|---|---|---|
| 96 | 1.5-2.5 | 0.768 | G'=2.5 | $3\ 10^{-2}$ | | [233] |
| 38.4 | | 0.28 | G'=20 G"=0.7-5 | $10^{-2} - 10^2$ | 20 | [137] |
| 10 | 5-6 | 0.033 | G'=0.3 G"=1 | 1 | | [64] |
| | | 0.1 | G'=0.6 G"= 1.2 | 1 | | |
| | | 0.2 | G'= 1.0 G"= 1.5 | 1 | | |

1. G(t)= Relaxational Shear Modulus, G', G"=Storage and Loss modulus, $G^* = \sqrt{(G'^2 + G''^2)}$

2. 1 mg/ml of actin = 24 $\mu$M

Table 4.4: Cell Deformation Techniques, Shear Modulus Extracted and the Model Adjunct. The effective shear modulus extracted for a cell depends on the experimental technique, cell type and the model adjunct

| Whole Cell | *In vivo* Structural Constant | Measurement Technique | Model Adjunct | Reference |
|---|---|---|---|---|
| Fibroblast | G'=300 G"=200 | AFM | Modified Hertz | [117] |
| | G=4 $10^3$ stable edge  G <(1000-1666) leading edge | AFM | Hertz | [161] |
| | G=566 V=4 $10^5$ | Bead Microrheology | Kelvin-Voigt | [153] |
| | G=$10^4$ V=$10^3$ | Bead Microrheology | 4 Element Mechanical | [10] |
| | G=333.33 | Microplates V=$10^4$ | 3 Element Mechanical | [196] |
| Epithelial | G=2500-3233 Normal cell  G=100-333 Cancer cell | AFM | Hertz | [109] |
| Macrophage | G=343 V=210 | Magnetic Bead Micro-rheometry | 4 Element Mechanical | [11] |
| Neutrophil | G=118 | Cell poker | Secant | [232] |

1. G=shear modulus in Pa , G',G"=storage and loss modulus in Pa and V=viscosity in Pa.s

2. The above calculations use a Poisson's ratio of 0.5 to convert from Young's modulus to shear modulus.

Table 4.5: Rate Constants and Time Constants of Key Actin Processes. The time scale associated with transient crosslinking is $\sim \frac{1}{k_-}$, while that associated with severing or capping is $\sim \frac{1}{k_+ * \rho_{protein}}$

| Protein | Association Rate $k_+$ $\mu M^{-1}s^{-1}$ | Dissociation Rate $k_-$ $s^{-1}$ | $K_d = \frac{k_+}{k_-}$ | $\rho_{protein}$ Acanthamoeba $\mu M$ | $k_+ * \rho_{protein}$ $s^{-1}$ | Reference |
|---|---|---|---|---|---|---|
| F-Actin | 1.3 (p)[1] 11.6 (b)[1] | 0.8 (p) 1.4 (b) | 0.61 $\mu$M 0.12 $\mu$M | 100 100 | | [150] |
| Capping Protein CapZ | 3.5 | 3 $10^{-4}$ | $\sim$ 0.1 nM | 1.0 | 3.5 | [168] |
| ADF (Cofilin) | $k_n$=0.037 $\mu M^{-2}s^{-1}$ $k_e$=130 $\mu M^{-1}s^{-1}$ | 0.035 | | 20 | 3.7 | [157] |
| Gelsolin | 2.5 excess EGTA[2] | 1.7 $10^{-4}$ | 0.07 nM | 1.0 (imag.) | 2.5 | [173] |
| | 10.0 presence of $Ca_2^+$ | $10^{-4}$ | 0.01 nM | 1.0 (imag.) | 10.0 | |
| $\alpha$-actinin | 1.0 | 2.7 | 2.7 $\mu$M | 4.0 | | [209] |
| Filamin (or ABP) | 1.3 | 0.6 | 0.46 $\mu$M | 1.0 (imag.) | | [63] |
| Arp 2/3 | 1-10 | 0.5-5 | 0.5 $\mu$M | 2-4 | | [134] |

[1] p - pointed end of actin filament and b - barbed end of actin filament

[2] EGTA condition - 1 mM MgCl$_2$, 100 mM KCl, pH 7.5, 37 degrees C

# Chapter 5

# Models for a Eukaryotic Cell in the Stretcher

## 5.1 Introduction

Chapter 3 discusses a linear thick shell (hollow interior) continuum model for a cell with a predominant actin cortex, assuming that actin is the main and only contributor to the structural response of the cell. However, the exact contribution of an isotropic actin network to cell strength and the conditions under which it can explain the cell's entire strength are described quantitatively in Chapter 4. Although Chapter 4 acknowledges the dynamical structural behavior of an isotropic actin network and its important role in cell strength, an actin network is not the only structural element in a cell. Hence, this chapter discusses the continuum and finite element (FEM) structural models created by us for a cell deforming in the stretcher, in order to incorporate the interior assembly of microtubules, and the nucleus and study their contribution to the structural response. Our continuum model also includes to first order the interaction between the actin cortex and the microtubules, by varying the boundary conditions.

All the above analytical and FEM models for a cell in the stretcher are linear elastic models. If actin is assumed to play a key role in the structural response of cells, a linear model is valid as long as the laser power used in the optical stretcher experiment does not stretch the cell beyond actin's linear response. *In vitro* rheological studies on actin filaments have shown that the material nonlinear properties of

actin (strain hardening) become important at strains greater than 10 percent [141]. An *in vivo* actin network may behave non-linearly beyond a different value of strain, but for large deformations, a nonlinear model which takes into account both the material nonlinearity and the geometric nonlinearity is required. So, this chapter also briefly explores how a nonlinear FEM model for a cell with a predominant actin cortex might be created.

Finally, recent viscoelastic data obtained by deforming normal as well as cancerous fibroblasts in the optical stretcher are analyzed by us with a three-element mechanical model. The structural parameters extracted are then used to gain an understanding of the polymer properties of the cytoskeleton - in particular, the actin cytoskeleton. The analysis of structural parameters from the mechanical model can also be combined with the deformation response of our analytical or FEM cell models, to incorporate the geometry of the cell. This permits an extraction of elastic and viscous parameters from experimental data, which include the effect of cell geometry.

## 5.2 Modeling a Eukaryotic Cell in the Optical Stretcher

### 5.2.1 Linear Elastic Analytical Model

Our study develops a model for a eukaryotic cell, which takes into account not just the actin cortex but other structural elements in the cell as well, to observe their role in cellular mechanics. Experimental evidence from Heidemann et al. [78] suggests that one possible structural model for the whole cell is a three-layered solid, with the three layers being the outer actin cortex, the interior network of microtubules and intermediate filaments and finally the nucleus (Figure 5.1). Such a

structural model, thus, assigns effective, homogeneous structural properties to each of the continuum layers: the actin cortex, the interior polymer network and the nucleus. As in the thick shell model, our continuum cell model (three-layered sphere model) calculations yield deformations for any rotationally symmetric stress acting on a cell in the stretcher set up. However, the calculations and results presented here are for only one typical stretcher-induced stress profile on the cell surface - $\sigma = \sigma_0 \ cos^2 \phi$ (Figure 2.2).
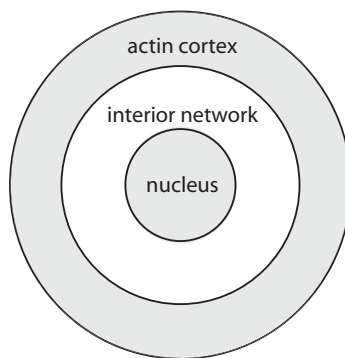


Figure 5.1: A three layered structural model of a eukaryotic cell, with the three layers being the actin cortex, the interior assembly of microtubules and finally the nucleus

The analytical techniques used to obtain the deformation of this model cell to such a stress are very similar to that of the thick hollow shell [112], where the deformation is calculated using legendre polynomials as the basis and using the principle of linear superposition too. Here, each layer can be treated individually as a ring (the cortex and the interior network layers) or as a sphere (nucleus), both of which can be solved analytically. The complexity of this problem lies in dealing with multiple boundary conditions. For each of the three layers, the boundary conditions must be satisfied everywhere on the interface. At each interface, no-slip boundary

conditions are used if the two layers are rigidly attached (non-penetrating). The no-slip conditions involve matching the radial and meridional displacements ($w$ and $v$) and also the radial and meridional stresses ($\sigma_r$ and $\sigma_{r\phi}$) on the boundary.

However, in order to create a continuum model which incorporates to first order the interaction between the actin cortex and the interior assembly of micro-tubules [74], slip boundary conditions, written as follows, can be used.

$$w_2 = w_1$$

$$(\sigma_r)_1 = (\sigma_r)_2$$

$$(\sigma_{r\phi})_1 = (\sigma_{r\phi})_2$$

$$(\sigma_{r\phi})_1 = 0,$$

where 1 and 2 are two surfaces with a common boundary.

More realistically, the mixed boundary conditions (combination of slip and no-slip conditions) given below are used in the problem, to incorporate the actin-microtubule interaction.

$$\alpha(\sigma_r)_2 = \beta(w_2 - w_1)$$

$$\alpha(\sigma_{r\phi})_2 = \beta(v_2 - v_1)$$

$$(\sigma_r)_1 = (\sigma_r)_2$$

$$(\sigma_{r\phi})_1 = (\sigma_{r\phi})_2,$$

where the parameters $\alpha$ and $\beta$ can be adjusted anywhere between 0 and 1 to obtain a boundary condition that varies from no-slip to slip.

Numerical values for the radial deformation of our whole cell continuum model are now calculated for both the no-slip and the mixed boundary conditions

by using representative values. The value used for the Young's modulus of the actin cortex is 500 Pa, while that used for the microtubules is 50000 Pa. Intermediate filaments are believed to play a role in the structural response only at large deformations [214] and are not considered in our structural model. From Guilak et al.'s work [72], the Young's modulus of the nucleus is taken to be 1000 Pa. The Poisson's ratio used for all the layers is 0.45. The actin cortex is assumed to be twenty percent of the cell radius, the interior network fifty percent and the nucleus thirty percent of the cell radius of 10 $\mu$m. With the above parameters and a stress of $\sigma = cos^2\phi$ on the cell ($\sigma_0 = 1$), the radial deformation obtained from the model at the outer layer, along the laser axis ($\phi = 0$) is $\sim$ 4.35 nm with no-slip boundary conditions and $\sim$ 80 nm with mixed boundary conditions ($\alpha$=1/2, $\beta$=1/2 for the actin-microtubule interface), which shows that the boundary conditions used are important in determining the deformation.

### 5.2.2 Linear Elastic Finite Element Model

To incorporate cytoskeletal architecture, numerical FEM models for a cell have also been created by us, using the commercial FEM package ABAQUS [1]. An ABAQUS program involves specifying the geometry of the model (mesh), the structural properties of the model's material, boundary conditions and the distribution of the applied load. The output of the model that interests us is the displacement observed for the prescribed stress.

The linear elastic FEM models created by us include a thick shell model to study the actin cortex alone, a layered thick shell model (with each layer having slightly different structural properties) for the actin cortex, a thick shell and rods

83

model for the cortex and microtubules respectively and finally a model for the cortex, microtubules and nucleus. All our FEM models which include microtubules enable us to model the structure of the microtubules, as hollow rods, more realistically than in the continuum model. Also, an analytical model for a thick shell with several rods does not seem easily solvable and a numerical FEM model seems to be required. For computational ease, our whole cell model consists of only half a sphere, with a thick shell for the actin cortex, a small nucleus in the center and rod-like microtubules that emanate from just above the nucleus to the inner surface of the actin cortex, as shown in Figure 5.2.

Before discussing our whole cell model, our thick shell FEM model is explained (Appendix D.2 contains our input file - named vtshell.inp). The shell is constructed using several twenty-node brick elements (ABAQUS element C3D20R). The thickness of the shell can be changed by varying the number of layers (of brick elements) and by varying the size of the brick elements used to construct the shell. The model consists of only one eighth of a shell, due to the axisymmetry of our problem (rotationally symmetric stress on a cell in the stretcher). So, the boundary conditions constrain the nodes in the XY plane to move only in the XY plane (no motion in the z direction); similar boundary conditions apply to the nodes in the YZ and XZ planes. Any axisymmetric stress can be applied to the FEM shell with an ABAQUS subroutine to define the stress on the entire shell. The deformation of this model, on which all our other cell models are based, is quantitatively compared with that of the analytical continuum thick shell model, detailed in Chapter 3, for two stress distributions (a uniform pressure of 1 Pa on the cell and a non-uniform pressure distribution of $cos^2\phi$) and for various structural parameters. These results are shown for different mesh discretizations and layers of the thick shell, along with error calculations, in Table 5.1. Table 5.1 reveals that the error or difference in de-
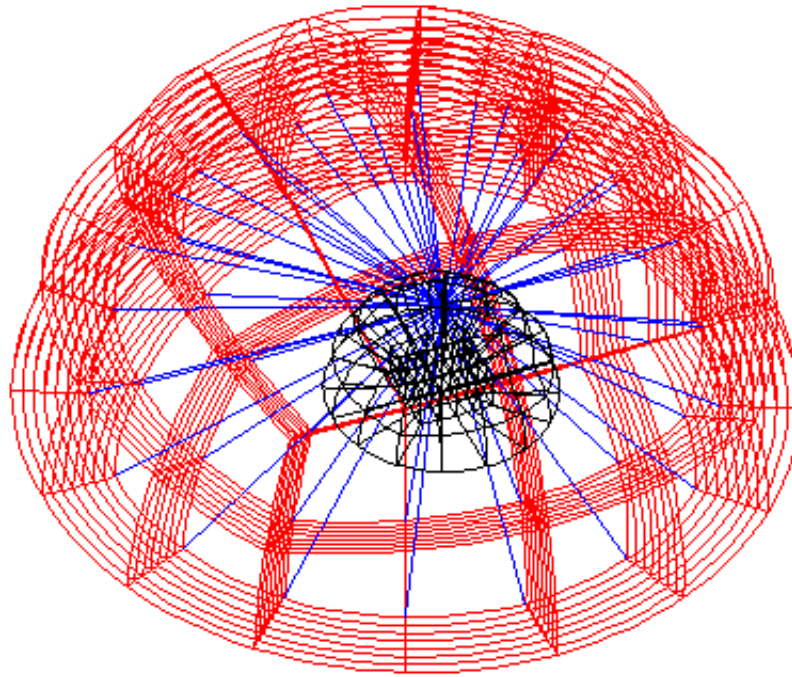
Figure 5.2: Finite element model (FEM) of a cell which includes three structural components - the actin cortex (red), microtubules (blue) and nucleus (black). The number of microtubules estimated *in vivo* is $\sim 1500$. However, the number of rods (microtubules) seen in this figure is much less ($\sim 60$), for clarity

formation predicted by the analytical model and the FEM model is very small even for the coarsest mesh discretization used (12 squares seen on the surface of one-eight of a shell). This error decreases as the mesh is made finer but at successively smaller rates, while the computational time increases significantly for finer meshes with more layers. Hence, the mesh chosen depends on the accuracy required of the solution (for instance, in the optical stretcher experiment, there is a minimum detection error in the deformation of 1 pixel or $\sim 0.6\%$ for a 100X magnification objective, which is much greater than the error of our FEM model). The high accu-

racy of our FEM thick shell model, as seen from Table 5.1, enables us to build upon it, to create more complex models such as a whole cell model.

In our whole cell FEM model, the actin shell is created as before with twenty-node brick elements. The nucleus is modeled as a sphere using twenty-node brick elements, while the microtubules are modeled as hollow rods with an outer radius of 12 nms and a thickness of 5 nms (ABAQUS element B31, which is a Timoshenko beam that can be used as a slender or thick beam and can carry transverse shear). All the rods have two nodes, with a common node located at the top of the nucleus and another node on the inner surface of the thick shell. The moduli and sizes of the cortex, microtubules and nucleus are the same as those used in the continuum model. With these parameters and the stress $\sigma = cos^2\phi$ on the model, the radial deformation along the laser axis can be obtained. This deformation, however, also depends on the number of rods (microtubules) in the model. So, the number of microtubules *in vivo* has been estimated by us, with a knowledge of the amount of tubulin found *in vivo* [138] and the microtubule structure and is found to be $\sim$ 1500. A cell model with a thick shell and $\sim$ 1500 microtubules, then, yields an extension of 65 nm along the laser axis. The observed deformation from our model with the cortex and microtubules can be used to get an idea of the contribution of microtubules to the entire structural response of the cell - by comparing it to the deformation from our model with the cortex alone (thick shell model) and attributing the response in each case to that of a homogeneous sphere. For a model with a twenty percent thick actin shell of Young's modulus 500 Pa and Poisson's ratio 0.45 and microtubules of Young's modulus 50000 Pa, the contribution of the microtubules to cell strength is estimated to be 20 percent but is only 5 percent for a cortex of modulus 3000 Pa (Figure 5.3).
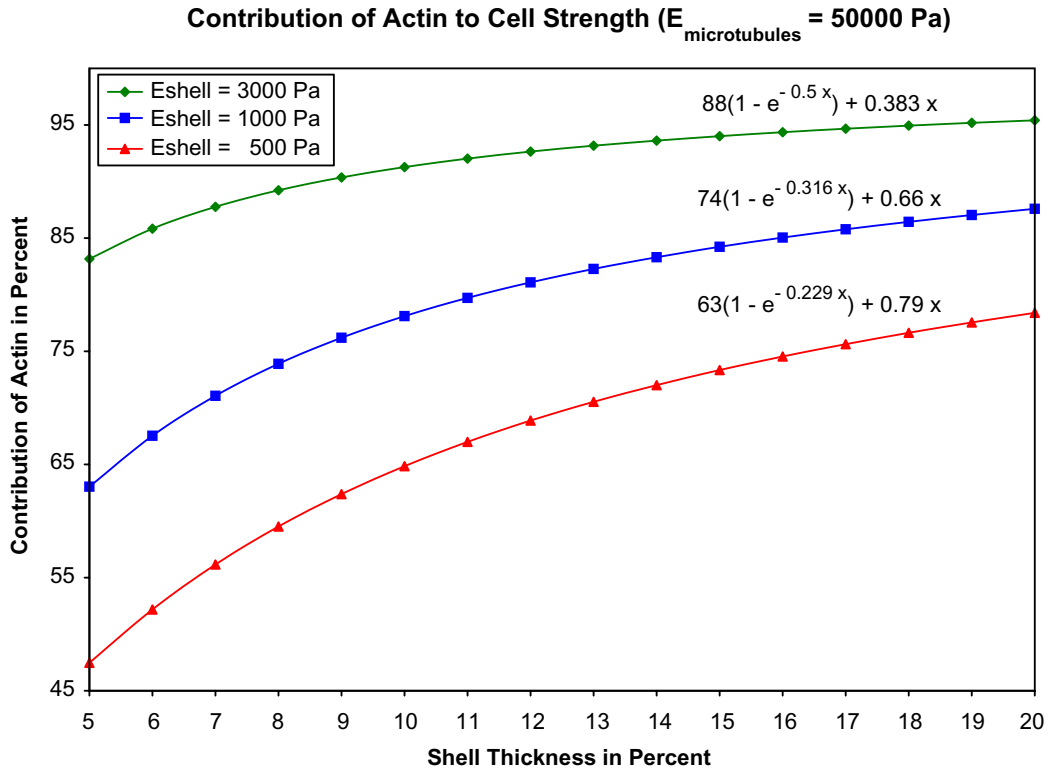
Figure 5.3: Contribution of actin to cell strength from studies with the FEM model with the actin cortex and microtubules, assuming $E_{microtubules} = 50000$ Pa

The numerical model has also been used to study the effect of an increase in microtubules from 0 to 1500 (Figure 5.4, with $E_{microtubules} = 50,000$ Pa) and a change in their modulus (Figure 5.5, for 1500 microtubules) on the observed deformation. A model with a thick shell, nucleus and 2000 microtubules (the *in vivo* microtubule estimate increases due to the space occupied by the nucleus) also results in an extension of $\sim 65$ nm along the laser axis. Both our analytical and numerical calculations imply that a peak stress $\sigma_0$ much higher than 1 $N/m^2$ needs to be applied to a normal cell in the stretcher, for the radial extension to be easily detectable or measurable - the extension must be $> 1$ pixel, which is $\sim 130$ nms for

the 100X magnification objective used in the experiment.
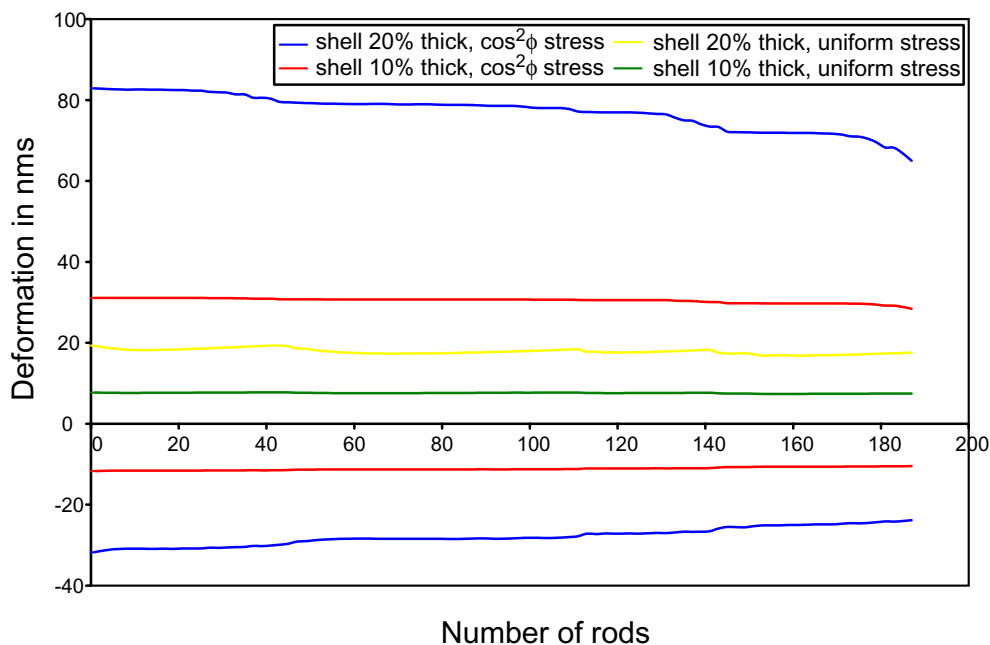


Figure 5.4: An increase in the number of microtubules leads to a lower deformation or stiffening of the model cell (thick shell and microtubules) along and perpendicular to the laser axis

Another effect studied by us in our whole cell FEM model (with half a sphere), which would be very difficult to study in an analytical model, is the effect of asymmetry of the nucleus. Many images of cells show (J. Guck, unpublished data) that the nucleus is not situated symmetrically (right in the center) in the cell. Our whole cell FEM model allows us to displace the nucleus anywhere in the XY plane. The results obtained suggest that the effect of the asymmetry on structural response is not significant.
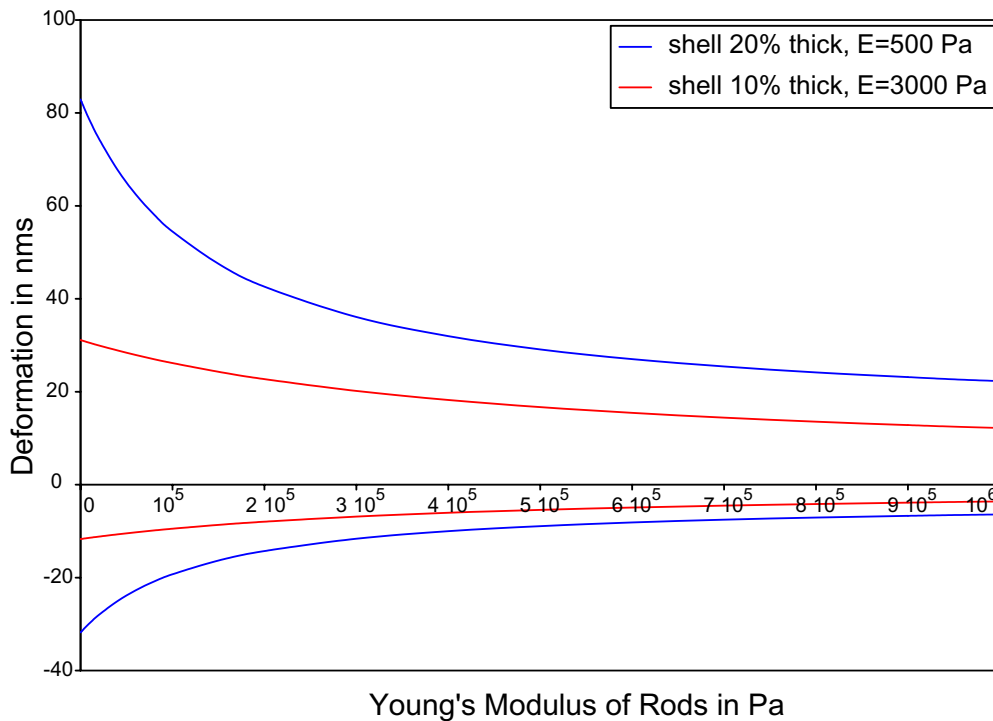
Figure 5.5: An increase in the microtubule modulus leads to a lower deformation or stiffening of a model cell (thick shell and microtubules), subjected to a stress $\sigma = \sigma_0 \; cos^2\phi$

### 5.2.3 Nonlinear Thick Shell Finite Element Model

As the laser power in the stretcher is increased, the cell's structural elements may respond nonlinearly - as mentioned earlier, actin displays a strain hardening behavior at high strains ($>$ 10 percent). Therefore, at these strains, a nonlinear thick shell model for the cortex, with a strain-hardening stress-strain behavior is required. Creating an analytical nonlinear model to analyze deformations is extremely difficult, since the principle of linear superposition, relied on to solve the linear problem analytically, does not hold any longer. Therefore, a numerical FEM model using

ABAQUS has been created. ABAQUS has available certain potentials (derivative of potential with respect to strain is stress) that satisfy this condition - for example, the Mooney-Rivlin, Odgen and Arruda-Boyce potentials are strain-hardening at high strains. The main reason for using the Arruda-Boyce is its inherent stability. The Arruda Boyce potential has the form

$$
\begin{aligned}
U &= \mu(\frac{1}{2}(I_1 - 3) + \frac{1}{20\lambda^2}(I_1^2 - 9) + \frac{11}{1050\lambda^4}(I_1^3 - 27) + \frac{19}{7000\lambda^6}(I_1^4 - 81) \\
&\quad + \frac{519}{673750\lambda^8}(I_1^5 - 243) + ...) + \frac{1}{D}(\frac{J_{el}^2 - 1}{2} - lnJ_{el})
\end{aligned}
\tag{5.1}
$$

where $\lambda$, $\mu$ and $D$ are the three material (fit) parameters in the potential, which are calculated by the program, once the stress-strain data are given as input. $I_1$ is the first deviatoric strain invariant, while $J^{el}$ is the elastic volume ratio. The nonlinear model also takes into account geometric nonlinearities at high strain. Figure 5.6 shows that the deformation obtained from the nonlinear model at $\phi = 0$ is 1.75 percent lower than that from the linear model.

However, the nonlinear model and the potential considered may not be realistic for a cell model. Also, the potential used is perturbative - the modulus extracted from it at small strains is the same as the linear modulus, while at higher strains, there are positive higher order corrections to the modulus. At high strains, though, if the brownian fluctuations of the network are overcome and the filaments straightened, the network becomes extremely rigid (like stiff rods). Due to these limitations, the nonlinear model proposed here mainly gives an idea of how such a model might be created and solved using numerical FEM techniques.
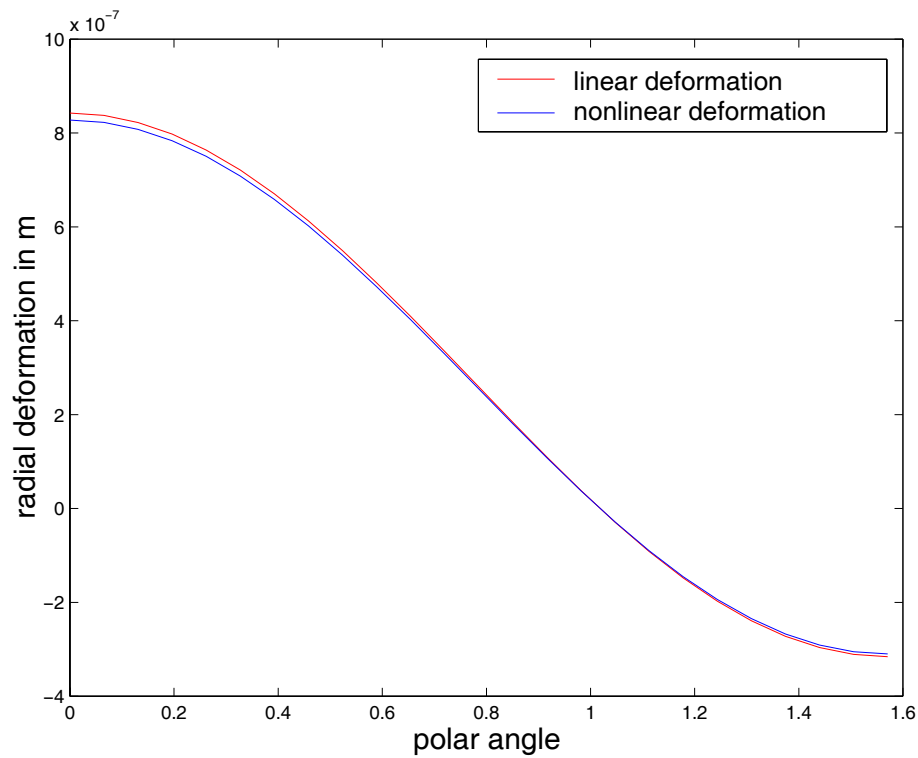
Figure 5.6: Preliminary results from a nonlinear thick (actin) shell model (Arruda Boyce potential) for a cell in the stretcher - Radial deformation versus polar angle of a thick shell of Young's Modulus 500 Pa, Poisson's ratio 0.45 and shell thickness 20%, subjected to a stress of $\sigma = 10\ cos^2\phi$. The deformation at $\phi = 0$ is 1.75 percent lower than that from the linear model

## 5.3 Extraction of Structural Parameters from the Stretcher Experiment Using Viscoelastic Models

### 5.3.1 Extraction of Viscoelastic Parameters without Incorporating Cell Geometry

The previous chapters and sections have discussed the deformation and other predictions of our cell models, based on our knowledge of the structural prop-

erties of the cytoskeletal polymer networks, with an emphasis on actin. This section analyzes the viscoelastic experimental data from the optical stretcher experiment [169], [221], to extract structural parameters using the models developed by us and to gain an understanding of the behavior of the *in vivo* cytoskeletal polymer networks. Normal NIH-3T3 and BALB-3T3 fibroblasts as well as cancerous SV-T2 fibroblasts (fifty cells of each type) have been deformed for approximately one second in the stretcher with 1.7 Watts in each laser beam. The peak stress on the cell depends on the laser power as well as other factors and experimental conditions such as the cell size and the distance between the fiber ends. However, an average estimate of the peak stress on the cell for the laser power used is 10-13 Pa.

As the first step to understanding the data and the difference in the structural response of the three cell types, the average maximum deformation (of the fifty cells) of each cell type is plotted (Figure 5.7). Figure 5.7 shows that the cancerous SV-T2 fibroblasts have a higher average deformation than the normal NIH-3T3 and BALB-3T3 fibroblasts. To extract structural parameters from the data for a preliminary estimate of cell strength, the cell is modeled as a homogeneous elastic sphere - the model yields the following mean shear moduli for the normal and cancerous cells: $G = 36\pm10$ Pa for the NIH fibroblasts, $G = 33\pm19$ Pa for the BALB fibroblasts and $G = 18\pm4.5$ Pa for the SV-T2 fibroblasts. However, more data are required to reduce the error or variability in measurement and help clearly differentiate the normal and cancerous cell types. Hence, presently, work is underway to automate the stretcher experiment, to acquire a large amount of data in a short period of time.

The structural analysis above with the homogeneous sphere model assumes an elastic behavior of the cells, while the observed behavior of the cells to the applied step stress is viscoelastic. The cells show a sharp increase in deformation
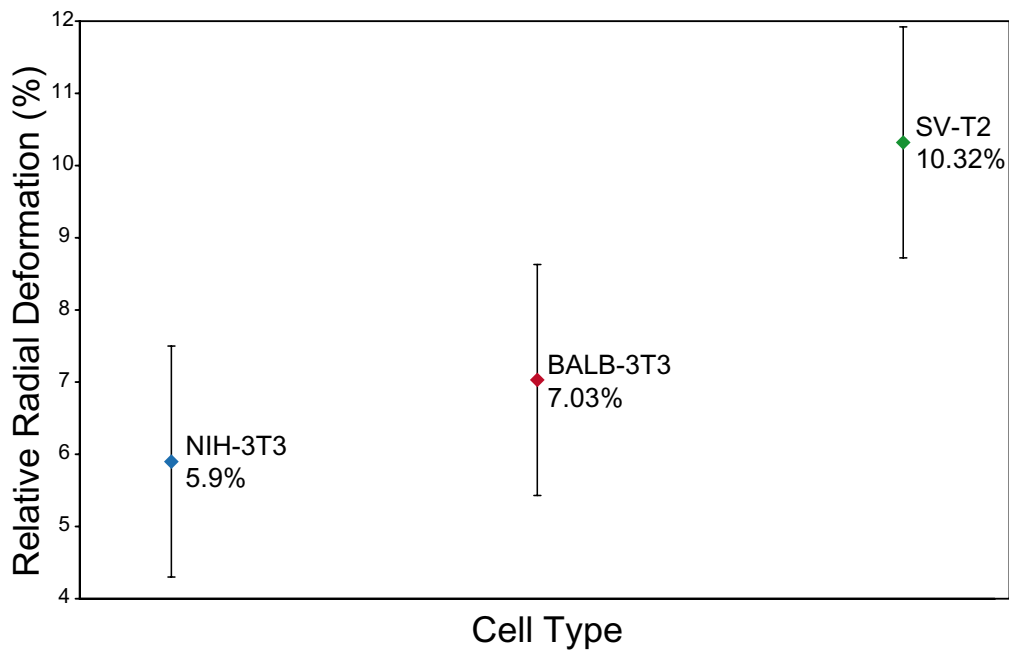
Figure 5.7: The average deformation of NIH, BALB and SV-T2 fibroblasts deformed in the stretcher [221], [169]. The average deformation of the SV-T2 cancerous cells is higher than that of the normal NIH and BALB cells

along the laser axis due to the applied stress, for approximately 0.2 seconds after the laser is switched on and then display a slower increase or viscous behavior for the remaining time that the laser is on. Deformation data are also taken along the laser axis for one second or more after the laser is switched off, to study the relaxation behavior of the cell. Such viscoelastic data are commonly analyzed using a mechanical model, which is a combination of springs and dashpots. Different mechanical models can be tried, in order to fit the data; a Voigt model (model with a spring and dashpot in parallel) with a dashpot in series (Figure 5.8) is the simplest model found to fit the observed viscoelastic behavior. The additional dashpot is used since the cell does not relax fully even after several seconds, when the laser is off. Figures 5.9 and 5.10 show the model's fit (line) to the experimental data (dots)

of a representative normal cell and a cancerous cell. The exact mathematical form of the model equations used to fit our cell deformation data and extract elastic and viscous parameters is as follows.

$$\frac{\Delta r(t)}{r} = \frac{\sigma_0}{E}(1 - e^{-(t-t_0)E/\eta_1}) + \frac{\sigma_0 (t - t_0)}{\eta_2} \ \ for \ \ t_0 < t < t_1 \qquad (5.2)$$

$$\frac{\Delta r_1(t)}{r_1} = \frac{\sigma_0}{E}(1 - e^{-(t_1-t_0)E/\eta_1})e^{-(t-t_1)E/\eta_1} + \frac{\sigma_0 (t_1 - t_0)}{\eta_2} \ \ for \ \ t > t_1 \qquad (5.3)$$

where $\frac{\Delta r(t)}{r}$ is the relative deformation, $E$ is the elasticity of the spring, $\eta_1$ and $\eta_2$ the viscosities of the two dashpots, $t_0$ is the time the laser is switched on ($t_0 = 0$ in our experiment) and $t_1$ is the time the laser is switched off.

Our evaluation of the stretcher data using macroscopic mechanical models, such as the modified Voigt model, is now explained in detail. A total of three elastic constants and two viscous constants are extracted from the data, to describe the deformation and relaxation behavior of the fibroblast cells. As mentioned earlier, the cells show an elastic behavior for the first 0.2 seconds of stretch. This elasticity arises, most likely, from the fact that the actin filaments in the cortex are crosslinked on this time scale, and this allows the network to behave like an elastic, permanently crosslinked gel - the binding time of known actin crosslinkers, such as $\alpha$-actinin, ABP/filamin and the Arp 2/3 complex, is $\geq$0.2 seconds. So, a spring of elasticity $E_{elastic}$ is used by us to model the cell's behavior in the first 0.2 seconds. Beyond this time scale, the transient nature of the crosslinks comes into play; as the crosslinkers begin to unbind from the actin filaments, the cell starts to display a viscous behavior. This viscoelastic deformation or creep is seen in Figures 5.9

94
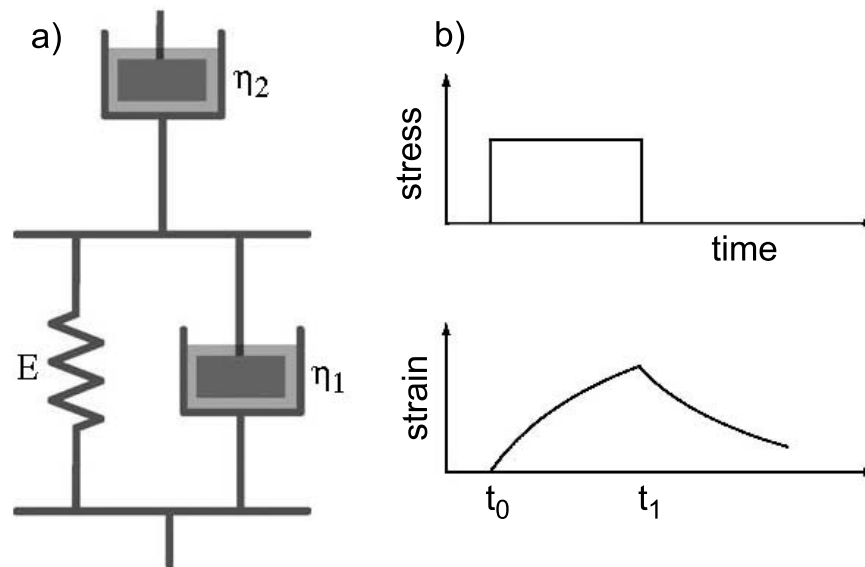
Figure 5.8: a) Mechanical model - Voigt element with a dashpot in series - used to fit the viscoelastic data from the stretcher experiment b) The structural response curve (strain) of this model for a step stress. The strain does not decay to zero even at longer times due to the response of the dashpot

and 5.10 and is fit with Equation 5.2 of the modified Voigt model (red line). The modulus of the spring, $E_0$, obtained from the fit is close to $E_{elastic}$, because a stress applied to the model first extends the spring, and then acts on the dashpots. In addition to $E_0$, the fit yields the viscosities $\eta_0$ and $\eta_1$ of the dashpots. The relaxation behavior of the cell after the laser is switched off can be seen in Figures 5.9 and 5.10 and can also be modeled using the modified Voigt model (Equation 5.3). However, it is found that Equation 5.3 fits the relaxation phase of the behavior, only if the elasticity of the spring in the model is changed from $E_0$ to $E_1$ (the dashpot values are still held at $\eta_0$ and $\eta_1$). A possible explanation for the change in elasticity after the deformation is the effect of the deformation itself on the structural state of the cell. The values of $E_{elastic}$, $E_0$ and $E_1$ and also $\eta_0$ and $\eta_1$ for the three cell types (NIH, BALB and SV-T2 fibroblasts) obtained with the models are summarized in
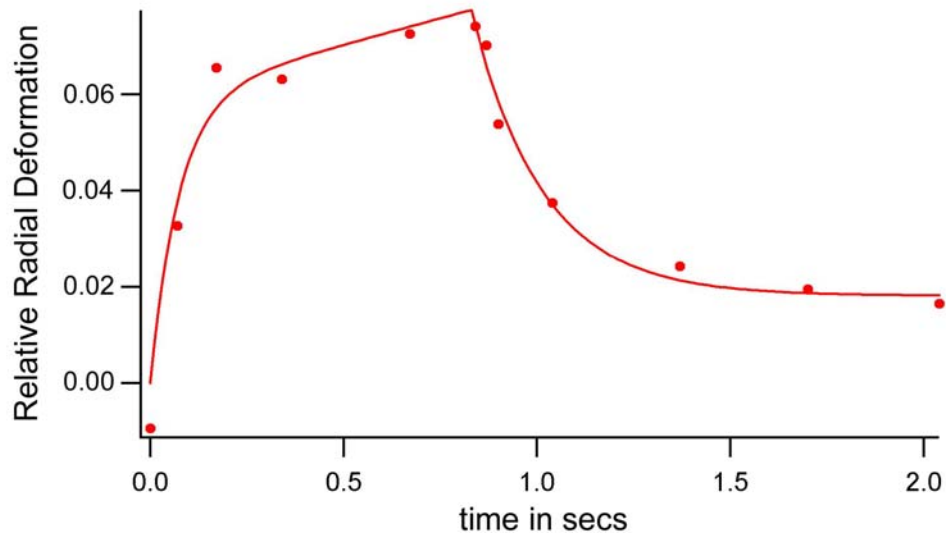
Figure 5.9: Experimental data points and fit using the voigt model with a dashpot in series for a representative NIH fibroblast being deformed in the stretcher

the tables below.

| Cell Type | $E_{elastic}$ Pa | $E_0$ Pa | $E_1$ Pa |
|-----------|------------------|----------|----------|
| NIH | $414.89 \pm 39.5$ | $421.12 \pm 35.18$ | $43.3 \pm 7.34$ |
| BALB | $366.16 \pm 47.14$ | $333.48 \pm 38.32$ | $37.01 \pm 8.55$ |
| SV-T2 | $228.6 \pm 17.87$ | $216.13 \pm 19.99$ | $13.24 \pm 5.47$ |

| Cell Type | $\eta_0$ Pa.s | $\eta_1$ Pa.s |
|-----------|---------------|---------------|
| NIH | $31.6 \pm 4.86$ | $1645.75 \pm 337.22$ |
| BALB | $33.67 \pm 6.08$ | $1734.98 \pm 411.78$ |
| SV-T2 | $15.89 \pm 1.39$ | $971.73 \pm 134.59$ |

The above numerical values for elasticity (of fibroblasts), extracted from the mechanical model, are now understood from the polymer physics or molecular

96
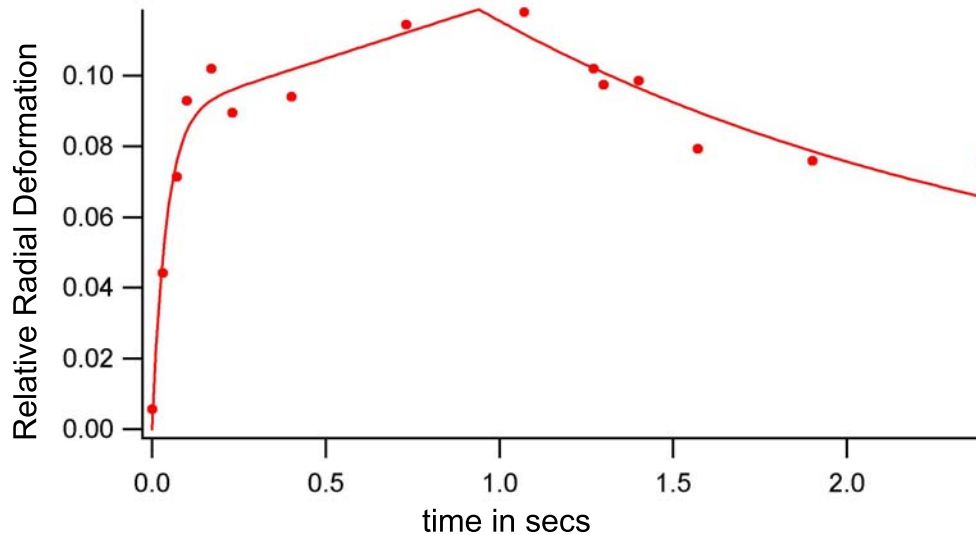
Figure 5.10: Experimental data points and fit using the voigt model with a dashpot in series for a representative SV-T2 fibroblast being deformed in the stretcher

properties of the cytoskeleton - specifically the actin cytoskeleton, with the partially (transiently) crosslinked actin network model developed in Chapter 4. The network model is employed to find a realistic parameter set of actin and crosslinker concentrations and cortex (shell) thickness that can explain the stretcher data. In conjunction with an assumed actin concentration that is physiologically relevant (between 8.4 and 11.3 mg/ml for fibroblasts - see Table 1.1) and a given elasticity, the model yields an estimate for the actin crosslinker concentration *in vivo*. An actin concentration of 10 mg/ml is postulated for the NIH cells, since the elasticity, $E_0$, extracted from the stretcher data is the highest for this cell type, while a concentration of 9.5 mg/ml is assumed for the BALB fibroblasts (since their elasticity is slightly lower than that of the NIH cells). Finally, an actin concentration of 9 mg/ml is used for the SV-T2 cells, which show the lowest elasticity. A corresponding actin crosslinker concentration is, then, calculated for each cell type, from the partially

crosslinked network model, and the values obtained for crosslinker concentration are found to be physiologically relevant. Also, if both NIH and BALB cells are inferred to have a cortex thickness of ∼20 %, from fluorescence images of these cells taken in our group, then the shell (cortex) thickness of SV-T2 cells is computed by considering the total actin content in cancerous fibroblasts to be ∼35% lower than in their normal counterparts. So, if the presumed actin concentration of 9 mg/ml in the SV-T2 cells is integrated over the shell, the shell thickness of 13% obtained for these cells is smaller that that of the normal fibroblasts. By obtaining a realistic parameter set that explains the data, our analysis suggests that the transient crosslinking of actin networks controls the deformation response of cells. The table below summarizes the parameter set obtained from our analysis.

|  | NIH | BALB | SV-T2 |
|---|---|---|---|
| $\rho_{actin}$ | 10 mg/ml | 9.5 mg/ml | 9 mg/ml |
| $\rho_{CL}$ corresponding to $E_0$ | 10.01 $\mu$M | 9.75 $\mu$M | 8.7 $\mu$M |
| $\rho_{CL}$ corresponding to $E_1$ | 3.62 $\mu$M | 3.66 $\mu$M | 2.49 $\mu$M |
| Shell thickness | 20% | 20% | 13% |

### 5.3.2   Extraction of Viscoelastic Parameters Incorporating Cell Geometry

The material constants extracted from the stretcher data with mechanical models do not consider the geometry of the cell. Although this study does not present final values for these structural parameters, that incorporate cell geometry, it proposes a method to approach the problem. Our analysis here assumes, for simplicity, that the modified Voigt model can be used to fit the stretcher data with the same value for the elasticity of the spring, $E$, in the deformation and

98

relaxation phases. In this case, only three material constants are required to describe the data, namely, $E$, $\eta_0$ and $\eta_1$. An equation for the relaxational modulus $G(t)$ can, then, be obtained, by inverting the strain or deformation equation (Equation 5.2), to relate the stress of the model to an applied unit step strain (since $L[G(t)]L[J(t)] = \frac{1}{2(1+\nu)\ s^2}$, where $L$ is the Laplace Transform, $J(t)$ is the time dependent creep or unit strain and $\nu$, the Poisson's ratio of the material [105]). For our model, the relaxational modulus calculated is the following.

$$G(t) = \frac{E\ e^{\frac{-t\ E}{\eta_1+\eta_2}}}{2(1+\nu)(1+\frac{\eta_1}{\eta_2})^2} + \frac{\eta_1\ \delta(t)}{2(1+\nu)(1+\frac{\eta_1}{\eta_2})}. \tag{5.4}$$

Since our study uses the modified Voigt element to model the cytoskeleton, Equation 5.4 for $G(t)$ provides insight into the material property or relaxational modulus of the *in vivo* cytoskeletal polymer network. However, to incorporate the spherical geometry of the cell, the structural response of one of our cell models, such as the thick shell model, the three-layered sphere model or the FEM model, needs to be considered. If the thick shell model is considered (for simplicity), its geometric effect along the laser axis (geometric factor $F_G$) can be obtained from Figure 3.3. Figure 3.3 shows that the geometric factor $F_G$ (along the laser axis) for a given stress profile depends on the shell thickness and Poisson's ratio (for a homogeneous sphere, $F_G \sim 0.58$ along the laser axis for a $cos^2\phi$ stress and a Poisson's ratio of 0.45). From our knowledge of the linear elastic-viscoelastic correspondence principle (Appendix C.3), a material property function (equation for $G(t)$) that incorporates both viscoelasticity and geometry is then equal to the expression derived for $G(t)$ from the mechanical model (Equation 5.4) multiplied by the geometric factor $F_G$, or mathematically, it is

$$G(t) = \frac{F_G \; E \; e^{\frac{-t \; E}{\eta_1 + \eta_2}}}{2(1 + \nu)(1 + \frac{\eta_1}{\eta_2})^2} + \frac{F_G \; \eta_1 \; \delta(t)}{2(1 + \nu)(1 + \frac{\eta_1}{\eta_2})}. \tag{5.5}$$

The above calculation shows that, if a structural response function for the material or data can be determined, then the effect of material geometry can be incorporated by multiplying each viscoelastic parameter extracted ($E$, $\eta_1$ and $\eta_2$) by the geometric factor $F_G$. It is difficult to deduce such an equation for the stretcher data, since the elasticity of the spring $E$ in the modified Voigt model is found to change on cell deformation; so, no further analysis of the data has been carried out to relate the observed deformation to the molecular properties of the actin cytoskeleton (such as actin and crosslinker concentrations, cortex thickness), by including cell geometry. However, the above example illustrates how a mathematical function that incorporates viscoelasticity and geometry can be derived and used to differentiate the structural response of the normal and cancerous cells. For example, the geometric factor of the cancer cells is different than that of the normal cells, if they have a thinner cortex (shell) or are smaller in size. Also, Figures 5.9 and 5.10 indicate that the viscoelastic response itself (model fit) of the normal and cancer cells is different. Hence, it is possible to use the viscoelastic response alone or the combined material property behavior (linear viscoelasticity and geometry) as a signature to distinguish these cell types. However, if the cancer cells deform beyond the linear regime (say >10 percent), a nonlinear equation for their structural response will have to be developed and used. The difference between the nonlinear response equation for the cancer cells and the linear equation for the normal cells (whose smaller deformations are more likely to be in the linear regime) may clearly separate the two cell types.

## 5.4 Results and Discussions

Our three-layered continuum model for a cell shows that the boundary conditions used in the analysis are important in determining the deformation. If mixed boundary conditions are used at the actin-microtubule interface in the three-layered model, the value obtained for the radial deformation is not much lower than the value obtained with a thick shell model for the actin cortex alone. The deformation results of our thick shell FEM model show a low percent error, when compared with the analytical thick shell results (Table 5.1). This model has been tested for various stress distributions on the shell, mesh discretizations and number of layers and hence can be used as a basis for creating more complex FEM models. Our whole cell FEM model incorporates observed cytoskeletal architecture such as the rod-like microtubules and a displaced nucleus. This numerical model shows quantitatively (Figures 5.4, 5.5) how the addition of microtubules results in a stiffening behavior or a smaller observed deformation, but no analytical result or scaling law for how the stiffening of the structure depends on the number of rods (microtubules) in the model has been established here. However, for a fixed number of microtubules, an estimate can be obtained of the contribution of microtubules to cell strength, which shows that their contribution diminishes as the cortex strength or modulus increases. In our model, the nucleus can be placed asymmetrically about the origin and this is found to have an insignificant effect on the structural response. Our analytical and numerical models show that only a much higher peak stress $\sigma_0$ than 1 $N/m^2$ on a normal cell results in a deformation that can be easily detected or measured. In the case of the optical stretcher experiment, this implies the use of higher laser powers (greater than 1.5 Watts in each beam) while stretching fibroblasts and other eukaryotic cells.

Our experiments in the stretcher on deforming normal and cancerous fibroblasts by applying a step stress with 1.7 Watts in each laser beam shed light on the viscoelastic behavior of cells. To enable a quantitative understanding of the observed structural response, our study extracts elastic and viscous material constants from the stretcher data, using a mechanical model. With the help of such viscoelastic parameters, our work is beginning to shed light on the molecular properties of the *in vivo* cytoskeletal polymer network of these different cell types; it suggests that the transient crosslinking of actin can help explain the dynamic behavior observed in the stretcher data and is a sensitive parameter controlling the strength of cells. Our preliminary results also indicate that these material constants can be used to differentiate normal and cancerous cells.

## 5.5    Summary

By combining both analytical and numerical techniques, it has been possible for us to create a variety of models for a eukaryotic cell that take into account both its geometry (spherical shape) and architecture (rod-like microtubules and nucleus). Using these models, the effect of different cellular features has been studied - these range from a first order model for the interaction between the cytoskeletal polymers incorporated in our continuum model to the asymmetry of the nucleus studied with our FEM model. A study of these effects, in conjunction with our study of the cytoskeletal polymers, enables us to create a comprehensive structural model of a cell and to begin relating the structural properties of the individual *in vivo* polymer assemblies and their interactions to the macroscopic deformation of the whole cell. So, the model has then been used to predict or quantify the observed deformation of a cell in the optical stretcher subjected to an arbitrary, rotationally symmetric stress.

From the experimental side, it has also been possible to extract and analyze structural parameters from the optical stretcher data on normal and cancerous fibroblasts. These viscoelastic parameters, which reflect the state of the cytoskeleton, may be the key to distinguishing cell types, such as normal and cancerous cells, at an early stage.

Table 5.1: Results from the Numerical Thick Shell FEM Model

Discretization of the thick shell mesh

| Thickness of shell = 20 % | | Thickness of shell = 10 % | |
| Young's modulus of shell = 500 Pa | | Young's modulus of shell = 3000 Pa | |

Uniform  Stress

| Mesh | No of layers in thick shell | Deformation nms $\phi$=90 | Error % | Deformation nms $\phi$=0 | Error % | Deformation nms $\phi$=90 | Error % | Deformation nms $\phi$=0 | Error % |
|---|---|---|---|---|---|---|---|---|---|
| 4 by 4 | 5 | 19.272 | -0.2020 | 19.257 | -0.2796 | 7.7380 | 0.0918 | 7.7340 | 0.0401 |
| | 10 | 19.261 | -0.2589 | 19.247 | -0.3314 | 7.7370 | 0.0789 | 7.7334 | 0.0323 |
| | 15 | 19.258 | -0.2745 | 19.245 | -0.3418 | 7.7367 | 0.0750 | 7.7333 | 0.0310 |
| | 20 | 19.257 | -0.2796 | 19.245 | -0.3418 | 7.7364 | 0.0711 | 7.7333 | 0.0310 |
| 6 by 6 | 5 | 19.289 | -0.1139 | 19.286 | -0.1295 | 7.7294 | -0.0194 | 7.7282 | -0.0349 |
| | 10 | 19.280 | -0.1605 | 19.275 | -0.1864 | 7.7286 | -0.0298 | 7.7274 | -0.0453 |
| | 15 | 19.277 | -0.1761 | 19.272 | -0.2020 | 7.7284 | -0.0323 | 7.7273 | -0.0466 |
| | 20 | 19.275 | -0.1864 | 19.271 | -0.2071 | 7.7283 | -0.0336 | 7.7273 | -0.0466 |
| 8 by 8 | 5 | 19.301 | -0.0518 | 19.301 | -0.0518 | 7.7294 | -0.0194 | 7.7289 | -0.0259 |
| | 10 | 19.295 | -0.0829 | 19.293 | -0.0932 | 7.7286 | -0.0298 | 7.7280 | -0.0375 |
| | 15 | 19.292 | -0.0984 | 19.290 | -0.1087 | 7.7283 | -0.0336 | 7.7278 | -0.0401 |
| | 20 | 19.290 | -0.1087 | 19.288 | -0.1191 | 7.7282 | -0.0349 | 7.7276 | -0.0427 |
| 10 by 10 | 5 | 19.307 | -0.0207 | 19.306 | -0.0259 | 7.7299 | -0.0129 | 7.7298 | -0.0142 |
| | 10 | 19.303 | -0.0414 | 19.302 | -0.0466 | 7.7293 | -0.0207 | 7.7290 | -0.0246 |
| | 15 | 19.300 | -0.0570 | 19.299 | -0.0621 | 7.7290 | -0.0246 | 7.7287 | -0.0285 |
| | 20 | 19.299 | -0.0621 | 19.297 | -0.0725 | 7.7289 | -0.0259 | 7.7286 | -0.0298 |
| 12 by 12 | 5 | 19.309 | -0.0104 | 19.309 | -0.0104 | 7.7303 | -0.0078 | 7.7303 | -0.0078 |
| | 10 | 19.307 | -0.0207 | 19.306 | -0.0259 | 7.7299 | -0.0129 | 7.7297 | -0.0155 |
| | 15 | 19.305 | -0.0311 | 19.304 | -0.0362 | 7.7296 | -0.0168 | 7.7294 | -0.0194 |
| | 20 | 19.304 | -0.0362 | 19.303 | -0.0414 | 7.7295 | -0.0181 | 7.7293 | -0.0207 |
| Analytical Result | | 19.311 | | 19.311 | | 7.7309 | | 7.7309 | |

Thickness of shell = 20 %
Young's modulus of shell = 500 Pa

Thickness of shell = 10 %
Young's modulus of shell = 3000 Pa

$\cos^2\phi$ stress

| Mesh | No of layers in thick shell | Deformation nms $\phi=0$ | Error % | Deformation nms $\phi=90$ | Error % | Deformation nms $\phi=0$ | Error % | Deformation nms $\phi=90$ | Error % |
|---|---|---|---|---|---|---|---|---|---|
| 4 by 4 | 5 | 82.967 | 0.0434 | -31.862 | 0.1666 | 31.143 | 0.0900 | -11.711 | 0.1625 |
| | 10 | 83.005 | 0.0892 | -31.887 | 0.2452 | 31.151 | 0.1157 | -11.716 | 0.2053 |
| | 15 | 83.026 | 0.1146 | -31.899 | 0.2829 | 31.154 | 0.1253 | -11.717 | 0.2138 |
| | 20 | 83.037 | 0.1278 | -31.905 | 0.3018 | 31.156 | 0.1318 | -11.717 | 0.2138 |
| 6 by 6 | 5 | 82.901 | -0.0362 | -31.810 | 0.0031 | 31.116 | 0.0032 | -11.696 | 0.0342 |
| | 10 | 82.900 | -0.0374 | -31.815 | 0.0189 | 31.118 | 0.0096 | -11.697 | 0.0428 |
| | 15 | 82.904 | -0.0326 | -31.818 | 0.0283 | 31.119 | 0.0129 | -11.698 | 0.0513 |
| | 20 | 82.907 | -0.0289 | -31.821 | 0.0377 | 31.120 | 0.0161 | -11.698 | 0.0513 |
| 8 by 8 | 5 | 82.909 | -0.0265 | -31.805 | -0.0126 | 31.112 | -0.0096 | -11.692 | 0.0000 |
| | 10 | 82.903 | -0.0338 | -31.806 | -0.0094 | 31.112 | -0.0096 | -11.693 | 0.0086 |
| | 15 | 82.902 | -0.0350 | -31.807 | -0.0063 | 31.113 | -0.0064 | -11.693 | 0.0086 |
| | 20 | 82.902 | -0.0350 | -31.808 | -0.0031 | 31.113 | -0.0064 | -11.693 | 0.0086 |
| 10 by 10 | 5 | 82.918 | -0.0157 | -31.806 | -0.0094 | 31.113 | -0.0064 | -11.692 | 0.0000 |
| | 10 | 82.913 | -0.0217 | -31.806 | -0.0094 | 31.112 | -0.0096 | -11.692 | 0.0000 |
| | 15 | 82.910 | -0.0253 | -31.806 | -0.0094 | 31.112 | -0.0096 | -11.692 | 0.0000 |
| | 20 | 82.909 | -0.0265 | -31.806 | -0.0094 | 31.112 | -0.0096 | -11.692 | 0.0000 |
| 12 by 12 | 5 | 82.923 | -0.0096 | -31.807 | -0.0063 | 31.113 | -0.0064 | -11.692 | 0.0000 |
| | 10 | 82.919 | -0.0145 | -31.807 | -0.0063 | 31.113 | -0.0064 | -11.692 | 0.0000 |
| | 15 | 82.917 | -0.0169 | -31.806 | -0.0094 | 31.113 | -0.0064 | -11.692 | 0.0000 |
| | 20 | 82.916 | -0.0181 | -31.806 | -0.0094 | 31.113 | -0.0064 | -11.692 | 0.0000 |
| Analytical Result | | 82.931 | | -31.809 | | 31.115 | | -11.692 | |

'Effective Cell'

From the error analysis above, a 8 by 8 mesh with 5 layers for a thick shell seems
a reasonable model.
To take into account the effect of the rods and nucleus, the thick shell of 20% would have to have
 an effective Young's modulus of 625 Pa (25% change), while the thick shell of 10% percent
would have to have an effective modulus of 3300 Pa (10% change)

105

# Chapter 6

# Conclusions and Future Work

In this thesis, a detailed structural model of a eukaryotic cell has been created, by incorporating the molecular properties as well as the architecture of the cytoskeletal polymers, namely the actin cortex and the microtubules. Our modeling work starts with creating a thick shell continuum model for a cell in which the actin cortex predominates and goes on to more complex models (numerical finite element models) that incorporate the rod-like microtubules and the nucleus. These models have been used to study the individual contribution of the polymer assemblies to the entire structural response of the cell and to obtain the deformation of the model cell to an arbitrary rotationally symmetric surface stress, as in our cell deformation experiment - the optical stretcher.

Our model cell allows us to extract structural parameters for different cells such as normal and cancer cells and show theoretically that the strength obtained depends sensitively on cytoskeletal polymer properties such as actin concentration and cortex thickness - hence, the structural response of cancer cells versus normal cells is a good parameter to distinguish them. Experimental evidence from the stretcher and other experiments indicates that the structural response of normal and cancerous cells differs considerably, due to the altered cytoskeleton of cancer cells. This observation has been quantified in our study by extracting elastic and viscous parameters from the optical stretcher data on normal and cancerous fibrob-

lasts. Our preliminary analysis of these viscoelastic parameters in various time regimes shows that they can be used to differentiate normal and cancer cells. An attempt is then made to relate the structural constants extracted to the molecular properties of the actin cytoskeleton of these two cell types - specifically the actin and crosslinker concentrations and the cortex thickness. Our results suggest that the transient crosslinking of actin can help explain the dynamic (viscoelastic) behavior seen in the stretcher data and is a sensitive parameter controlling the strength of cells. With such a mathematical approach, the structural properties of the *in vivo* polymer assemblies and their individual contribution to the structural response of a cell are just beginning to be understood from the data.

Our study of the cytoskeletal polymers suggests that the actin cortex can account for the structural properties of the cell, only under tight localization of the actin in the cell and its crosslinking proteins. The shear modulus of cells is much higher than our estimate for the modulus of a fully crosslinked actin network of cellular concentration, distributed homogeneously through the cell. However, when all the *in vivo* actin in acanthamoeba (assuming homogeneous filaments one micron long) is in a cortex of 13 percent thickness and the crosslinking protein in a shell of 5 percent thickness, the cortex has a modulus of $\sim 1000$ Pa, close to the shear modulus of fibroblasts. The addition of the rod-like microtubules to our FEM model results in a stiffening of the cell structure. However, the addition of microtubules alone may not be enough to account for the versatile structural properties of cells. The intermediate filament network has not been studied in this thesis.

Hence, possible future directions to this work, include a structural study of intermediate filaments and its subsequent incorporation into our model. Another important step is an experimental as well as a theoretical study (through polymer

107

physics, and not simple boundary conditions) of the structural contribution of cytoskeletal interactions. There is sufficient experimental evidence [176] for the interaction of actin filaments and microtubules via MAPS (microtubule associated proteins) and other proteins and hence the actin-microtubule interaction could be a starting point for the study. First, an *in vitro* rheology experiment could be performed to obtain the strength of a mixture of actin and microtubules. The value obtained could be compared to the strength of an actin or microtubule network alone from rheology, to estimate the effect of interaction. In order to study the actin-microtubule interaction theoretically, a form of the interaction potential is required - either experimentally or otherwise. It is then possible to calculate stress, strain, and modulus from the potential and hence its effect on the structural strength. The next step would be to study the interaction *in vivo*, but this seems a huge challenge. The other interactions (actin-intermediate filaments, microtubule-intermediate filaments) could also be studied similarly. A different interaction not captured in our model is that between polymer filaments and active motor proteins - for example between actin filaments and myosin motors. The influence of these motor proteins on the structural response of the cell could be investigated in further models.

Further modifications and improvements can be made to our model too, although our thick shell analytical model and finite element models are quite versatile and accurate. The thickness of the shell in our hollow, 3D thick shell model can be varied. So, it can be used to model a red blood cell with a thin 2D cytoskeleton as well as a fibroblast and other eukaryotic cells with a much more extensive 3D cytoskeleton. When the shell is very thin, the deformation of the shell model is exactly that of a thin shell or membrane, and when it is very thick (inner radius almost zero), the deformation is the same as that of a solid sphere. Also, the deformation of our finite element thick shell model compares very accurately to that

of our analytical thick shell model. However, all these models are linear, elastic models and no detailed non linear model for a cell undergoing large deformation has been presented in this thesis. Such a model may be required for the stretcher experiment on cancer cells, since their average radial deformation is greater than that of normal cells. In addition, we have modeled the viscoelasticity of cells with a simple mechanical model. It is possible, though, to create a more sophisticated viscoelastic FEM model of a cell. The structural elements of the cell such as the actin cortex and the microtubules could be assigned viscoelastic properties and the interior of the cell could be filled with a viscoelastic medium.

An extension to modeling a spherical suspended cell is to model the mechanics of an attached cell (which has a non regular shape), including the effect of the actin stress fibers. As opposed to the isotropic actin cortex, the stress fibers are anisotropic, long, actin bundles. Modeling the mechanics of these anisotropic bundles is one step in a complex model for an attached cell. Our work on the structural response of single cells could also be extended to studying the structural response of two interacting cells. It could then be used as the basis for multicellular studies, to understand the mechanical properties of tissue. Another application of our cell model is in tumor growth and its dynamics. The damaging effect of a tumor arises when its hard elastic spherical interior pushes on the surrounding polymer network - the results of our single cell model could be valuable in creating a suitable tumor growth model. Hence, the extensions and applications of our cell model and studies on polymer networks to other problems in this new field of modeling complex biophysical phenomena are numerous, varied and exciting.

109

**Appendices**

110

# Appendix A

# Appendix for Red Blood Cells

## A.1 Extraction of Structural Parameters from Some Red Blood Cell Experiments

This appendix discusses how the models created to accompany different red blood cell deformation experiments are used to extract structural parameters.

### A.1.1 Micropipette Aspiration of Cells

There are cells which behave structurally like a solid, while others can be modeled as a liquid surrounded by an elastic cortical shell. For example, neutrophils and red blood cells are considered to be soft cells, while chondrocytes and endothelial cells are more rigid. Therefore, the model for a cell being aspirated into a micropipette, depends on the type of cell.

**Extraction of the cortical shear modulus $\mu$ and the cytoplasmic viscosity $\eta$ ($N/m^2$) for a Red Blood Cell**

A red blood cell is modeled as a Newtonian liquid of viscosity $\eta$ surrounded by an elastic shell or membrane, which is defined by a cortical shear modulus, $\mu$ (where $\mu = Gt$, where $G$ is the conventional shear modulus ($N/m^2$) and $t$ is the shell thickness ($m$)) and Poisson's ratio, $\nu$. In order to analyze the deformation

of a red blood cell aspirated in a pipette and extract structural parameters from experiment, a model of an infinite plane membrane being sucked into a cylindrical pipette is used (Figure A.1). The model also assumes that the deformation takes place at a constant surface area, which results in the following equation relating the aspiration pressure and the observed deformation [37], [22], [217].

$$\frac{\Delta P R_p}{\mu} = 2.45 \frac{L_p}{R_p},$$ (A.1)

where $\frac{L_p}{R_p} > 1$, $\Delta P$ is the negative pressure drop within the pipette, associated with aspiration, $L_p$ is the net axial extension into the pipette and $R_p$ is the radius of the pipette. Experimentally, a plot of $\Delta P$ versus $L_p$ yields $\mu$.
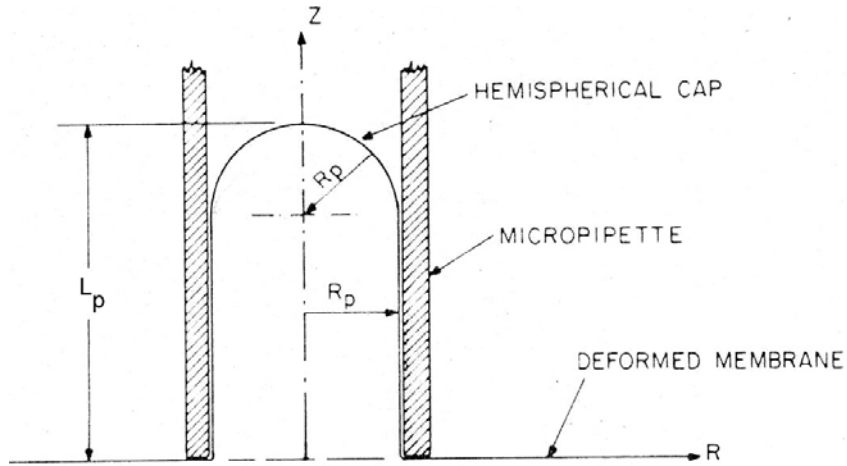


Figure A.1: A hemispherical cap model for an infinite plane membrane being sucked into a cylindrical pipette of radius $R_p$, taken from [22]. The problem is analyzed in terms of cylindrical coordinates

The viscosity, $\eta$ is given by

$$\eta = \frac{R_p \Delta P}{m(1 - R_p/R)\frac{dL_p}{dt}},$$   (A.2)

where $m$ is a constant obtained from theory ($\approx 6$ for red blood cells), $R$ is the initial radius of the cell and $\frac{dL_p}{dt}$ is the initial rate of cell extension into the pipette.

## A.1.2   Electric Field Deformation of Cells

The deforming force on a cell stretched by a high frequency electric field arises due to the polarization of the cell [97], [36]. The elongation of the cell is proportional to the square of the electric field, for small deformations. The shear modulus of a red blood cell is extracted using thin shell theory to calculate the deformation [36] of a sphere into an ellipse, under an axisymmetric stress (Figure A.2). The shear modulus is given by $\mu = 1.38A^2 [\frac{dU}{dq}]^2$, where $U$ is the applied voltage and $q$ is the ratio of the long axis to the short axis of the deformed ellipse. $A$ is given by $A^2 = 2.25\, \epsilon\, \epsilon_0\, r_s/s^2$, where $r_s$ is radius of the spherical cell, $\epsilon$ is the permittivity of the medium in which the cell is present and $s$ is a constant of the instrument, which can be calculated (s=1.1 in Engelhardt et. al.'s experiment). Therefore, by calculating the initial slope of the $U$ versus $q$ data plot and by calculating $A$, $\mu$ can be determined.

In order to calculate the viscosity, jump experiments are performed, which relate $q$ and $t$, from which the response time of the cellular deformation $\tau$ can be found. The viscosity $\eta$ is then given by $\mu\, \tau$.

113
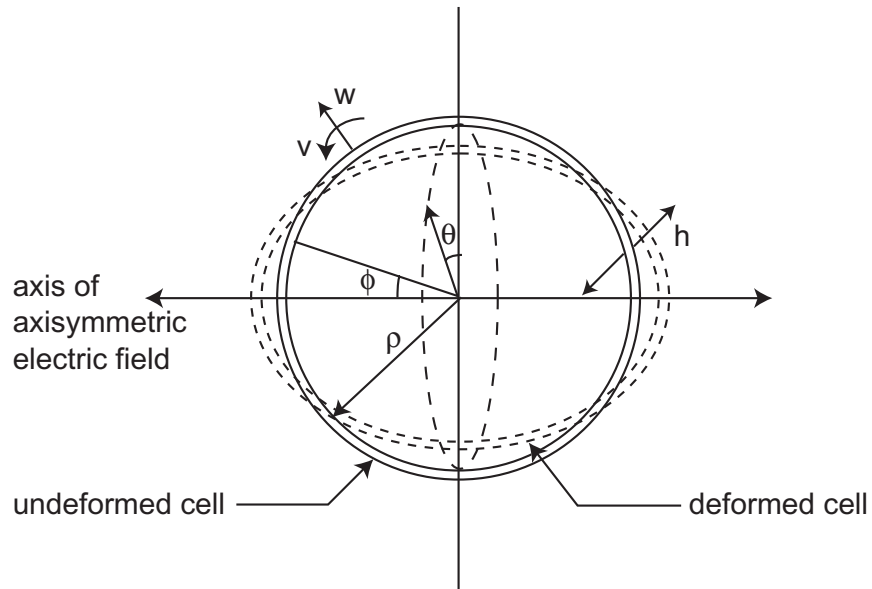
Figure A.2: Thin shell model for the deformation ($v$ and $w$ - meridional and radial deformations) of a red blood cell deforming in an axisymmetric electric field

### A.1.3 Optical Tweezer

Henon et al. [80] use an optical tweezer to deform swollen as well as discoid, unswollen red blood cells and extract structural parameters from their experiment with the following models.

An osmotically swollen red blood cell is modeled as a spherical thin shell (Figure A.3). In an optical tweezer, two silica beads, placed at the poles, are each pulled by a point force $F$; the deformation of a thin shell in the direction perpendicular to these point forces is given by

$$D = D_0 - \frac{F}{2\pi\mu}, \tag{A.3}$$

where $D$ is the equatorial diameter of the stretched cell, $D_0$, the original diameter, $F$, the applied force and $\mu$ is the shear modulus in $N/m$. The slope of the graph of the deformed cell diameter, $D$, versus the applied force, $F$, gives $\mu$.
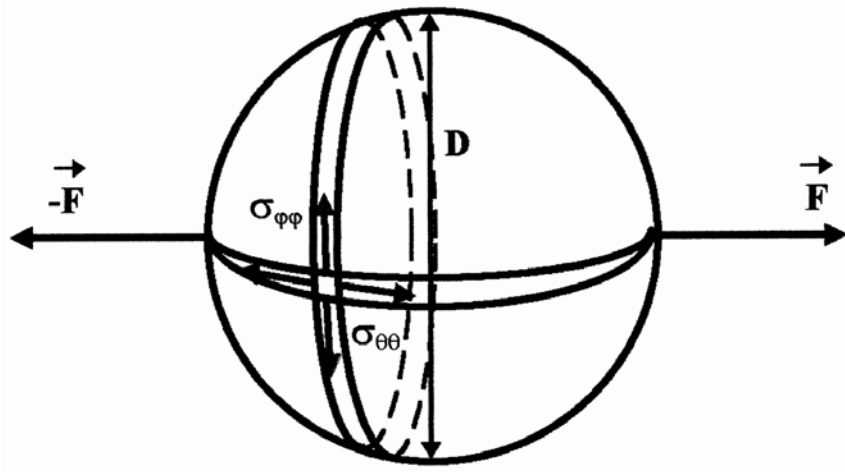


Figure A.3: Elastic thin shell model for an osmotically swollen, spherical red blood cell in a tweezer, deforming under diametrically-opposed loads at the poles, taken from [80]

A discotic, unswollen red blood cell of diameter $D_0$ is modeled by two parallel discs (Figure A.4). The deformation of the discs is calculated under the action of two opposing forces $F$ at two ends of the disc diameter. The deformation perpendicular to $F$ is given by

$$D = D_0 - \frac{F}{2\pi\mu}(1 + (1 - \frac{\pi}{2})\frac{\mu}{K}), \tag{A.4}$$

where $D$ is the stretched diameter, $D_0$, the original diameter, $F$ is the applied force, $\mu$ is the shear modulus in $N/m$ and $K$ is the area compressibility modulus. For a red blood cell, $\mu \ll K$, and so

$$D = D_0 - \frac{F}{2\pi\mu}. \tag{A.5}$$

The slope of the graph of deformed cell diameter, $D$, versus applied force, $F$, gives $\mu$.
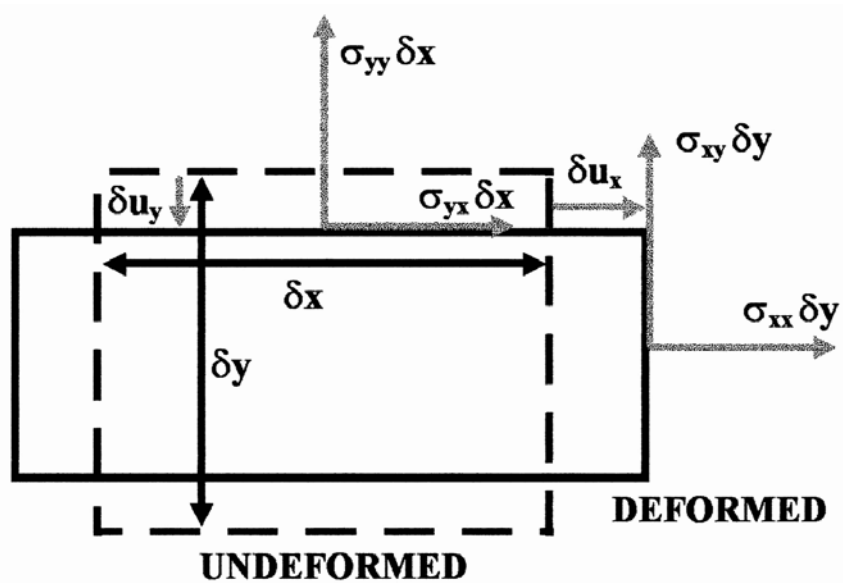


Figure A.4: Membrane model for an unswollen, discoid red blood cell deforming in a tweezer, taken from [80]. The membrane thickness is assumed to be constant and the problem is purely two dimensional

### A.1.4    Flicker Spectroscopy in Red Blood Cells

A measurement of the flicker phenomenon of red blood cells, measured at two points (correlation function), can be used to estimate the area compressibility modulus of a red blood cell [14], [189], [238]. The correlation function is characterized by a length scale $\lambda_w$, which is a function of frequency $w$ and can be obtained experimentally. In order to relate $\lambda_w$ to the curvature modulus $K$, Brochard et al. [14] model the red blood cell as two thin membranes separated by a distance $d$, which is filled with a Newtonian fluid of viscosity $\eta$ at velocity $v$ (Figure A.5). A detailed analysis of this model gives us the following relation

$$\lambda_w = (\frac{Kd^3}{24\eta w})^{1/6}.$$

(A.6)

Therefore, a knowledge of $d$, $\eta$ and $\lambda$ at a particular $w$ leads to a determination of $K$.
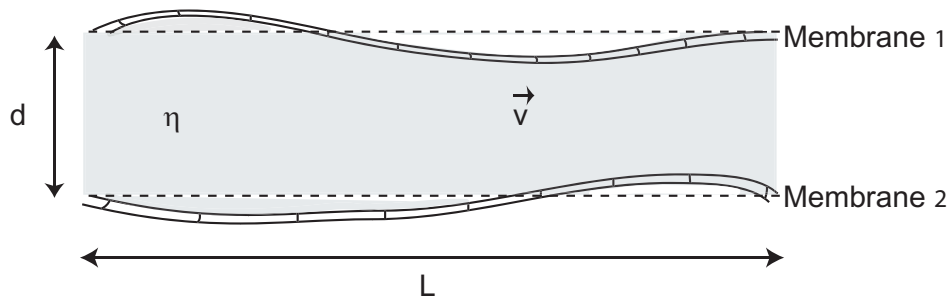


Figure A.5: Membrane model of a red blood cell to analyze its flicker phenomenon or thickness fluctuations

117

## A.2 Ray Optics Calculations to Determine the Surface Stress on a Cell in the Stretcher Set up
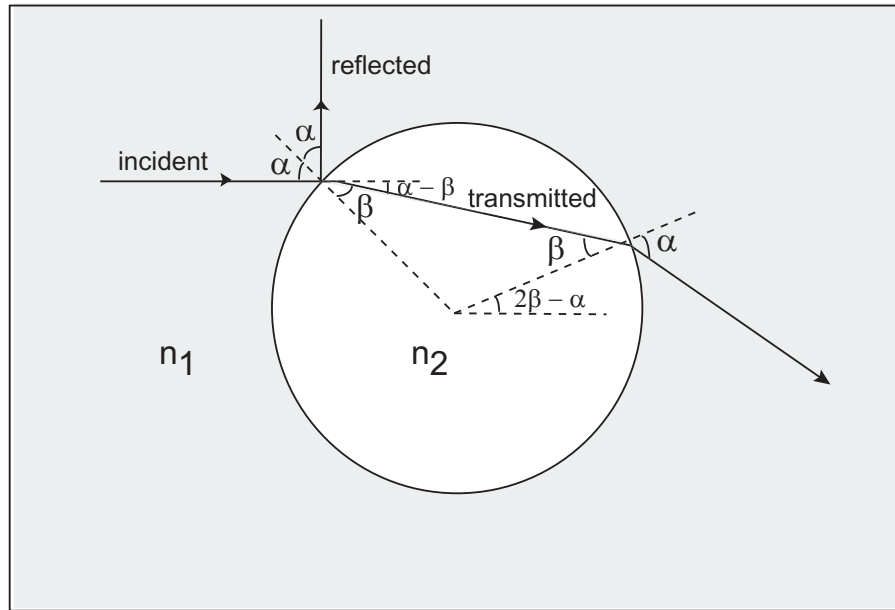


Figure A.6: Ray optics is used to calculate the surface stress on a cell in the stretcher. Shown here is the path of a beam from the laser, on the left side, hitting a cell at an angle $\alpha$

Since the cell size (microns) is much greater than the wavelength of light used in the experiment (785 nms), ray optics is used to explain the normal, outward, stretching force experienced by a cell placed between two counter propagating laser beams [68], [69]. The physics lies in the net outward momentum transfer that occurs when a beam of laser light both enters and leaves the cell. The initial momentum of the beam $p_i$ is $p_i = E/c$, where $E$ is its energy and $c$ is the velocity of light. If it hits the cell at an angle $\alpha$ (Figure A.6), it will be refracted according to Snell's law, $n_1 sin\alpha = n_2 sin\beta$, where $n_1$ is the refractive index of the medium

surrounding the cell, $n_2$ is the refractive index of the cell ($n = \frac{n_2}{n_1}$) and $\beta$ is the angle of the transmitted ray. The momentum of the initial ray changes in magnitude and direction, upon hitting the cell. Due to the conservation of momentum, the difference in momentum $\Delta p$ between the incident ray and the reflected and transmitted rays ($\Delta p = p_i + p_r - p_t$) is experienced by the cell as a surface force $F = \frac{\Delta p}{\Delta t}$.

The momentum $\Delta p$ transferred to the cell can be decomposed into a parallel and perpendicular (perp) component as follows:

$$
\begin{aligned}
\Delta p_{front}^{parallel} &= cos(0) - R\, cos(\pi - 2\alpha) - n\,(1 - R)\, cos(2\pi - \alpha + \beta) \\
&= 1 + R(\alpha)\, cos(2\alpha) - n\,(1 - R(\alpha))\, cos(\alpha - \beta) \\
&= \Delta p_{front}(\alpha)\, cos\phi
\end{aligned}
\tag{A.7}
$$

and

$$
\begin{aligned}
\Delta p_{front}^{perp} &= sin(0) - R\, sin(\pi - 2\alpha) - n\,(1 - R)\, sin(2\pi - \alpha + \beta) \\
&= R(\alpha)\, sin(2\alpha) + n\,(1 - R(\alpha))\, sin(\alpha - \beta) \\
&= \Delta p_{front}(\alpha)\, sin\phi
\end{aligned}
\tag{A.8}
$$

where $\phi$ is the angle between the beam axis and the direction of momentum transferred, $R(\alpha)$, the reflection coefficient is calculated as $R(\alpha) = \frac{r_{\parallel}^2(\alpha) + r_{\perp}^2(\alpha)}{2}$ - $r_{\parallel}$ and $r_{\perp}$ are the reflection coefficients for TE and TM fields when interacting with surfaces.

Similarly, for the back surface, the following equations are obtained for the momentum components.

$$\Delta p_{back}^{parallel} = (1 - R(\alpha)) [n\, cos(\alpha - \beta)$$
$$+ n\, R(\beta) cos(3\beta - \alpha) - (1 - R(\beta))\, cos(2\alpha - 2\beta)]$$
$$= \Delta p_{back}(\alpha) cos\phi \qquad\qquad (A.9)$$

and

$$\Delta p_{back}^{perp} = (1 - R(\alpha)) [-n\, sin(\alpha - \beta)$$
$$+ n\, R(\beta)\, sin(3\beta - \alpha) - (1 - R(\beta))\, sin(2\alpha - 2\beta)]$$
$$= \Delta p_{back}(\alpha)\, sin\phi \qquad\qquad (A.10)$$

The total magnitude of the transferred momentum is now given by

$$\Delta p_{front/back}(\alpha) = \sqrt{((\Delta p_{front/back}^{parallel})^2 + (\Delta p_{front/back}^{perp})^2)} \qquad (A.11)$$

while its direction is given by

$$\phi_{front/back}(\alpha) = arctan(\frac{\Delta p_{front/back}^{perp}}{\Delta p_{front/back}^{parallel}}) \qquad\qquad (A.12)$$

Using the above equation for $\phi(\alpha)$, it can be shown mathematically that $\Delta p(\alpha)$ is always normal to both the front and back surfaces and outward for every incident angle $\alpha$.

Finally, the surface stress on the cell, as a function of the incident angle $\alpha$ is

120

$$\sigma_{front/back}(\alpha) = \frac{n_1 \Delta p_{front/back}(\alpha) I(\alpha)}{c} \qquad \text{(A.13)}$$

where the light intensity $I(\alpha) = \frac{2P}{\pi\omega^2(z)} e^{-2\rho^2 sin^2(\alpha)/\omega^2(z)}$, $P$ is the laser power, $\omega$, the beam waist of a gaussian beam and $\rho$, the radius of the cell.

Thus, the cell surface stress considered above due to a single laser beam depends on the ratio $\frac{\omega}{\rho}$ and $n$. There is a net force on the cell due to a single laser beam, which accelerates the cell. However, if the cell is hit by two equal counter propagating beams, the surface stresses are additive, while the net force on the cell is zero. Hence the cell remains stationary or stably trapped and the axisymmetric, normal surface stress deforms the cell.

## A.3   Bending and Membrane Energy of a Thin Shell

As mentioned in Chapter 2, membrane theory assumes that the bending forces are negligible compared to the membrane forces. This is valid when the changes in curvature of the shell are small and the moment terms in the equations for equilibrium are considered to be unimportant. The formulae for the bending energy $U_b$ and membrane energy $U_m$ of a thin shell are as follows [206].

The Bending Energy $U_b$ is given by

$$U_b = \frac{D}{2} \int \int_A [(\chi_\phi + \chi_\theta)^2 - 2(1-\nu)(\chi_\phi\chi_\theta - \chi_{\phi\theta}^2)]dxdy \qquad \text{(A.14)}$$

Using spherical coordinates, due to the the geometry of the problem (Figure A.7), the governing equations for axisymmetrical loading are

$$\chi_\phi = \frac{1}{\rho^2}(\frac{d}{d\phi}(v + \frac{dw}{d\phi})) \tag{A.15}$$

$$\chi_\theta = (v + \frac{dw}{d\phi})\frac{cot\phi}{\rho^2} \tag{A.16}$$

$$D = \frac{E\ h^3}{12(1 - \nu^2)} \tag{A.17}$$

where $\chi_\phi$ and $\chi_\theta$ are the changes in curvature in the $\phi$ and $\theta$ (polar and azimuthal) directions respectively, $\chi_{\phi\theta}$ is zero and $v$, $w$ are the meridional and radial displacements respectively. Also, as before, $E$ is the membrane's Young's modulus, $\nu$ is the material's Poisson ratio, $\rho$, the shell radius and $h$ its thickness.

The Membrane Energy $U_m$ is given by

$$U_m = \frac{E\ h}{2(1 - \nu^2)}\int\int_A [(\epsilon_\phi + \epsilon_\theta)^2 - 2(1 - \nu)(\epsilon_\phi\epsilon_\theta - \frac{1}{4}\gamma_{\phi\theta})^2]dxdy \tag{A.18}$$

The relevant equations in spherical coordinates for axisymmetric loading are the following.

$$\epsilon_\phi = \frac{1}{\rho}(\frac{dv}{d\phi} - w) \tag{A.19}$$

122

$$\epsilon_\theta = \frac{1}{\rho}(v \, cot\phi - w) \tag{A.20}$$

where $\epsilon_\phi$ and $\epsilon_\theta$ are the strains in the $\phi$ and $\theta$ directions respectively and $\gamma_{\phi\theta}$, the shear strain, is zero.

The equations for the bending and membrane energy of a thin shell are now used to calculate their ratio explicitly for the stress profile $\sigma_r = \sigma_0 \, cos^2\phi$. The meridional and radial deformations for this stress profile are

$$v(\phi) = \frac{\rho^2 \sigma_0}{Eh}[(\frac{1+\nu}{2}) \, cos\phi \, sin\phi] \tag{A.21}$$

and

$$w(\phi) = \frac{\rho^2 \sigma_0}{Eh}[(\frac{1+\nu}{4} + 1) \, cos^2\phi - \frac{1+\nu}{4}] \tag{A.22}$$

and the ratio $\frac{U_b}{U_m}$ is proportional to $\frac{4h^2}{3\rho^2}$, which is $\approx 10^{-4}$ for red blood cells.

## A.4 Deformation Equations for a Thin Shell

The total energy of a thin shell subjected to an axisymmetric radial stress $\sigma_r$ consists of the membrane energy and the work done due to $\sigma_r$. Neglecting the bending energy, the total energy is then given by [124], [206]

$$V = 2\pi\rho^2 \int [\frac{E \, h}{2(1-\nu^2)}[\epsilon_\phi^2 + \epsilon_\theta^2 + 2\nu\epsilon_\phi\epsilon_\theta] - \sigma_r \, w]sin\phi \, d\phi, \tag{A.23}$$

where $E$ is the Young's modulus of the thin shell, $\nu$ is the material's Poisson ratio, $\rho$, the shell radius and $h$ its thickness. The strain in the polar or $\phi$ direction $\epsilon_\phi$ and the strain in the azimuthal or $\theta$ direction $\epsilon_\theta$ due to the applied stress can both be expressed in terms of the meridional and radial displacements ($v$ and $w$) of the shell as follows.

$$\epsilon_\phi = \frac{1}{\rho}(\frac{dv}{d\phi} - w) \tag{A.24}$$

$$\epsilon_\theta = \frac{1}{\rho}(v\ cot\phi - w). \tag{A.25}$$

If the variational principle (Euler's equations) is used to extremize the total energy $V$ with respect to $v$ and $w$, the two equations obtained are

$$\frac{1}{\rho}\frac{d}{d\phi}\frac{dF}{dv'} - \frac{dF}{dv} = 0 \tag{A.26}$$

$$\frac{1}{\rho}\frac{d}{d\phi}\frac{dF}{dw'} - \frac{dF}{dw} = 0, \tag{A.27}$$

where $F$ is the integrand of the energy functional $V$, $v' = \frac{1}{\rho}\frac{dv}{d\phi}$ and $w' = \frac{1}{\rho}\frac{dw}{d\phi}$.

The differential equations obtained in terms of $v$ and $w$ and their derivatives, when the form of $F$ is substituted, are given below.

$$\frac{dv}{d\phi} + v\ cot\phi - 2\ w = \frac{-\rho^2(1-\nu)}{E\ h} \tag{A.28}$$

124

$$\frac{d^2v}{d\phi^2} + cot\phi\,\frac{dv}{d\phi} - (1+\nu)\frac{dw}{d\phi} - v\,cot^2\phi - \nu\,v = 0. \qquad (A.29)$$

These coupled differential equations can be solved for $v$ and $w$. Note that the form of the equations from membrane theory (Equations 2.1 and 2.2) used by us to solve for $v$ and $w$ are different. They are obtained from the two stress equilibrium equations. If the equilibrium equations are combined with the stress-strain relations, the equations obtained are the same as the equations derived from the variational principle (Equations A.28 and A.29).
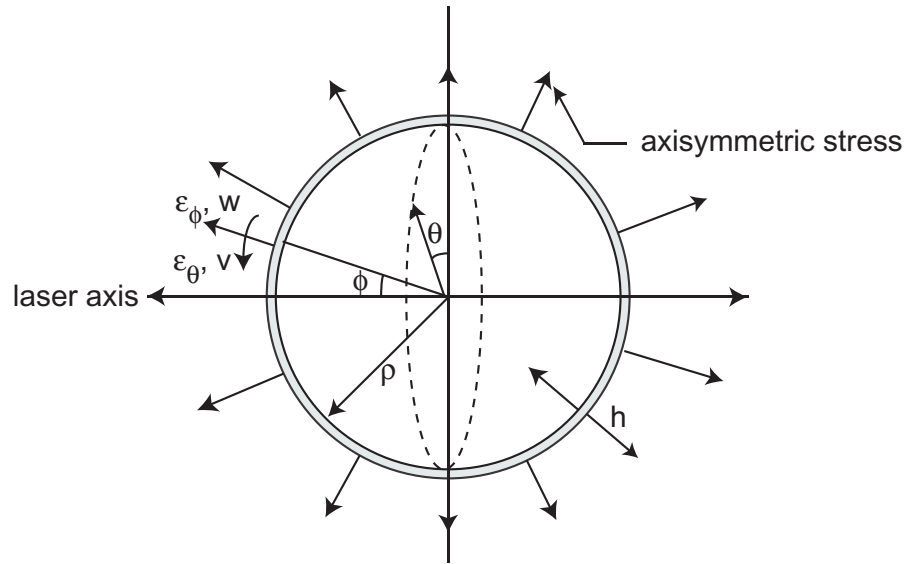


Figure A.7: The deformation of a red blood cell in the stretcher is modeled as a thin shell under an axisymmetric stress, where $\epsilon_\theta$ and $\epsilon_\phi$ are the meridional and radial strains respectively and $v$ and $w$ are the meridional and radial displacements

# Appendix B

# Appendix for Thick Shell Model of a Eukaryotic Cell Deforming in the Stretcher

## B.1  Deformation Equations for a Thick Shell

A thick spherical shell of outer radius $r_0$ and inner radius $r_1$ (hollow interior) subjected to an axisymmetric load displays a radial deformation $w$ and a meridional deformation $v$, as shown in Figure B.1. The radial deformation is considered here, since it alone can be observed experimentally. The general expression for the radial deformation due to an axisymmetric stress is [112]

$$
\begin{aligned}
w \;=\; & [Ar^{n+1}(n+1)(n-2+4\nu) + Br^{n-1}n]P_n(cos\phi) \\
& + [\frac{C}{r^n}n(n+3-4\nu) - \frac{D(n+1)}{r^{n+2}}]P_n(cos\phi)
\end{aligned}
\tag{B.1}
$$

where $r$ is the radial distance from the center of the sphere, $\nu$, the Poisson's ratio of the material and $\phi$ is the polar angle. For an axisymmetric stress, the solution does not depend on the azimuthal angle $\theta$.

To obtain $w$ for a specific problem, the external radial stress applied at the outer surface $r_0$ and the internal internal radial stress applied at the inner surface $r_1$ is written as a linear combination of Legendre polynomials $P_n$, which form a complete basis. In the optical stretcher set up, only an external axisymmetric radial

stress is applied. The applied shear stress is written in terms of the derivatives of the Legendre polynomials, but is zero in the optical stretcher experiment. The total radial displacement $w$ is a summation over $n$, where $n$ is the order of the Legendre polynomial in the nonzero coefficients of the radial stress expansion. The constants $A$, $B$, $C$, $D$ are solved for every $n$ by evaluating four equations - the radial and meridional stresses, $\sigma_r$ and $\sigma_{r\phi}$ respectively, at $r = r_0$ and $r = r_1$. These are given below.

$$
\begin{aligned}
\frac{1}{2G}\sigma_r &= [A(n+1)(n^2 - n - 2 - 2\nu)r^n + Bn(n-1)r^{n-2}]P_n(cos\phi) \\
&+ [-\frac{Cn}{r^{n+1}}(n^2 + 3n - 2\nu) + \frac{D(n+1)(n+2)}{r^{n+3}}]P_n(cos\phi) \quad \text{(B.2)}
\end{aligned}
$$

$$
\begin{aligned}
\frac{1}{2G}\sigma_{r\phi} &= [A(n^2 + 2n - 1 + 2\nu)r^n + B(n-1)r^{n-2}]\frac{d}{d\phi}P_n(cos\phi) \\
&+ [\frac{C}{r^{n+1}}(n^2 - 2 + 2\nu) - \frac{D(n+2)}{r^{n+3}}]\frac{d}{d\phi}P_n(cos\phi) \quad \text{(B.3)}
\end{aligned}
$$

Here, below the meridional deformation $v$ is also included, for the sake of completeness and for its use in our continuum models in Chapter 5.

$$
\begin{aligned}
v &= [Ar^{n+1}(n + 5 - 4\nu) + Br^{n-1}]\frac{dP_n(cos\phi)}{d\phi} \\
&+ [\frac{C}{r^n}(-n + 4 - 4\nu) + \frac{D}{r^{n+2}}]\frac{dP_n(cos\phi)}{d\phi} \quad \text{(B.4)}
\end{aligned}
$$
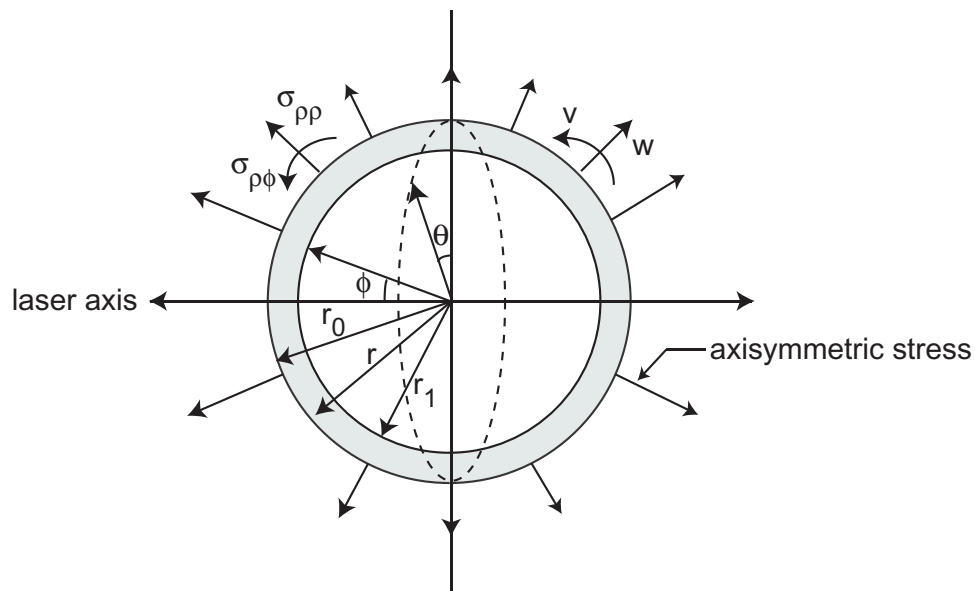
Figure B.1: A eukaryotic cell with a predominant actin cortex deforming in the stretcher is modeled as a thick shell. The axisymmetric deformation of a thick shell of outer radius $r_0$ and inner radius $r_1$ is shown. $w$ is the radial deformation and $v$, the meridional, while $\phi$ is the polar angle and $\theta$, the azimuthal angle

The thick shell deformation equations developed in this appendix for any axisymmetric stress are implemented in the mathematica program below, to extract structural parameters from experimental data.

**Mathematica Program to Extract the Shear Modulus of a Thick Shell from Experimental Data**

$$Clear["Global` * "]$$
$$SetDirectory["C : default directory"];$$
$$peakdata = ReadList["data.dat",$$
$$\{Number, Number, Number, Number, Number, Number, Number\}];$$

r0 = radius of cell in [m],

r1 = inner radius of cell/shell (I consider a hollow shell) 10-20% thickness of actual diameter,

m = 1/$\nu$, where $\nu$ is the poisson's ratio,

x = polar angle,

G = shear modulus,

ytot = deformation at every point on the shell,

yt1 = deformation at the pole / along the laser axis

obsdefper = experimentally observed deformation in percent

peakstress = peak stress calculated from program "stress profile (dimension like in "stress profile")

x = exponent for cos (gotten with stressprofilecurrentfib.m)

$r0 = 1;$

$r = r0;$

$potenz = Table[\{peakdata[[j, 5]]\}, \{j, 1, Length[peakdata]\}];$

$con0 = Table[\{\frac{1}{2} \int_{-1}^{1} LegendreP[0, Cos[x]]Cos^{potenz[[j]]}[x]dCos[x]\},$
$\{j, 1, Length[peakdata]\}\}];$

$ytot = Table[\{(con0[[j]]/(2 * G)) \left(\frac{(m-2)r0^3 r}{(m+1)(r0^3 - r1^3)} + \frac{r0^3 r1^3}{2(r0^3 - r1^3)r^2}\right)\},$
$\{j, 1, Length[peakdata]\}];$

$For[n = 2, n <= 100, n = n + 2,$

$con = Table[\{\left(\frac{2n+1}{2}\right) \int_{-1}^{1} LegendreP[n, Cos[x]]Cos^{potenz[[j]]}[x]dCos[x]\},$
$\{j, 1, Length[peakdata]\}];$

$r10 = (r1/r0);$

$r0n = r0^n;$

$r10n = (r10)^n;$

$one = a(n + 1) \left(n^2 - n - 2 - \frac{2}{m}\right) r10n + b(n)(n - 1)(r10n)(r10)^{-2}$
$- c(n) \left(n^2 + 3n - \frac{2}{m}\right)/(r10n\ r10) + d(n + 1)(n + 2)/(r10n\ (r10)^3);$

$two = a \left(n^2 + 2n - 1 + \frac{2}{m}\right) r10n + b(n-1)(r10n)(r10)^{-2}$

$+c \left(\left(n^2 - 2 + \frac{2}{m}\right)/(r10n \, r10) - d(n+2)/(r10n \, (r10)^3\right);$

$three = a(n+1)\left(n^2 - n - 2 - \frac{2}{m}\right) + b(n)(n-1) - c(n)(n^2 + 3n - \frac{2}{m}) +$

$d(n+1)(n+2) - 1;$

$four = a \left(n^2 + 2n - 1 + \frac{2}{m}\right) + b(n-1) + c \left(n^2 - 2 + \frac{2}{m}\right) - d(n+2);$

$abcd = Solve[\{one == 0, two == 0, three == 0, four == 0\}, \{a, b, c, d\}];$

$aa = First[(a/r0n)/.abcd];$

$bb = First[(b \, r0^2/r0n)/.abcd];$

$cc = First[(c \, r0 \, r0n)/.abcd];$

$dd = First[(d \, r0^3 \, r0n)/.abcd];$

$yy = \left((n+1)(n-2+4/m)aa \, r^{n+1} + bb \, n \, r^{n-1} + \frac{n(n+3-(4/m))cc}{r^n} - \frac{dd(n+1)}{r^{n+2}}\right) /$

$(2*G);$

$ytot = Table[\{ytot[[j]] + con[[j]] * yy(LegendreP[n, Cos[x]])\},$

$\{j, 1, Length[peakdata]\}];$

]

$yt1 = Table[\{100ytot[[j]]/r0/.\{G-> 1, r1-> 0.01 * r0,$

$m-> 2.2222222, x-> 0\}\}, \{j, 1, Length[peakdata]\}];$

(yt1 multiplied with peak stress is what we need)

$peakstress = Table[peakdata[[j, 4]], \{j, 1, Length[peakdata]\}];$

$obsdefper = Table[peakdata[[j, 3]], \{j, 1, Length[peakdata]\}];$

$G = Table[\{j, peakdata[[j, 5]], peakstress[[j]] * yt1[[j]]/obsdefper[[j]]\},$

$\{j, 1, Length[peakdata]\}];$

$OutputForm[TableForm[G]] >> youngmodulusnih.dat$

## B.2 The Elastic-Viscoelastic Correspondence Principle

When the Laplace transform of the linear viscoelastic boundary value problem (stress-strain relation, strain-displacement relation, momentum conservation equations and boundary conditions constitute a boundary value problem) is considered, it takes the same form as that of the linear elastic boundary value problem under the following replacements [105]

1. L[viscoelastic variable] = elastic variable (where L[s] is the Laplace transform).

2. s L[G(s)] = $G_{elastic}$ (shear modulus)

   s L[K(s)] = $K_{elastic}$ (bulk modulus) and similarly for other structural parameters.

Thus, the Laplace transformed solution to the viscoelastic boundary value problem can be obtained from the solution to the corresponding elastic boundary value problem. The final viscoelastic solution is obtained by taking the inverse Laplace transform.

If, for example, the elastic solution for the radial displacement, $w$, of an object is a function of $G$, $\nu$ and $\sigma$, the surface stress, the corresponding viscoelastic solution $w(t)$ can be found by taking the Laplace transform of the equation for radial displacement. Also, as noted above, $G$ is replaced by $sL[G]$, $\nu$ by $sL[\nu]$ and $\sigma$ by $L[\sigma]$. It is assumed here that the time dependencies of $G$, $\nu$ and $\sigma$, and hence their Laplace transforms, are known, as the equation must be expressed in terms of known structural quantities. The final result for $w(t)$ is obtained by taking the inverse transform.

The viscoelastic response of a cell with mainly the actin cortex (assume a crosslinked network) can be calculated similarly from the elastic solution, when

$G(t)$ is known. The correspondence principle can be applied to an entangled actin network in its linear viscoelastic regime - the network is found to be linearly viscoelastic till a strain of 10 percent at a concentration of 1 mg / ml (uncrosslinked network [141]). Hence, our linear viscoelastic shell model for the cell is appropriate as long as the strain or deformation in our stretcher experiment is in this regime.

In the internal dynamics regime, for high frequencies, $G(\omega) = a_1(i\omega)^{3/4}$. $G(t)$ can be obtained by using Abel's Theorem, which states that

$$F^{-1}[(i\omega)^{-z}] = \frac{1}{\Gamma(z)} t^{z-1} H(t), \tag{B.5}$$

where $H(t)$ is the heaviside step function; the result is $G(t) = a_2 t^{-3/4}$. The correspondence principle then yields the following in the internal dynamics regime; the time dependent radial displacement of a cell with mainly the actin cortex, subjected to an axisymmetric stress is of the form

$$\frac{w(t)}{r_0} = a_3 \sigma_0 t^{3/4} F_G(\nu, r, \phi, r_1, r_0) \tag{B.6}$$

where $a_1$, $a_2$ and $a_3$ are constants and $F_G(\nu, r, \phi, r_1, r_0)$ is known from the corresponding elastic solution. The solution above for $w(t)$ is valid only for small $t$ ($t < 0.001$ sec), as the form of $G(\omega)$ used to calculate it is valid for large $\omega$. At intermediate time scales ($0.001 < t < 0.01$ sec), a recent theoretical derivation for $G(t)$ of a solution of relatively stiff actin filaments ($L < L_p$) (Pasquali et al., 2001) shows that $G(t) \sim t^{-5/4}$. The radial displacement, $w(t)$, at intermediate times can be obtained with an analysis similar to that in the internal dynamics regime. At a longer time ($t > 0.01$ sec), the structural response of the actin shell is elastic, as $G$ has no time dependence in the plateau region. Hence, the deformation of a

crosslinked actin shell is predicted to be dominantly elastic. Finally, it is important to note that although AFM data reveal that the extent of the rubber plateau and the transition to the internal dynamics regime are the same in both cells and *in vitro* actin networks [117], there are additional factors that create a difference in the viscoelastic response of a cell and an actin shell [230].

## B.3   Extraction of Structural Parameters from our Deformation Experiment - the Optical Stretcher

The correspondence principle described in Appendix B.2 can be used to extract structural parameters from the stretcher experiment, for any form of the stress profile (generally, the relaxation modulus $G(t)$ is obtained only under constant strain conditions, but this method enables us to obtain $G(t)$ for any stress profile). Consider the elastic solution for $w$, the radial displacement of a thick shell subjected to a stress profile $\sigma = \sigma_0 \, cos^2(\phi)$, which is of the form

$$\frac{w}{r_0} = \frac{\sigma_0}{G} F_G\big(\nu, r, \phi, r_1, r_0\big). \tag{B.7}$$

Here, $\sigma_0$, the peak applied stress can be time dependent and $F_G(\nu, r, \phi, r_1, r_0)$, the geometric factor, is a function of $r$, the radial distance from the center of the sphere, $\phi$, the polar angle, $r_1$, the inner radius of the shell, $r_0$, the outer radius of the shell and $\nu$, the Poisson's ratio.

The Laplace transform of the above equation is performed to obtain the following viscoelastic solution.

$$L[w] = \frac{L[\sigma_0]}{sL[G]}sL[F_G(\nu, r, \phi, r_1, r_0)]. \tag{B.8}$$

This Laplace equation can be used to obtain $G$ as follows. $L[w(t)]$ is known from the optical stretcher experiment, and so is $\sigma_0$, the peak stress applied. Also, if $\nu$ is constant, $L[\nu] = \frac{\nu}{s}$. Hence, the above equation can be inverted to extract the structural parameter $G(t)$.

## B.4 Extraction of Structural Parameters from Other Cell Deformation Experiments

Many experimental techniques have been developed to deform cells. This section describes how the models created to accompany different experiments are used to extract structural parameters.

### B.4.1 Cell Poker

The cell poker experiment [232] is an older version of the AFM experiment and consists of a poker of radius $a$, which probes a cell of radius $R$. In order to obtain force-indentation curves, two models are considered: a liquid drop model (Figure B.2) and a neo-hookean model (Figure B.3). An analysis of the two models leads to a dimensionless force indentation curve which is, for the liquid-drop model $\frac{F}{2\pi aT}$ versus $\frac{u}{a}$, where $F$ is the indenting force, $T$ is the tension, and for the neo-hookean model, $\frac{F}{\mu a^2}$ versus $\frac{u}{a}$, where $F$ is the applied force and $\mu$ is the shear modulus. The force applied is calculated by multiplying a typical indentation with the stiffness, which is the initial slope of the experimental force-indentation curve. Hence, a knowledge of the force applied and the force-indentation curves of the

neo-hookean model enables an estimation of the shear modulus $\mu$.
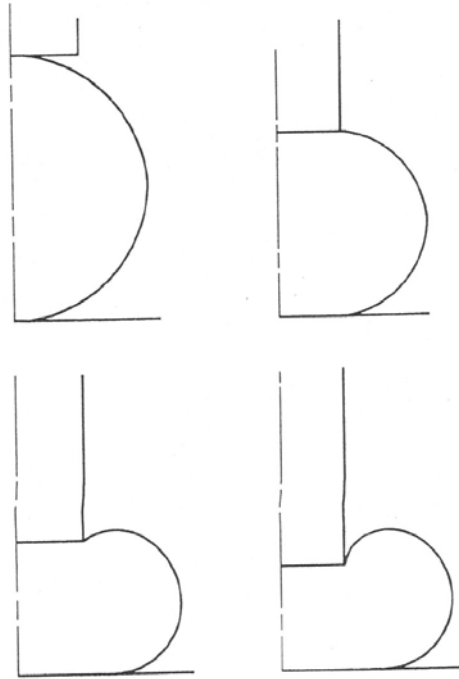


Figure B.2: A liquid drop with constant surface tension being deformed by a rigid indentor, as a model for a cell probed by the cell poker tip, taken from [232]

## B.4.2 Atomic Force Microscopy (AFM)

The Hertz model or a variation of it has been commonly used for an AFM tip probing a cell to study its structural properties [117], [152], [109], [160], [161]. As shown in Figure B.4, the Hertz model comprises an elastic half-space being indented by a hard axisymmetric indentor. The cell surface is approximated as an elastic half space, under the assumption that the indentation depth is much less than the radius of the cell. The tip is modeled as a paraboloid of radius $R$ at the contact

135
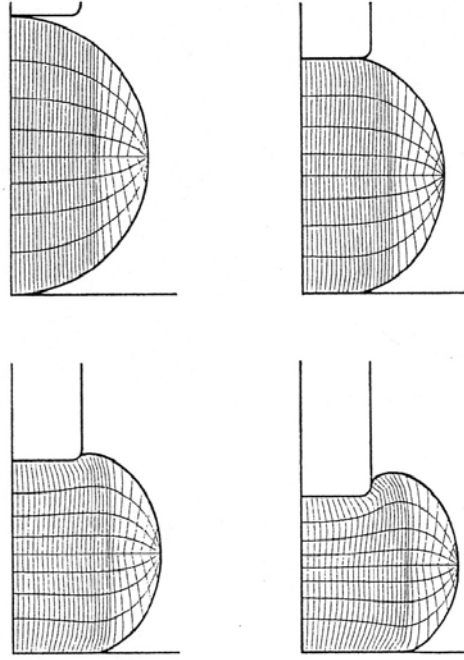
Figure B.3: An incompressible hyperelatic (neo-hookean) sphere being deformed by a rigid indentor, as a model for a cell probed by the cell poker tip, taken from [232]. It is assumed that the contact between the poker, sphere and substrate is smooth

point. From the analysis of this model, the relation that emerges for the indentation $\delta$ versus the applied force $F$ is

$$F = \frac{4}{3} R^{0.5} \delta^{1.5} E',$$

(B.9)

where $R$ is the radius of the tip and $E'$ is the effective Young's modulus given by $E' = \frac{E_{cell}}{1 - \nu_{cell}^2}$, where $\nu_{cell}$ is the Poisson's ratio of the cytoskeleton. Therefore, the indentation versus force curve allows an estimation of the effective modulus (and hence the Young's modulus of the cell).
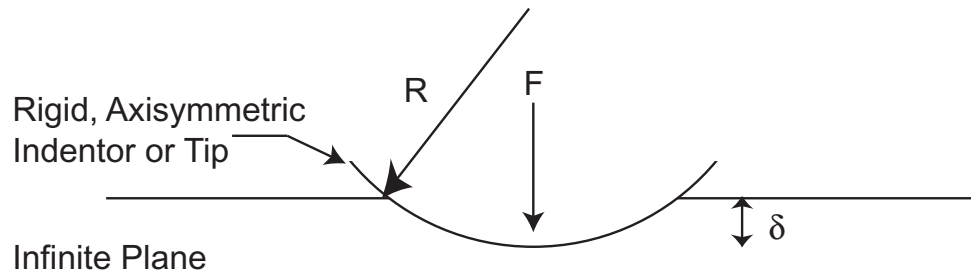
Figure B.4: The Hertz model - a rigid axisymmetric identor exerting a force F on an infinite plane, causing an indentation $\delta$ - for an atomic force microscope (AFM) tip probing a cell

### B.4.3   Microplate Manipulation

The microplate experiment by Thoumine et al. [196] uses a 3 element mechanical model to extract two elastic moduli and a viscosity from their traction experimental data and oscillatory tests. They use a Kelvin model, as shown in Figure B.5, with one spring of elasticity $k_0$ (in $N/m^2$) in parallel with a series combination of a second spring of elasticity $k_1$ and a dashpot of viscosity $\mu$. The slope of the stress-strain curve from traction data gives the sum $k_0 + k_1$ of the two elastic constants, while the stress relaxation curve gives gives the time constant $\tau$ ($\tau = \frac{\mu}{k_1}$) and the spring constant $k_0$. $k_0$, $k_1$ and $\mu$ can also be extracted from oscillation data.

### B.4.4   Magnetic Bead Microrheometry

In order to extract structural parameters from their magnetic microbead microrheometry data, Bausch et al. [10] use the 4-element mechanical model (Kelvin model with a dashpot in series) shown in Figure B.6 a). The viscoelastic response of the cell can be characterized by three parameters, by reducing the four parame-

137
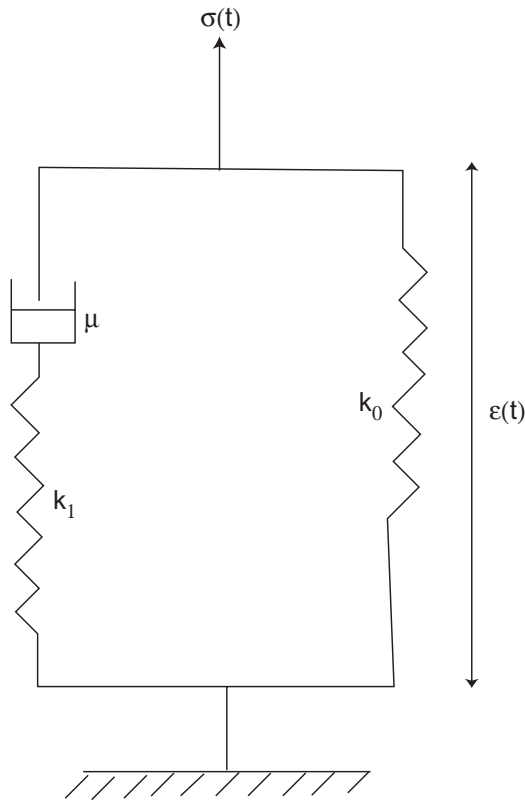
Figure B.5: Three-element mechanical model for a cell being deformed by two parallel microplates

ters of the mechanical model: an effective elastic constant $k = k_0 + k_1$, a relaxation time $\tau = \frac{\gamma_1(k_0+k_1)}{k_0 k_1}$ and a viscosity $\gamma_0$. These viscoelastic parameters are obtained by analyzing the experimental creep response and relaxation curves. To relate $k$, $\tau$ and $\gamma_0$ to the viscoelastic moduli of the cell, the cell membrane and actin cortex together are modeled as a thin elastic plate of shear modulus $\mu*$ coupled to the cytoplasm, which is modeled as a viscoelastic layer (viscosity $\eta_c$) fixed to a solid support on the opposite side (Figure B.6 b). $\mu*$ is obtained from the displacement of the magnetic beads and the effective elasticity $k$ of the viscoelastic model. The

3D shear modulus of the cell envelope is then related to $\mu*$ by $\mu = \frac{\mu*}{h}$, where $h$ is the thickness of the membrane and cortex. The viscosity of the cytoplasm is connected to the mechanical model parameter $\gamma_0$ by the relation $\eta_c = \frac{\gamma_0 d_c}{\pi R^2}$, where $R$ is the radius of the contact area between membrane and bead and $d_c$ is the thickness of the viscous medium the bead moves in (cytoplasm).
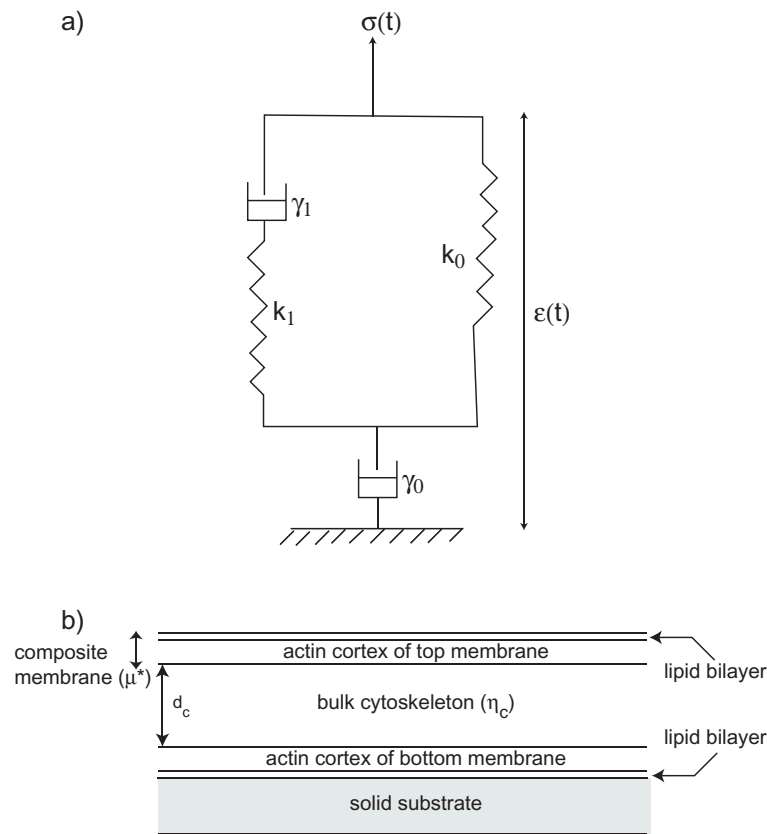


Figure B.6: a) 4-element mechanical model of a cell used to analyze magnetic bead microrheometry data. b) Cell model used to relate the viscoelastic parameters obtained from the mechanical model to those of the cell

### B.4.5   Micropipette Aspiration of Cells

There are cells which behave structurally like a solid; for example chondro-cytes and endothelial cells are more rigid [96], [194]. Therefore, the model for a cell being aspirated in a pipette, depends on the type of cell.

**Extraction of $E$ (Young's modulus) and $\eta$ for a Chondrocyte or Endothelial cell**

A solid cell being aspirated in a micropipette is modeled as an infinite half space [194]. The loading due to the micropipette of inner radius $a$ is represented as a constant pressure in a circular region (of radius $a$) on the half-space, while the contact between the cell and the micropipette is represented as a stress in the annular region $a > r > b$ ($b - a$ is the micropipette thickness), as shown in Figure B.7. The model uses two boundary conditions in the annular contact region $a > r > b$ (force model and punch model) but gives the following identical relation between the suction pressure $\Delta P$ and the extension of the cell into the pipette $L_p$ in both these cases.

$$\Delta P = \frac{2\pi}{3} \frac{E L_p \Phi}{R_p},$$
(B.10)

where $E$ is the Young's modulus and $\Phi$ depends on the ratio of pipette wall thickness to radius of the pipette (a typical value of $\Phi$ is 2.1 and so $\frac{2\pi\Phi}{3}$ is 4.4). The slope of $\Delta P$ versus $\frac{L_p}{R_p}$ divided by 4.4 gives $E$. The calculation assumes that both the radius and thickness of the micropipette are smaller than the thickness of the cell or half space.

To obtain viscosity, $\eta$, $\frac{dL_p}{dt}$ is measured from experiment. An analysis of the half-space model along with the standard viscoelastic model yields $\eta$.
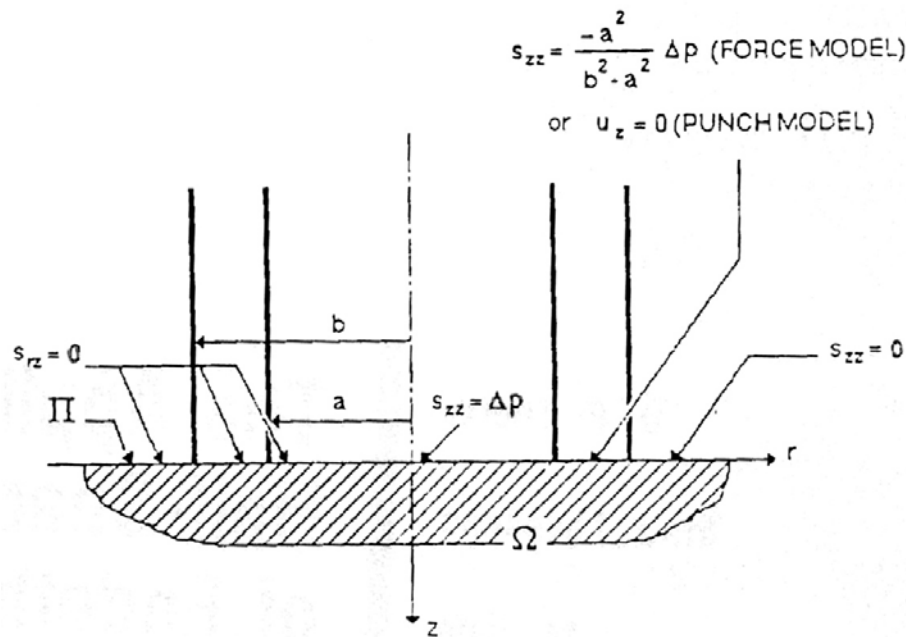


Figure B.7: The half-space model with the boundary conditions used to represent a solid cell being aspirated in a micropipette, taken from [194]. $\Omega$ is the half-space representing the cell and $\Pi$ is the boundary of $\Omega$. $s_{zz}$ and $s_{rz}$ are the stresses in cylindrical coordinates (r,z), while $u_z$ is the displacement along the $z$ axis. $a$ and $b$ are the inner and outer radius of the pipette.

## B.4.6   Microstructural Models of the Cytoskeleton for Adherent Cells

### B.4.6.1   Open Cell Foam Networks

The open cell foam network depicts the actin cytoskeleton as a network of interconnected struts, as shown in Figure B.8 [182]. The contribution of the network to the structural response of the cell is calculated by considering the bending of the

struts to an applied force on the cell and is as follows [182]

$$E^* = C E \phi^2, \tag{B.11}$$

where $C$ is a constant approximately equal to 1, $E$ is the Young's modulus of an individual actin filament, $E^*$ is the effective Young's modulus and $\phi = \frac{\rho^*}{\rho}$, the ratio of the mass density of the actin network to that of the individual filament.
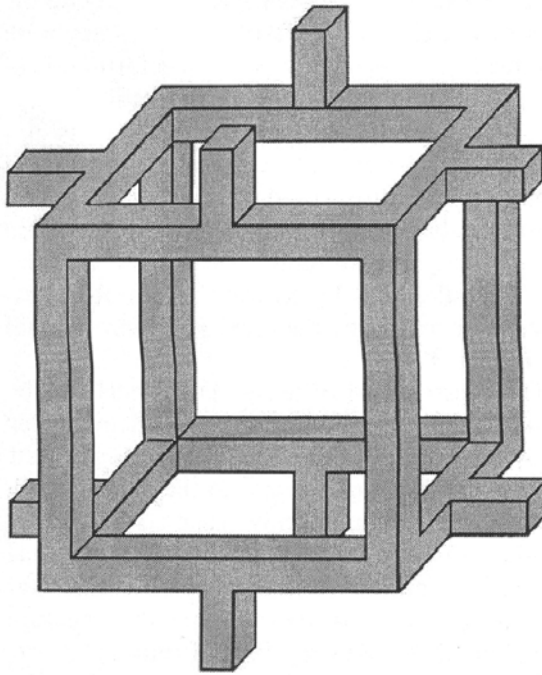


Figure B.8: Microstructural unit of an open cell foam as a model for the elastic properties of the actin cytoskeleton, taken from [182]

### B.4.6.2 Prestressed Cable Nets

In the prestressed cable net model, the initial tension in the actin filaments determines the overall mechanical response of the cell. The actin filaments are thought to be cables, which carry a prestress, due to the actomyosin function, osmotic pressure and cell spreading. This prestress is balanced partly by other cellular structures such as microtubules and the nucleus. Taking into consideration the prestress or the normal force transmitted by the cables across a unit area, an expression for the Young's modulus $E^*$ can be found and is as follows.

$$E^* \geq \frac{F\phi}{2r^2\pi}, \tag{B.12}$$

where $F$ is the uniform tensile force in the cables, $r$ is the filament radius and $\phi$ is the volumetric fraction of actin in the cells.

The tensegrity structure, shown in Figure B.9, is a special form of the prestressed cable structure, where the cable tension is initially balanced entirely by the local compression of the supporting struts. For a model in which six struts are interconnected with 24 cables by frictionless pin joints, and in which the struts are elastic and buckle beyond the critical value of compression force, $E^*$ is calculated as follows

$$E^* = \frac{5.85F(1 + 4\epsilon)}{l^2(1 + 12\epsilon)}, \tag{B.13}$$

where $F$ is the initial cable tension, $l$ is the initial length of an individual cable and $\epsilon$ is the initial cable strain. This formula highlights the importance of the initial

143

tension and microstructural geometry of the actin network. The above two formulae can be used to calculate bounds for $E^*$.

Another way of expressing $E^*$ is as follows.

$$E^* = \frac{6.4P(1 + 4\epsilon)}{L^2(1 + 12\epsilon)},$$
(B.14)

where $L$ is the initial strut length and $P$ is the initial compression in the cable. This formula highlights the importance of buckling of compression bearing elements.
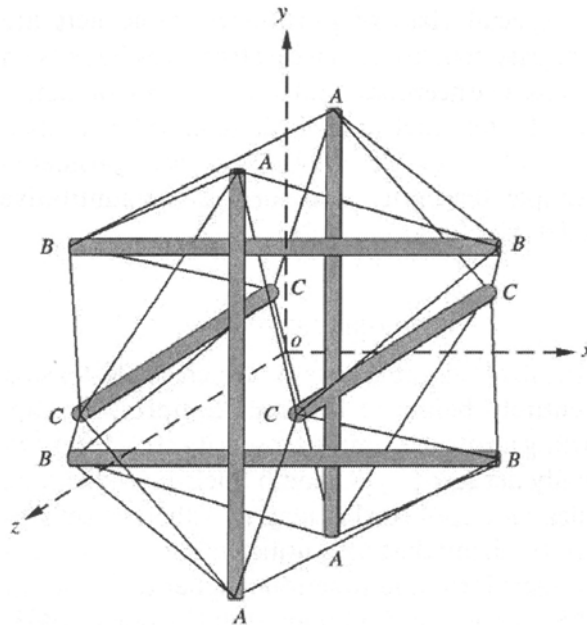


Figure B.9: Six-strut tensegrity model to represent cytoskeletal mechanics, taken from [182]. The cables - shown as thin lines - carry a tensile force initially which is balanced by compression in the struts - gray columns

# Appendix C

# Appendix for the Role of Isotropic Actin Networks in Cells

## C.1  A Network of Actin Filaments and Bundles

Here, the strength or shear modulus of an isotropic network of a mixture of actin filaments and bundles is estimated by us [4], by modifying existing isotropic polymer network theories for the strength of an isotropic, permanently crosslinked actin network of filaments [113], [103]. Our calculation for the strength of a network of actin filaments is based, as before, on MacKintosh et al.'s theory of a permanently crosslinked network [113], which estimates the entropic elasticity of an actin network by considering the force-extension relation of a filament segment 'pinned' between two entanglement points. Their assumption that the applied force is parallel to the filament length seems reasonable *in vivo*, where the short actin filaments (whose lengths $l$ are of the order of their entanglement length $l_e$) can align themselves continuously along the load direction, when crosslinked by flexible crosslinkers such as $\alpha$-actinin and ABP. In order to calculate the strength of a network of actin bundles, our study modifies Kroy et al.'s theory of a permanently crosslinked network (Kroy et al., 1996). This theory generalizes MacKintosh et al.'s work and considers a variable angle between the applied load and filament length and hence (in addition to entropic elasticity) the bending of long filaments ($l > l_e$) 'clamped' at their entanglement points - the Kroy et al. model reduces to the MacK-

intosh et al. model, if the variable angle $\theta$ between the filament and load in the Kroy model is assumed to be 0. Thus, the Kroy et al. model seems more appropriate for a bundle of long filaments than MacKintosh et al.'s model, due to the joint stiffness of the bundles. Our strength calculation differs from Kroy et al.'s theory as each filament is considered to be a bundle - a continuum approach is used to model each bundle as a cylinder of radius $R$. Hence, the number of filaments in each bundle depends on the value of the bundle size $R$, which can be varied. The parameters that change for a network of bundles, from Kroy's theory for a network of filaments, are the mesh size and persistence length which become $R$*mesh size of a network of filaments and $R^4$*times persistence length of a filament in a network of filaments. The total strength (shear modulus $G$) of this network of a mixture of filaments and bundles is then given by

$$G_{total} = G_{filament} + G_{bundles} + \beta * G_{filament} * G_{bundles}$$

$$G_{total} = \frac{l_p^2}{24.8 \; \xi_m^2 \; le^3 \; 10} + \frac{l_{p1}}{24.8 \; (4\pi/3) \; (\xi_{m1}/2)^3 \; l_{e1} \; 10} + \beta * G_{filament} * G_{bundles}$$

$$(C.1)$$

where the mesh size of the network of filaments is $\xi_m = (\rho \, (1 - x))^{-0.5}$, the mesh size of the networks of bundles is $\xi_{m1} = R(\rho \, x)^{-0.5}$, where $\rho$ is the actin concentration and $(1 - x)$ is the fraction of total actin in the network of filaments and $x$ is the fraction in the network of bundles. The entanglement length for the network of filaments is $l_e = 5.37671 \; \xi_m^{0.8} \; l_p^{0.2}$ ($l_p = 17$) and that of the network of bundles is $l_{e1} = 5.37671 \; \xi_{m1}^{0.8} \; l_{p1}^{0.2}$ ($l_{p1} = 17 \, R^4$). Also, $\beta$ is a parameter that characterizes the interaction between filaments and bundles.

Figures C.1, C.2 and C.3 show our results for the total shear modulus G' of a network of filaments and bundles for different values of $R$, the bundle size,

146

and for different values of the interaction parameter $\beta$, as a function of the fraction of total actin that forms the network of bundles ($x$). The total concentration of actin (in the network of filaments and the network of bundles) is assumed to be 10 mg/ml in our calculations. Our results show that if there is no interaction between the network of filaments and bundles, the modulus of a network of filaments alone is always greater than the modulus of a network of filaments and bundles. As the bundle size $R$ increases, the bundles sap the actin filaments and degrade the strength of the network of filaments. Although the strength of the network of filaments and bundles increases beyond a certain fraction of bundled network ($x > x_1$ (say)), the rapid decrease in strength before $x_1$ cannot be overcome, even when the network is made of bundles alone ($x = 1$) - bundled networks are not inherently stronger than filament networks. Now, if there is an interaction between the filaments and bundles, there is a possibility that the strength of a network of filaments and bundles is greater than that of a network of filaments alone. The graph with $\beta = 0.01$ is not very different from the graph with $\beta = 0$ (no interaction). However, when $\beta = 0.05$, and $R = 1.5,3$ and 5, there is a local maximum in the strength of the network, for slightly different values of the fraction of bundled network $x$ in each case.
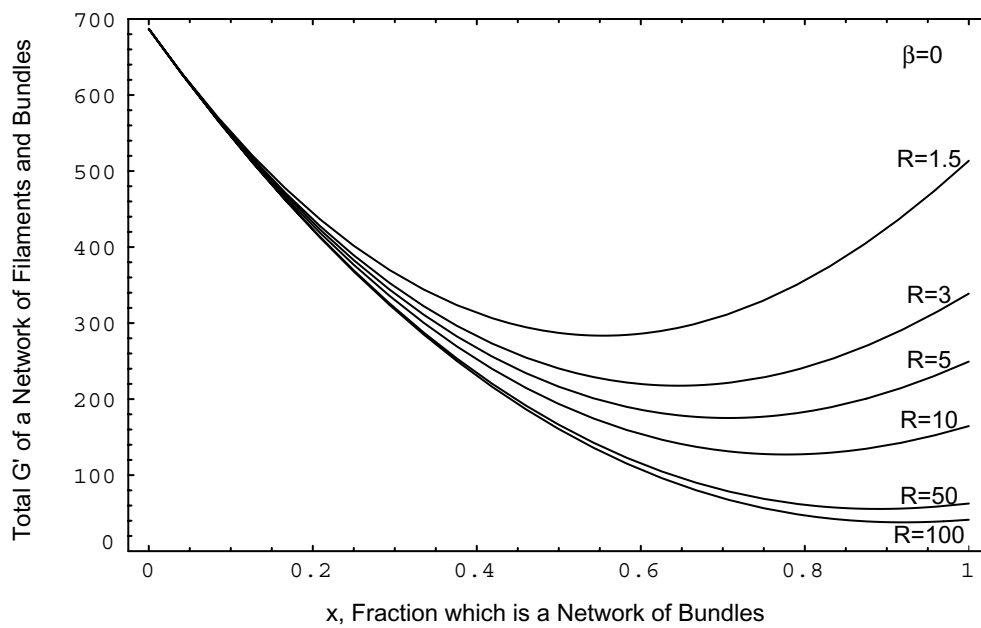
Figure C.1: Shear modulus, $G'$, of a network filaments and bundles, with no interaction between the two networks
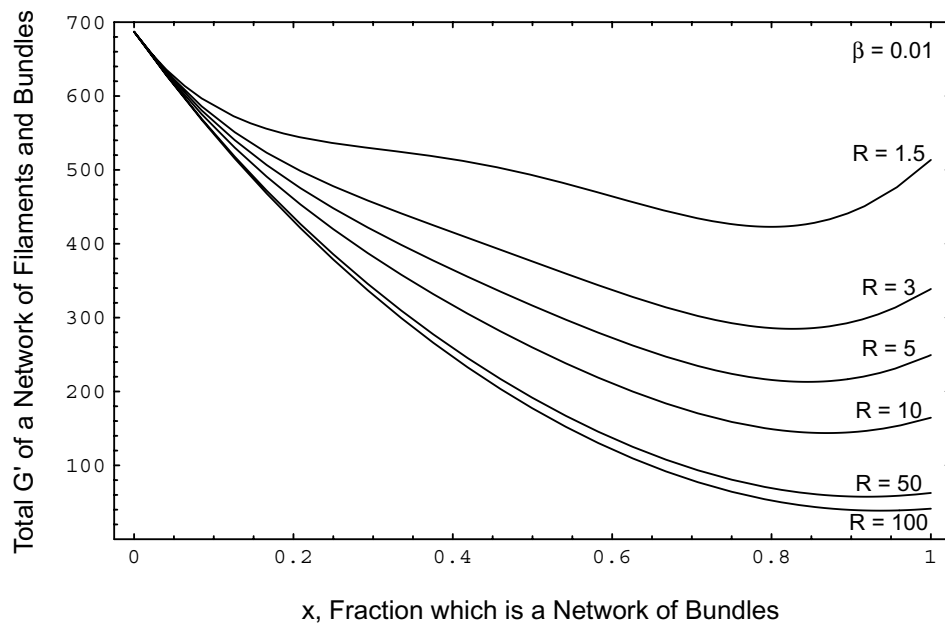
Figure C.2: Shear modulus, $G'$, of a network of filaments and bundles, with an interaction between the two networks (interaction parameter $\beta$=0.01)
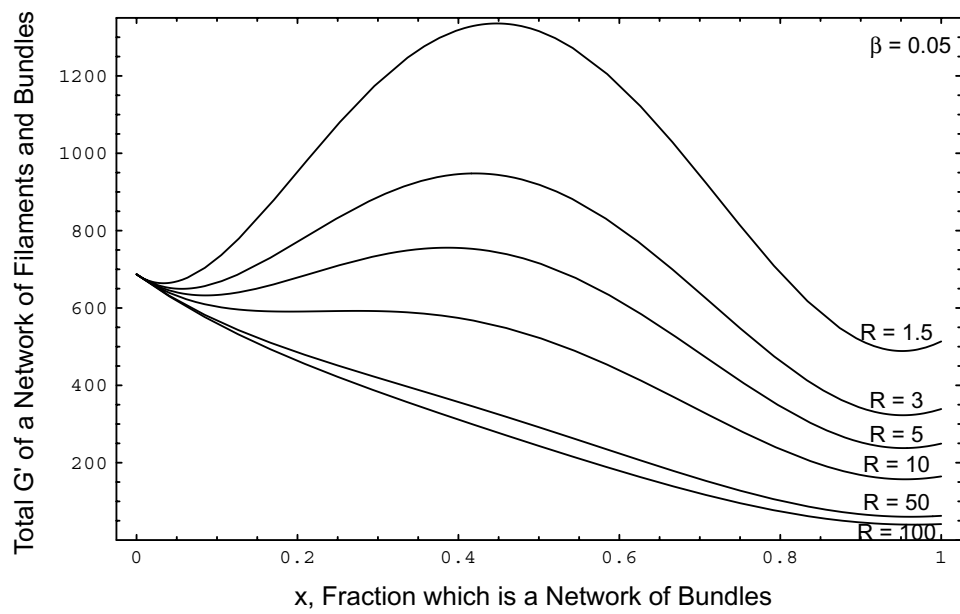
Figure C.3: Shear modulus, $G'$, of a network of filaments and bundles, with an interaction between the two networks (interaction parameter $\beta$=0.05)

150

# Appendix D

# Appendix for Models for Eukaryotic Cells

## D.1  Buckling of Microtubules

This appendix deals with a simple calculation to estimate the deformation of a cell in the stretcher which can cause the *in vivo* microtubules to buckle. Assuming the microtubule to be a thin beam, the deformation $\delta_{critical}$ at which a beam buckles is obtained from Euler's bucking criterion and is given by

$$\delta_{critical} = \frac{EI\pi}{LEr^2},\tag{D.1}$$

where $EI$ is the flexural rigidity of the beam (microtubule), $L$ its length and $r$ is radius. Substituting the values for microtubules of $EI$ = 2.2 $10^{-23}$ Nm [55], $L$ = 8 $\mu m$ and $r$ = 12.5 nm [16], the formula above yields $\delta_{critical}$ of 1 $\mu m$. The maximum compression, and likelihood of buckling, of a microtubule in a cell being deformed in the stretcher occurs at the equator (perpendicular to the laser axis). The compression at the equator of a cell subjected to a stress $\sigma = cos^2\phi$ is of the order of a few tens of nms from our analytical model (without the microtubules) and our FEM model (with the microtubules). So, the buckling limit of microtubules is not reached for linear deformations of a cell in the stretcher.

151
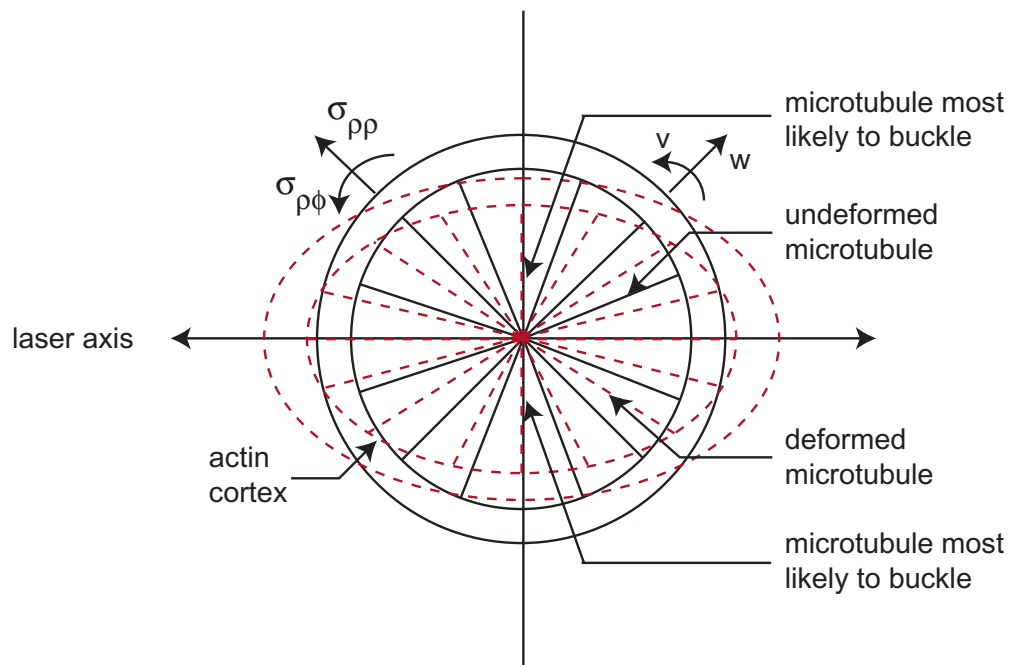
Figure D.1: Schematic figure to depict the possible buckling of a microtubule in our cell model (thick shell and microtubules) or in the optical stretcher experiment

## D.2   An ABAQUS Program or Finite Element Model of a Thick Shell Subjected to a Uniform Stress

*HEADING

SPHERICAL CAVITY, C3D20R, R=1,2,4,8, FX, 1-1-11-4

*PREPRINT,ECHO=NO,MODEL=NO,HISTORY=NO

*RESTART, WRITE, FREQUENCY=1

*NODE,SYSTEM=S,NSET=IN

1,18E-6,0.,90.

25,18E-6,90.,0.

601,18E-6,0.,0.

613,18E-6,45.,0.

313,18E-6,45.,35.26439

325,18E-6,45.,0.

*NODE,SYSTEM=S,NSET=OUT

14001,20.E-6,0.,90.

14025,20.E-6,90.,0.

14601,20.E-6,0.,0.

14613,20.E-6,45.,0.

14313,20.E-6,45.,35.26439

14325,20.E-6,45.,0.

*NGEN,LINE=C,NSET=IN

1,25,1

1,601,25

25,325,25

601,613,1

13,313,25

313,325,1

26,38,1

51,63,1

76,88,1

101,113,1

126,138,1

151,163,1

176,188,1

201,213,1

226,238,1

251,263,1

276,288,1

301,313,1

302,602,25

303,603,25

304,604,25

305,605,25

306,606,25

307,607,25

308,608,25

309,609,25

310,610,25

311,611,25

312,612,25

38,50,1

63,75,1

88,100,1

113,125,1

138,150,1

163,175,1

188,200,1

213,225,1

238,250,1

263,275,1

288,300,1

*NGEN,LINE=C,NSET=OUT

14001,14025,1

14001,14601,25

14025,14325,25

14601,14613,1

14013,14313,25

14313,14325,1

14026,14038,1

14051,14063,1

14076,14088,1

14101,14113,1

14126,14138,1

14151,14163,1

14176,14188,1

14201,14213,1

14226,14238,1

14251,14263,1

14276,14288,1

14301,14313,1

14302,14602,25

14303,14603,25

14304,14604,25

14305,14605,25

14306,14606,25

14307,14607,25

14308,14608,25

14309,14609,25

14310,14610,25

14311,14611,25

14312,14612,25

14038,14050,1

14063,14075,1

14088,14100,1

14113,14125,1

14138,14150,1

14163,14175,1

14188,14200,1

14213,14225,1

14238,14250,1

14263,14275,1

14288,14300,1

*NFILL

IN,OUT,20,700

*NSET,NSET=XSYM,GENERATE

1,25,1

701,725,1

1401,1425,1

2101,2125,1

2801,2825,1

3501,3525,1

4201,4225,1

4901,4925,1

5601,5625,1

6301,6325,1

7001,7025,1

7701,7725,1

8401,8425,1

9101,9125,1

9801,9825,1

10501,10525,1

11201,11225,1

11901,11925,1

12601,12625,1

13301,13325,1

14001,14025,1

*NSET,NSET=YSYM,GENERATE

1,601,25

701,1301,25

1401,2001,25

2101,2701,25

2801,3401,25

3501,4101,25

4201,4801,25

4901,5501,25

5601,6201,25

6301,6901,25

7001,7601,25

7701,8301,25

8401,9001,25

9101,9701,25

9801,10401,25

10501,11101,25

11201,11801,25

11901,12501,25

12601,13201,25

13301,13901,25

14001,14601,25

*NSET,NSET=ZSYM,GENERATE

25,325,25

725,1025,25

1425,1725,25

2125,2425,25

2825,3125,25

3525,3825,25

4225,4525,25

4925,5225,25

5625,5925,25

6325,6625,25

7025,7325,25

7725,8025,25

8425,8725,25

9125,9425,25

9825,10125,25

10525,10825,25

11225,11525,25

11925,12225,25

12625,12925,25

13325,13625,25

14025,14325,25

601,613,1

1301,1313,1

2001,2013,1

2701,2713,1

3401,3413,1

4101,4113,1

4801,4813,1

5501,5513,1

6201,6213,1

6901,6913,1

7601,7613,1

8301,8313,1

9001,9013,1

9701,9713,1

10401,10413,1

11101,11113,1

11801,11813,1

12501,12513,1

13201,13213,1

13901,13913,1

14601,14613,1

*NSET,NSET=OUT1

14001,14026,14051,14076,14101,14126,14151,14176,14201,14226,14251,14276,

14301,14326,14351,14376,14401,14426,14451,14476,14501,14526,14551,14576,

14601

*ELEMENT,TYPE=C3D20R,ELSET=ALL

1,1,51,53,3,1401,1451,1453,1403,26,52,28,2,1426,1452,1428,

1402,701,751,753,703

2,3,53,55,5,1403,1453,1455,1405,28,54,30,4,1428,1454,1430,

1404,703,753,755,705

3,5,55,57,7,1405,1455,1457,1407,30,56,32,6,1430,1456,1432,

1406,705,755,757,707

4,7,57,59,9,1407,1457,1459,1409,32,58,34,8,1432,1458,1434,

1408,707,757,759,709

5,9,59,61,11,1409,1459,1461,1411,34,60,36,8,1434,1460,1436,

1408,709,759,761,711

78,311,361,315,313,1711,1761,1715,1713,336,362,314,312,

1736,1762,1714,1712,1011,1061,1015,1013

90,361,411,317,315,1761,1811,1717,1715,386,412,316,362,

1786,1812,1716,1762,1061,1111,1017,1015

102,411,461,319,317,1811,1861,1719,1717,436,462,318,412,

1836,1862,1718,1812,1111,1161,1019,1017

114,461,511,321,319,1861,1911,1721,1719,486,512,320,462,

1886,1912,1720,1862,1161,1211,1021,1019

126,511,561,323,321,1911,1961,1723,1721,536,562,322,512,

1936,1962,1722,1912,1211,1261,1023,1021

138,561,611,325,323,1961,2011,1725,1723,586,612,324,562,

1986,2012,1724,1962,1261,1311,1025,1023

*ELGEN,ELSET=ALL

1,12,2,1,6,50,12,10,1400,200

1,12,50,12,10,1400,200

2,12,50,12,10,1400,200

3,12,50,12,10,1400,200

4,12,50,12,10,1400,200

5,12,50,12,10,1400,200

78,10,1400,200

90,10,1400,200

102,10,1400,200

114,10,1400,200

126,10,1400,200

138,10,1400,200

*ELSET,ELSET=INEL,GENERATE

1,72,1

73,78,1

85,90,1

97,102,1

109,114,1

121,126,1

133,138,1

*ELSET,ELSET=OUTEL,GENERATE

1801,1872,1

1873,1878,1

1885,1890,1

1897,1902,1

1909,1914,1

1921,1926,1

1933,1938,1

*SOLID SECTION,ELSET=ALL,MATERIAL=ONE

*MATERIAL,NAME=ONE

*ELASTIC

1000,0.4

```
*BOUNDARY

XSYM,1

YSYM,2

ZSYM,3

*STEP

*STATIC

*DLOAD

OUTEL,P2,-1.0

*NODE PRINT,NSET=OUT1

U, COORD

*END STEP
```

# Bibliography

[1] ABAQUS online documentation - obtained by typing abaqus.doc, in the terminal where the ABAQUS program is run. The ABAQUS website is www.hks.com

[2] Alberts, B., Johnson, A., Lewis, J., Raff, M., Roberts, K. and P. Walter, Molecular Biology of the Cell, *Garland Science*, (4th Edition) (2002)

[3] Ananthakrishnan, R., Guck, J., Kas, J. and T. Moon, Gel-Sol Transitions in Eukaryotic Cells via Transient Crosslinking of F-Actin Networks, *Biophysical Journal* (to be submitted)

[4] Ananthakrishnan, R., Guck, J., Kas, J. and T. Moon, Structural Contributions of F-Actin Ensembles to Cytoskeletal Elasticity, *Biophysical Journal* (to be submitted)

[5] Ananthakrishnan, R., Guck, J., Kas, J. and T. Moon, Towards the structural characterization of eukaryotic cells, *Biophysical Journal* (to be submitted)

[6] Andre, E., Brink, M., Gerisch, G., Isenberg, G., Noegel, A., Schleicher, M,, Segall, J. E. and E. Wallraff, A Dictyostelium mutant deficient in severin, an F-actin fragmenting protein, shows normal motility and chemotaxis, *Journal of Cell Biology*, **108**(3):985 (1989)

[7] Andrianantoandro, E., Blanchoin, L., Sept, D., McCammon, J. A. and T. D. Pollard, Kinetic Mechanism of End-to-End Annealing of Actin Filaments, *Journal of Molecular Biology*, **312**(19):721 (2001)

165

[8] Arakawa, T. and C. Frieden, Interaction of Microtubule-associated Proteins with Actin Filaments, *Journal of Biological Chemistry*, **259**(19):11730 (1984)

[9] Atkins, H. and P. J. Anderson, Actin and tubulin of normal and leukaemic lymphocytes, *Biochemical Journal*, **207**(3):535 (1982)

[10] Bausch, A. R., Ziemann, F., Boulbitch, A. A., Jacobson, K. and E. Sackmann, Local Measurements of Viscoelastic Parameters of Adherent Cell Surfaces by Magnetic Bead Microrheometry, *Biophysical Journal*, **75**:2038 (1998)

[11] Bausch, A. R., Moller, W. and E. Sackmann, Measurement of local viscoelasticity and forces in living cells by magnetic tweezers, *Biophysical Journal*, **76**(1 Pt 1):573 (1999)

[12] Ben-Zeev, A., The Cytoskeleton in Cancer Cells, *Biochimica et Biophysica Acta*, **780**:197 (1985)

[13] Boey, S. K., Boal, D. H. and D. E. Discher, Simulations of the erythrocyte cytoskeleton at large deformation. I. Microscopic models, *Biophysical Journal*, **75**:1573 (1998)

[14] Brochard, F. and J. F. Lennon, Frequency Spectrum of the Flicker Phenomenon in Erythrocytes, *Le Journal De Physique*, **36**(11):1035 (1975)

[15] Caille, N., Thoumine, O., Tardy, Y. and J. Meister, Contribution of the nucleus to the mechanical properties of endothelial cells, *Journal of Biomechanics*, **35**:177 (2002)

[16] Campbell, N. A., Reece, J. B. and L. G. Mitchell, Biology, *Pearson Education, Inc.*, (5th Edition) (1999)

166

[17] Cano, M. L., Lauffenburger, D. A. and S. H. Zigmond, Kinetic analysis of F-actin depolymerization in polymorphonuclear leukocyte lysates indicates that chemoattractant stimulation increases actin filament number without altering the filament length distribution, *Journal of Cell Biology*, **115**(3):677 (1991)

[18] Casciari, J. J., Sotirchos, S. V. and R. M. Sutherland, Variations in Tumor Cell Growth Rates and Metabolism with Oxygen Concentration, Glucose Concentration, and Extracellular pH, *Journal of Cellular Physiology*, **151**:386 (1992)

[19] Castillo, H. E. and P. M. Goldbart, Semimicroscopic theory of elasticity near the vulcanization transition, *Physical Review E*, **62**(6):8159 (2000)

[20] Chaplain, M. A. J. and B. D. Sleeman, Modelling the growth of solid tumours and incorporating a method for their classification using nonlinear elasticity theory, *The Journal of Mathematical Biology*, **31**(5):431 (1993)

[21] Chen, C. and D. E. Ingber, Tensegrity and mechanoregulation: from skeleton to cytoskeleton, *Osteoarthritis and Cartilage*, **7**:81 (1998)

[22] Chien, S., Sung, K. L., Skalak, R., Usami, S. and A. Tozeren, Theoretical and experimental studies on viscoelastic properties of erythrocyte membrane, *Biophysical Journal*, **24**(2):463 (1978)

[23] Cramer, L. P., Briggs, L. J., and H. R. Dawe, Use of fluorescently labelled deoxyribonuclease I to spatially measure G-actin levels in migrating and non-migrating cells, *Cell Motility and the Cytoskeleton*, **51**(1):27 (2002)

[24] Cunningham, C. C., Gorlin, J. B., Kwiatowski, D. J., Hartwig, J. H., Janmey, P. A., Byers, H. R. and T. P. Stossel, Actin-Binding Protein Requirement for Cortical Stability and Efficient Locomotion, *Science*, **255**(5042):325 (1992)

[25] Discher, D. E., Boal, D. H. and S. K. Boey, Simulations of the erythrocyte cytoskeleton at large deformation. II. Micropipette aspiration, *Biophysical Journal*, **75**:1584 (1998)

[26] Discher, D. E., New insights into erythrocyte membrane organization and microelasticity, *Current Opinion in Hematology*, **75**:1584 (1998)

[27] Doi, M. and Edwards, S. F., The Theory of Polymer Dynamics, *Clarendon Press* (1986)

[28] Dong, C., Skalak, R. and K. P. Sung, Cytoplasmic Rheology of Passive Neutrophils, *Biorheology*, **28**:557 (1991)

[29] Drasdo, D., Kree, R. and J. S. McCaskill, Monte Carlo approach to tissue cell populations, *Physical Review E*, **52**(6):6635 (1995)

[30] Drasdo, D., Buckling Instabilities of One-Layered Growing Tissues, *Physical Review Letters*, **84**(18):4244 (2000)

[31] Edelstein-Keshet, L., A mathematical approach to cytoskeletal assembly, *European Biophysical Journal*, **27**:521 (1998)

[32] Edelstein-Keshet, L. and G. B. Ermentrout, Models for the Length Distributions of Actin Filaments: I. Simple Polymerization and Fragmentation, *Bulletin of Mathematical Biology*, **60**:449 (1998)

[33] Ermentrout, G. B. and L. Edelstein-Keshet, Models for the Length Distributions of Actin Filaments: II. Polymerization and Fragmentation by Gelsolin Acting Together, *Bulletin of Mathematical Biology*, **60**:477 (1998)

[34] Eichinger, L., Koppel, B., Noegel, A. A., Schleicher, M., Schliwa, M., Weijer, K., Witke, W. and P. A. Janmey, Mechanical perturbation elicits a phenotypic difference between Dictyostelium wild-type cells and cytoskeletal mutants, *Biophysical Journal*, **70**(2):1054 (1996)

[35] Elson, E. L., Cellular mechanics as an indicator of cytoskeletal structure and function, *Annual Review of Biophysics and Biophysical Chemistry*, **17**:397 (1988)

[36] Engelhardt, H. and E. Sackmann, On the measurement of shear elastic moduli and viscosities of erythrocyte plasma membranes by transient deformation in high frequency electric fields, *Biophysical Journal*, **54**(3):495 (1988)

[37] Evans, E. A., New membrane concept applied to the analysis of fluid shear- and micropipette-deformed red blood cells, *Biophysical Journal*, **13**(9):941 (1973)

[38] Evans, E. and A. Yeung, Apparent viscosity and cortical tension of blood granulocytes determined by micropipet aspiration, *Biophysical Journal*, **56**:151 (1989)

[39] Everaers, R., Julicher, F., Adjari, A. and A. C. Maggs, Dynamic Fluctuations of Semiflexible Filaments, *Physical Review Letters*, **82**(18):3717 (1999)

[40] Fabry, B., Maksym, G. N., Butler, J. P., Glougauer, M., Navajas, D. and J. J. Fredberg, Scaling the Microrheology of Living Cells, *Physical Review Letters*, **87**(14):148102-1 (2001)

[41] Flugge, W., Stresses in Shells, *Springer Verlag* (1973)

[42] http://www.itg.uiuc.edu/exhibits/gallery/fluorescencegallery.htm

[43] Forgacs, G., Foty, R. A., Shafrir, Y. and M. S. Steinberg, Viscoelastic Properties of Living Embryonic Tissues: a Quantitative Study, *Biophysical Journal*, **74**:2227 (1998)

[44] Fritz, M., Radmacher, M. and H. E. Gaub, *In Vitro* Activation of Human Platelets Triggered and Probed by Atomic Force Microscopy, *Experimental Cell Research*, **205**:187 (1993)

[45] Fuchs, E. and Y. Yang, Crossroads on Cytoskeletal Highways, *Cell*, **98**:547 (1999)

[46] Fujii, T., Hiromori, T., Hamamoto, M. and T. Suzuki, Interaction of Chicken Gizzard Smooth Muscle Calponin with Brain Microtubules, *Journal of Biochemistry*, **122**:344 (1997)

[47] Fujita, H., Suzuki, H., Kuzumaki, N., Mullauer, L., Ogiso, Y., Oda, A., Ebisawa, K., Sakurai, T., Nonomura, Y. and S. Kijimoto-Ochiai, A Specific Protein, p92, Detected in Flat Revertants Derived from NIH/3T3 Transformed by Human Activated c-Ha-ras Oncogene, *Experimental Cell Research*, **186**:115 (1990)

[48] Fung, Y. C. and P. Tong, Biophysical Journal, Theory of the sphering of red blood cells, *Biophysical Journal*, **8**(2):175 (1968)

[49] Galbraith, C. G., Skalak, R. and S. Chien, Shear Stress Induces Spatial Reorganization of the Endothelial Cell Cytoskeleton, *Cell Motility and the Cytoskeleton*, **40**:317 (1988)

[50] Gavin, R. H., Microtubule-Microfilament Synergy in the Cytoskeleton, *International Review of Cytology*, **173**:207 (1997)

[51] Gavin, R. H., Synergy of Cytoskeleton Components, *BioScience*, **49**(8):641 (1999)

[52] Geigant, E., Ladizhansky, K. and A. Mogilner, An integrodifferential model for orientational distributions of f-actin in cells, *SIAM Journal of Applied Mathematics*, **59**(3):787 (1998)

[53] Gisler, P. M. and S. B. Ross-Murphy, Shear creep of gelatin gels from mammalian and piscine collagens, *International Journal of Biological Macromolecules*, **29**(7):53 (2001)

[54] Gisler, T. and D. A. Weitz, Scaling of the Microrheology of Semidilute F-Actin Solutions, *Physical Review Letters*, **82**(7):1606 (1999)

[55] Gittes, F., Mickey, B., Nittleton, J. and J. Howard, Flexural Rigidity of Microtubules and Actin Filaments Measured from Thermal Fluctuations in Shape, *Journal of Cell Biology*, **120**(4):923 (1993)

[56] Gittes, F., Schnurr, B., Olmsted, P. D., MacKintosh, F. C. and C. F. Schmidt, Microscopic Viscoelasticity: Shear Moduli of Soft Materials Determined from Thermal Fluctuations, *Physical Review Letters*, **79**(17):3286 (1997)

[57] Gittes, F., Schnurr, B., Schmidt, C. F., Olmsted, P. D. and F. C. MacKintosh, Model for dynamic shear modulus of semiflexible polymer solutions, *Material Research Society Symposium Proceedings*, **489**:49 (1998)

[58] Gittes, F. and F. C. MacKintosh, Dynamic shear modulus of a semiflexible polymer network, *Physical Review E*, **58**(2):R1241 (1998)

[59] Gluck, U., Kwiatkowski, D. J. and A. Ben-Zeev, Suppression of tumori-genecity in simian virus 40-transformed 3T3 cells transfected with $\alpha-actinin$ cDNA, *Proceedings of the National Academy of Sciences, USA*, **90**:383 (1993)

[60] Goldbart, P. and N. Goldenfeld, Rigidity and Ergodicity of Randomly Cross-linked Macromolecules, *Physical Review Letters*, **58**(25):2676 (1987)

[61] Goldbart, P. and N. Goldenfeld, Microscopic theory for cross-linked macro-molecules. I. Broken symmetry, rigidity, and topology, *Physical Review A*, **39**(3):1402 (1989)

[62] Goldbart, P. and N. Goldenfeld, Microscopic theory for cross-linked macro-molecules. II. Replica theory of the transition to the solid state, *Physical Review A*, **39**(3):1412 (1989)

[63] Goldmann, W. H. and G. Isenberg, Analysis of filamin and $\alpha-actinin$ binding to actin by the stopped flow method, *FEBS*, **336**(3):408 (1993)

[64] Goldmann, W. H., Tempel, M., Sprenger, I., Isenberg, G. and R. M. Ezzell, Viscoelasticity of actin-gelsolin networks in the presence of filamin, *European Journal of Biochemistry*, **246**:373 (1997)

[65] Gonzalez, M., Cambiazo, V. and R. B. Maccioni, The Interaction of Mip-90 with Microtubules and Actin Filaments in Human Fibroblasts, *Experimental Cell Research*, **239**:243 (1998)

[66] Gowing, L. R., Tellam, R. L. and M. R. C. Banyard, Microfilament organiza-tion and total actin content are decreased in hybrids derived from the fusion of HeLa cells with human fibroblasts, *Journal of Cell Science*, **69**:137 (1984)

172

[67] Gregory, R. D., Milac, T. I. and F. Y. M. Wan, A thick hollow sphere compressed by equal and opposite concentrated axial loads: An asymptotic solution, *SIAM Journal of Applied Mathematics*, **59**(3):1080 (1999)

[68] Guck, J., Ananthakrishnan, R., Moon, T. J., Cunningham, C. C. and J. Kas, Optical Deformability of Soft Biological Dielectrics, *Physical Review Letters*, **84**:5451 (2000)

[69] Guck, J., Ananthakrishnan, R., Mahmood, H., Moon, T. J., Cunningham, C. C. and J. Kas, The optical stretcher: a novel laser tool to micromanipulate cells, *Biophysical Journal* **81**(2):767(2001)

[70] Guck, J., Ananthakrishnan, R., Cunningham, C. C. and J. Kas, Stretching Biological Cells with Light, *Journal of Physics: Condensed Matter* **14**(19):4843 (2002)

[71] Guck, J., Optical Deformability: Micromechanics from Cell Research to Biomedicine, *PhD Thesis*, UT Austin (2001)

[72] Guilak, F., Tedrow, J. R. and R. Burgkart, Viscoelastic Properties of the Cell Nucleus, *Biochemical and Biophysical Research Communications*, **269**:781 (2000)

[73] Haga, H., Sasaki, S., Kawabata, K., Ito, E., Ushiki, T. and T. Sambongi, Elasticity mapping of living fibroblasts by AFM and immunofluorescence observation of the cytoskeleton, *Ultramicroscopy*, **82**:253 (2000)

[74] Hart, T. N. and L. E. H. Trainor, The Two-Component Model for the Cytoskeleton in Development, *Physica D*, **44**:269 (1990)

[75] Hartwig, J. H., Actin filament architecture and movements in macrophage cytoplasm, *Ciba Foundation Symposium*, **118**:42 (1986)

[76] Hartwig, J. H. and D. J. Kwiatkowski, Actin-binding proteins, *Current Opinion in Cell Biology*, **3**:87 (1991)

[77] Hartwig, J. H., Mechanisms of actin rearrangements mediating platelet activation, *Journal of Cell Biology*, **118**(6):1421 (1992)

[78] Heidemann, S. R., Kaech, S., Buxbaum, R. E. and A. Matus, Direct Observations of the Mechanical Behaviors of the Cytoskeleton in Living Fibroblasts, *Journal of Cell Biology*, **145**(1):109 (1999)

[79] Helfer, E., Harlepp, S., Bourdieu, L., Robert, J., MacKintosh, F. C. and D. Chatenay, Buckling of Actin-Coated Membranes under Application of a Local Force, *Physical Review Letters*, **87**(8):088103-1 (2001)

[80] Henon, S., Lenormand, G., Richert, A. and F. Gallet, A new determination of the shear modulus of the human erythrocyte membrane using optical tweezers, *Biophysical Journal*, **76**(2):1145 (1999)

[81] Hinner, B., Temple. M., Sackmann, E., Kroy, K. and E. Frey, Entanglement, Elasticity and Viscous Relaxation of Actin Solutions, *Physical Review Letters*, **81**(12):2614 (1998)

[82] Hochmuth, R. M. and N. Mohandas, Uniaxial loading of the red-cell membrane, *Journal of Biomechanical Engineering*, **5**(5):501 (1972)

[83] Hochmuth, R. M., Measuring the mechanical properties of individual human blood cells, *Journal of Biomechanical Engineering*, **115**(4B):515 (1993)

[84] Hochmuth, R. M., Micropipette aspiration of living cells, *Journal of Biomechanics*, **33**:15 (2000)

[85] Honda, K., Yamada, T., Endo, R., Ino, Y., Gotoh, M., Tsuda, H., Yamada, Y., Chiba, H. and S. Hirohashi, Actinin-4, a Novel Actin-bundling Protein Associated with Cell Motility and Cancer Invasion, *The Journal of Cell Biology*, **140**(6):1383 (1998)

[86] Humphrey, D., Duggan, C., Saha, D., Smith, D. and J. Kas, Active fluidization of polymer networks through molecular, *Nature*, **416**(6879):413-6 (2002)

[87] Ingber, D. E., Cellular tensigrity: defining new rules of biological design that govern the cytoskeleton, *Journal of Cell Science*, **104**:613 (1993)

[88] Ingber, D. E., Tensigrity: the architectural basis of cellular mechanotransduction, *Annual Review of Physiology*, **59**:575 (1997)

[89] Ingber, D. E., The architecture of life, *Scientific American*, **278**(1):48 (1998)

[90] Janmey, P. A., Hvidt, S., Peetermans, J., Lamb, J., Ferry, J. D. and T. P. Stossel, Viscoelasticity of F-Actin and F-Actin/Gelsolin Complexes, *Biochemistry*, **27**:8218 (1988)

[91] Janmey, P. A., Hvidt, S., Lamb, J. and T. P. Stossel, Resemblance of actin-binding protein/actin gels to covalently crosslinked networks, *Nature*, **345**:89 (1990)

[92] Janmey, P. A., Euteneuer, U., Traub, P. and M. Schliwa, Viscoelastic Properties of Vimentin Compared with Other Filamentous Biopolymer Networks, *Journal of Cell Biology*, **113**(1):155 (1991)

[93] Janmey, P. A., A torsion pendulum for measurement of the viscoelasticity of biopolymers and its application to actin networks, *Journal of Biochemical and Biophysical Methods*, **22**:41 (1991)

[94] Janmey, P. A., Hvidt, S., Kas, J., Lerche, D., Maggs, A., Sachmann, E., Schliwa, M. and T. P. Stossel, The Mechanical Properties of Actin Gels, *The Journal of Biological Chemistry*, **269**(51):32503 (1994)

[95] Janmey, P. A., Shah, J. V., Tang, J. X. and T. P. Stossel, Actin Filament Networks, *Results and Problems in cell differentiation*, **32**:181 (2001)

[96] Jones, W. R., Ting-Beall, H. P., Lee, G. M., Kelley, S. S., Hochmuth, R. M. and F. Guilak, Alterations in the Young's modulus and volumetric properties of chondrocytes isolated from normal and osteoarthritic human cartilage, *Journal of Biomechanics*, **32**(2):119 (1999)

[97] Kage, H. S., Engelhardt, H. and E. Sackmann, A precision method to measure average viscoelastic parameters of erythrocyte populations, *Biorheology*, **27**(1):67 (1990)

[98] Kas, J., Strey, H., Tang, J. X., Finger, D., Ezzell, R., Sackmann, E. and P. A. Janmey, F-Actin, a Model Polymer for Semiflexible Chains in Dilute, Semidilute, and Liquid Crystalline Solutions, *Biophysical Journal*, **70**:609 (1996)

[99] Katsantonis, J., Tosca, A., Koukouritaki, S. B., Theodoropoulos, P. A., Gravanis, A. and C. Stournaras, Differences in the G/total actin ratio and microfilament stability between normal and malignant human keratinocytes, *Cell Biochemistry and Function*, **12**(4):267 (1994)

176

[100] Kerst, A., Chmielewski, C., Livesay, C., Buxbaum, R. E., and S. R. Heidemann , Liquid crystal domains and thixotropy of filamentous actin suspensions, *Proceedings of the National Academy of Sciences, USA*, **87**:4241 (1990)

[101] Kojima, H., Ishijima, A. and T. Yanagida, Direct measurement of stiffness of single actin filaments with and without tropomyosin by *in vitro* nanomanipulation, *Proceedings of the National Academy of Sciences, USA*, **91**:12962 (1994)

[102] Kraus, H., Thin Elastic Shells - An Introduction to the Theoretical Foundations and the Analysis of their Static and Dynamic Behavior, *Wiley* (1967)

[103] Kroy, K. and E. Frey, Force-Extension Relation and Plateau Modulus for Wormlike Chains, *Physical Review Letters*, **77**(2):306 (1996)

[104] Kundu, T., Bereiter-Hahn, J. and I. Karl, Cell Property Determination from the Acoustic Microscope Generated Voltage Versus Frequency Curves, *Biophysical Journal*, **78**:2270 (2000)

[105] Lakes, R. S., Viscoelastic Solids, *CRC Press* (1998)

[106] Leavitt, J., Latter, G., Lutomski, L., Goldstein, D. and S. Burbeck, Tropomyosin isoform switching in tumorigenic human fibroblasts, *Molecular and Cellular Biology* **6**(7):2721 (1986)

[107] Lee, J. C., Wong, D. T. and D. E. Discher, Direct measures of large, anisotropic strains in deformation of the erythrocyte cytoskeleton, *Biophysical Journal*, **77**(2):853 (1999)

[108] Leibler, L., Rubenstein, M. and R. H. Colby, Dynamics of Reversible Networks, *Macromolecules*, **24**:4701 (1991)

[109] Lekka, M., Laidler, P., Gil, D., Lekki, J., Stachura, Z. and A. Z. Hrynkiewicz, Elasticity of Normal and cancerous human bladder cells studied by scanning force microscopy, *European Biophysical Journal*, **28**:312 (1999)

[110] Lelievre, J. C., Bucherer, C., Geiger, S., Lacombe, C. and V. Vereycken, Blood Cell Biomechanics Evaluated by the Single Cell Micromanipulation, *Journal de Physique III*, **5**:1689 (1995)

[111] Lodish, H., Berk, A., Zipursky, L. S., Matsudaira, P., Baltimore, D. and J. Darnell, Molecular Cell Biology, *W. H. Freeman and Company*, (4th Edition) (2000)

[112] Lure, A. I., Three-dimensional Problems of the Theory of Elasticity, *Interscience Publishers* (1964)

[113] MacKintosh, F. C., Kas, J. and P. A. Janmey, Elasticity of Semiflexible Biopolymer Networks, *Physical Review Letters*, **75**(24):4425 (1995)

[114] MacKintosh, F. C., Gittes, F., Schnurr, B., Olmsted, P. D. and C. F. Schmidt, Viscoelasticity and its microscopic characterization in semiflexible biopolymer solutions, *Material Research Society Symposium Proceedings*, **489**:39 (1998)

[115] MacRae, E. K., Pryzwansky, K. E., Cooney, M. H. and J. K. Spitznagel, Scanning electron microscopic observations of early stages of phagocytosis of E. coli by human neutrophils, *Cell and Tissue Research*, **209**(1):65 (1980)

[116] Maggs, A. C., Two plateau moduli for actin gels, *Physical Review E*, **55**(6):7396 (1997)

[117] Mahaffy, R. E., Shih, C. K., MacKintosh, F. C. and J. Kas, Scanning Probe-Based Frequency-Dependent Microrheology of Polymer Gels and Biological Cells, *Physical Review Letters*, **85**(4):880 (2000)

[118] Mahaffy, R. E., Park, S., Gerde, E., Kas, J. and C. K. Shih, Quantitative analysis of the viscoelastic properties in thin regions of fibroblasts using AFM, *Biophysical Journal* (in review)

[119] Maniotis, A. J., Chen, C. S. and D. E. Ingber, Demonstration of mechanical connections between integrins, cytoskeletal filaments and nucleoplasm that stabilize nuclear structure, *Cell Biology*, **94**:849 (1997)

[120] Mason, T. G., Ganesan, K., van Zanten, J. H., Wirtz, D. and S. C. Kuo, Particle Tracking Microrheology of Complex Fluids, *Physical Review Letters*, **79**(17):3282 (1997)

[121] Mason, T. G., Gisler, T., Kroy, K., Frey, E. and D. A. Weitz, Rheology of F-actin solutions determined from thermally driven tracer motion, *Journal of Rheology*, **44**(4):917 (2000)

[122] Mathur, A. B., Truskey, G. A. and W. M. Reichert, Atomic force and total internal reflection fluorescence microscopy for the study of force transmission in endothelial cells, *Biophysical Journal*, **78**(4):1725 (2000)

[123] Mazars, M., Freely jointed chains in external potentials: analytic computations, *Journal of Physics A: Mat. Gen.*, **32**:1841 (1991)

[124] Mazurkiewicz, Z. E. and R. T. Nagorski, Shells of Revolution, *Elsevier* (1991)

[125] McGrath, J. L., Osborn, E. A., Tardy, Y. S., Dewey, C. F. Jr and J. H. Hartwig, Regulation of the actin cycle in vivo by actin filament severing, *Proceedings of the National Academy of Sciences, USA*, **97**(12):6532 (2000)

[126] Miyata, H., Yasuda, R. and K. Kinosita Jr., Strength and Lifetime of the bond between actin and skeletal muscle $\alpha$-actinin studied with an optical trapping technique, *Biochima et Biophysica Acta*, **1290**:83 (1996)

[127] Moreau, V. and M. Way, In vitro approaches to study actin and microtubule dependent cell processes, *Current Opinion in Cell Biology*, **11**:152 (1999)

[128] Morse, D. C., Viscoelasticity of Concentrated Isotropic Solutions of Semi-flexible Polymers. 1. Model and Stress Tensor, *Marcomolecules*, **31**(20):7030 (1998)

[129] Morse, D. C., Viscoelasticity of Concentrated Isotropic Solutions of Semi-flexible Polymers. 2. Linear Response, *Marcomolecules*, **31**(20):7044 (1998)

[130] Morse, D. C., Viscoelasticity of Concentrated Isotropic Solutions of Semi-flexible Polymers. 3. Nonlinear Rheology, *Marcomolecules*, **32**(18):5934 (1999)

[131] Morse, D. C., Viscoelasticity of tightly entangled solutions of semiflexible polymers, *Physical Review E*, **58**(2):R1237 (1998)

[132] Mullauer, L., Fujita, H., Suzuki, H., Katabami, M., Hitomi, Y., Ogiso, Y. and N. Kuzumaki, Elevated gelsolin and alpha-actin expression in a flat re-vertant R1 of Ha-ras oncogene-transformed NIH/3T3 cells, *Biochemical and Biophysical Research Communications*, **171**(2):852 (1990)

[133] Muller, O., Gaub, H. E., Barmann, M. and E. Sackmann, Viscoelastic Moduli of Sterically and Chemically Cross-linked Actin Networks in the Dilute to Semidilute Regime: Measurements by an Oscillating Disk Rheometer, *Macromolecules*, **24**:3111 (1991)

[134] Mullins, R. D., Heuser, J. A. and T. D. Pollard, The interaction of Arp2/3 complex with actin: Nucleation, high affinity pointed end capping and formation of branching networks of filaments, *Proceedings of the National Academy of Sciences, USA*, **95**:6181 (1998)

[135] Nagamalleswari, K. and D. Safer, Sequestered actin in chick embryo fibroblasts, *Molecular and Cellular Biochemistry*, **209**(1-2):63 (2000)

[136] Nossal, R., On the elasticity of cytoskeletal networks, *Biophysical Journal*, **53**:349 (1988)

[137] Nossal, R., Mechanical properties of biological gels, *Physica A*, **231**:265 (1996)

[138] Olins A. L., Herrmann, H., Lichter, P. and D. E. Olins, Retinoic Acid Differentiation of HL-60 Cells Promotes Cytoskeletal Polarization, *Experimental Cell Research*, **254**:130 (2000)

[139] Oster, G. F. and G. M.Odell, The Mechanochemistry of Cytogels, *Physica D*, **12D**:333 (1984)

[140] Palmer, A., Xu, J. and D. Wirtz, High-frequency viscoelasticity of crosslinked actin filament networks measured by diffusing wave spectroscopy, *Rheologica Acta*, **37**:97 (1998)

[141] Palmer, A., Mason, T. G., Xu, J., Kuo, S. C. and D. Wirtz, Diffusing Wave Spectroscopy Microrheology of Actin Filament Networks, *Biophysical Journal*, **76**(2):1063 (1999)

[142] Parker, K. H. and C. P. Winlove, The deformation of spherical vesicles with permeable, constant-area membranes: application to the red blood cell, *Biophysical Journal*, **77**(6):3096 (1999)

[143] Pasquali, M., Shankar, V. and D. C. Morse, Viscoelasticity of dilute solutions of semiflexible polymers, *Physical Review E*, **64**:020802(R) (2001)

[144] Paulitschke, M., Mikita, J., Lerche, D. and W. Meier, Elastic properties of passive leukemic white blood cells, *International Journal of Microcirculation: Clinical and Experimental*, **10**:67-73 (1991)

[145] Pedrotti, B., Colombo, R. and K. Islam, Interactions of Microtubule-Associated Protein MAP2 with Unpolymerized and Polymerized Tubulin and Actin Using a 96-Well Microtiter Plate Solid-Phase Immunoassay, *Biochemistry*, **33**:8798 (1994)

[146] Pedrotti, B. and K. Islam, Dephosphorylated but not phosphorylated microtubule associated MAP1B binds to microfilaments, *FEBS Letters*, **388**:131 (1996)

[147] Peng, W., Goldbart, P. M. and A. J. McKane, Connecting the vulcanization transition to percolation, arXiv:cond-mat/0104212 v1, 11 April 2001

[148] Podolski, J. L. and T. L. Steck, Length distribution of F-actin in Dictyostelium discoideum, *Journal of Biological Chemistry*, **265**(3):1312 (1990)

[149] Pollard, T. D., Selden, S. C. and P. Maupin, Interaction of Actin Filaments with Microtubules, *Journal of Cell Biology*, **99**(1):33s (1984)

[150] Pollard, T. D., Rate constants for the reactions of ATP- and ADP-actin with the ends of actin filaments, *Journal of Cell Biology*, **103**(6 Pt 2):2747 (1986)

[151] Pollard, T. D., Blanchoin, L. and R. D. Mullins, Molecular Mechanisms Controlling Actin Filament Dynamics in Nonmuscle Cells, *Annual Review of Biophysics and Biomolecular Structure*, **29**:545 (2000)

[152] Radmacher, M., Fritz, M., Kacher, C. M., Cleveland, J. P. and P. K. Hansma, Measuring the viscoelastic properties of human platelets with the atomic force microscope, *Biophysical Journal*, **70**(1):556 (1996)

[153] Ragsdale, G. K., Phelps, J. and K. Luby-Phelps, Viscoelastic Response of Fibroblasts to Tension Transmitted through Adherens Junctions, *Biophysical Journal*, **73**:2798 (1997)

[154] Rao, K. M. and H. J. Cohen, Actin cytoskeletal network in aging and cancer, *Mutation Research*, **256**(2-6):139 (1991)

[155] Rayleigh, The Theory of Sound, *MacMillan And Co., Limited* (1940)

[156] Rand, R. P. and A. C. Burton, Mechanical Properties of the Red Cell Membrane I. Membrane Stiffness and Intracellular Pressure, *Biophysical Journal*, **4**:115 (1964)

[157] Ressad, F., Didry, D., Xia, G., Hong, Y., Chu, N., Pantaloni, D. and M. Carlier, Kinetic Analysis of the Interaction of Actin-depolymerizing Factor (ADF)/Cofilin with G- and F-Actins, *The Journal of Biological Chemistry*, **273**(33):20894 (1998)

[158] Rivero, F., Koppel, B., Peracino, B., Bozzaro, S., Siegert, F., Weijer, C. J., Schleicher, M., Albert, R. and A. A. Noegel, The role of the cortical cytoskeleton: F-actin crosslinking proteins protect against osmotic stress, ensure cell size, cell shape and motility, and contribute to phagocytosis and development, *Journal of Cell Science*, **109**:2679 (1996)

[159] Rodionov, V. I., Hope, A. J., Svitkina, T. M. and G. G. Borisy, Functional coordination of microtubule-based and actin-based motility in melanophores, *Current Biology*, **8**(3):165 (1998)

[160] Rotsch, C., Braet, F., Wisse, E. and M. Radmacher, AFM imaging and elasticity measurements on living rat liver macrophages, *Cell Biology International*, **21**(11):685 (1997)

[161] Rotsch, C., Jacobson, K. and M. Radmacher, Dimensional and mechanical dynamics of active and stable edges in motile fibroblasts investigated by using atomic force microscopy, *Proceedings of the National Academy of Sciences, USA*, **96**(3):921 (1999)

[162] Rotsch, C. and M. Radmacher, Drug Induced Changes of Cytoskeletal Structure and Mechanics in Fibroblasts: An Atomic Force Microscopy Study, *Biophysical Journal*, **78**:520 (2000)

[163] Rufener, K., Palmer, A., Xu, J. and D. Wirtz, High Frequency solutions probed by diffusing wave spectroscopy: the case of concentrated solutions of F-actin, *Journal of Non-Newtonian Fluid Mechanics*, **82**:303 (1999)

[164] Sato, M., Schwartz, W. H. and T. D. Pollard, Dependence of the mechanical properties of actin/$\alpha$-actinin gels on deformation rate, *Nature*, **325**:828 (1987)

[165] Sato, M., Schwartz, W. H., Selden, S. C. and T. D. Pollard, Mechanical Properties of Brian Tubulin and Microtubules, *The Journal of Cell Biology*, **106**:1205 (1988)

[166] Sato, M., Theret, D. P., Wheeler, L. T., Ohshima, N. and R. M. Nerem, Application of the micropipette technique to the measurement of cultured porcine aortic endothelial cell viscoelastic properties, *Journal of Biomechanical Engineering*, **112**:263 (1990)

[167] Sattilaro, R., Interaction of Microtubule-associated Protein 2 with Actin Filaments, *Biochemistry*, **25**:2003 (1986)

[168] Schafer, D. A., Jennings, P. B. and J. A. Cooper, Dynamics of capping protein and actin assembly in vitro: uncapping barbed ends by polyphosphoinositides, *Journal of Cell Biology*, **135**(1):169 (1996)

[169] Schinkinger, S., Laser Induced Elasticity Measurements of Single Fibroblast Cells, *MA Thesis*, UT Austin (2002)

[170] Schliwa, M. and J. van Blerkom, Structural Interaction of Cytoskeletal Components, *The Journal of Cell Biology*, **90**:222 (1981)

[171] Schmidt, F. G., Hinner, B. and E. Sackmann, Microrheometry underestimates the values of the viscoelastic moduli in measurements on F-actin solutions compared to macrorheometry, *Physical Review E*, **61**(5):5646 (2000)

[172] Selden, S. C. and T. D. Pollard, Interaction of Actin Filaments with Microtubules Is Mediated by Microtubule-Associated Proteins and Regulated by Phosphorylation, *Annals NewYork Academy of Sciences*, pg 803 (1986)

[173] Selve, N. and A. Wegner, Rate constants and equilibrium constants for binding of the gelsolin-actin complex to the barbed ends of actin filaments in the presence and absence of calcium, *European Journal of Biochemistry*, **160**(2):379 (1986)

[174] Sept, D., Xu, J., Pollard, T. D. and J. A. McCammon, Annealing Accounts for the Length of Actin Filaments Formed by Spontaneous Polymerization, *Biophysical Journal*, **77**:2911 (1999)

[175] Shah, J. V., Flanagan, L. A., Bahk, D. and P. A. Janmey, Reptation of microtubules in f-actin networks: effects of filament stiffness and network topology on reptation dynamics, *Material Research Society Symposium Proceedings*, **489**:27 (1998)

[176] Sider, J. R., Mandato, C. A., Weber, K. L., Zandy, A. J., Beach, D., Finst, R. J., Skoble, J. and Bement, W. M., Direct observation of microtubule-f-actin interaction in cell free lysates, *Journal of Cell Science*, **112**(12):1947 (1999)

[177] Sit, P. S., Spector, A. A., Lue, A. J., Popel, A. S. and W. E. Brownell, Micropipette aspiration on the outer hair cell lateral wall, *Biophysical Journal*, **72**(6):2812 (1997)

[178] Sleep, J., Wilson, D., Simmons, R. and W. Gratzer, Elasticity of the red cell membrane and its relation to hemolytic disorders: an optical tweezers study, *Biophysical Journal*, **77**(6):3085-95 (1999)

[179] Small, J. V., Rottner, K. and I. Kaverina, Functional design in the actin cytoskeleton, *Current Opinion in Cell Biology*, **11**:54 (1999)

[180] Spiros, A. and L. Edelstein-Keshet, Testing a model for the dynamics of actin structures with biological parameter values, *Bulletin Mathematical Biology*, **60**(2):275 (1998)

[181] Stamatas, G. N. and L. V. McIntire, Rapid Flow-Induced Responses in Endothelial Cells, *Biotechnol. Prog.*, **17**:383 (2001)

[182] Stamenovic, D. and M. F. Coughlin, The Role of Prestress and Architecture of the Cytoskeleton and Deformability of Cytoskeletal Filaments in Mechanics of Adherent Cells: a Quantitative Analysis, *Journal of Theoretical Biology*, **201**:63 (1999)

[183] Stamenovic, D. and M. F. Coughlin, A Quantitative Model of Cellular Elasticity Based on Tensegrity, *Journal of Biomechanical Engineering*, **122**:39 (2000)

[184] Stamenovic, D. and N. Wang, Cellular Responses to Mechanical Stress. Invited Review: Engineering approaches to cytoskeletal mechanics, *Journal of Applied Physiology*, **89**:1663 (2000)

[185] Stark, R., Liebes, L. F., Nevrla, D., Conklyn, M. and R. Silber, Decreased actin content of lymphocytes from patients with chronic lymphocytic leukemia, *Blood*, **59**(3):536 (1982)

[186] Stossel, T. P. and J. H. Hartwig, Interactions of actin, myosin, and a new actin-binding protein of rabbit pulmonary macrophages. II. Role in cytoplasmic movement and phagocytosis, *Journal of Cell Biology*, **68**(3):602 (1976)

[187] Stossel, T. P., Contribution of Actin to the Structure of the Cytoplasmic Matrix, *The Journal of Cell Biology*, **99**(1):15s (1984)

[188] Stossel, T. P., Actin Organization and Remodeling in Cell Structure and Function, Course on Multiscale Dynamics in Soft Matter and Biophysics, July 4-18 (2000)

[189] Strey, H., Peterson, M. and E. Sackmann, Measurement of erythrocyte membrane elasticity by flicker eigenmode decomposition, *Biophysical Journal* **69**(2):478 (1995)

[190] Sung, K. L., Dong, C., Schmid-Schonbein, G. W., Chien, S. and R. Skalak, Leukocyte relaxation properties, *Biophysical Journal*, **54**(2):331 (1988)

[191] Tadokoro, S. Intracellular concentration and structural states of actin in human bladder carcinomas: New indices for malignancy, *Keio Journal of Medicine*, **34**:45 (1985)

[192] Taniguchi, S., Kawano, T., Kakunaga, T. and T. Baba, Differences in expression of a variant actin between low and high metastatic B-16 melanoma, *Journal of Biological Chemistry*, **261**(13):6100 (1986)

[193] Temple, M., Isenberg, G. and E. Sackmann, Temperature-induced sol-gel transition and microgel formation in $\alpha$-actinin cross-linked actin networks: A rheological study, *Physical Review E*, **54**(2):1802 (1996)

[194] Theret, D. P., Levesque, M. J., Sato, M., Nerem, R. M. and L. T. Wheeler, The application of a homogeneous half-space model in the analysis of endothelial cell micropipette measurements, *Journal of Biomechanical Engineering*, **110**(3):190 (1988)

[195] Theriot, J., The Polymerization Motor, *Traffic*, **1**:19 (2000)

[196] Thoumine, O. and A. Ott, Time scale dependent viscoelastic and contractile regimes in fibroblasts probed by microplate manipulation, *Journal of Cell Science*, **110**:2109 (1997)

[197] Thoumine, O. and A. Ott, Comparison of the mechanical properties of normal and transformed fibroblasts, *Biorheology*, **34**:09 (1997)

[198] Thoumine, O. and A. Ott, Biomechanical properties of fibroblasts, *Materials Research Symposium Bulletin*, Oct:22 (1999)

[199] Thoumine, O., Cardoso, O. and J. Meister, Changes in the mechanical properties of fibroblasts during spreading: a micromanipulation study, *European Biophysical Journal*, **28**:222 (1999)

[200] Ting, T. C. T., The Remarkable Nature of Radially Symmetric Deformation of Spherically Uniform Linear Anisotropic Elastic Solids, *Journal of Elasticity*, **53**:47 (1999)

[201] Tolomeo, J. A. and M. C. Holley, Mechanics of Microtubule Bundles in Pillar Cells from the Inner Ear, *Biophysical Journal*, **73**:2241 (1997)

[202] Torres, M. and T. D. Coates, Function of the cytoskeleton in human neutrophils and methods for evaluation, *Journal of Immunological Methods*, **232**:89 (1999)

[203] Tsai, M. A., Waugh, R. E. and P. C. Keng, Passive Mechanical behavior of Human Neutrophils: Effect of Cochline and Paclitaxel, *Biophysical Journal*, **74**:3282 (1998)

[204] Tseng, Y. and D. Wirtz, Mechanics and Multiple-Particle Tracking Micro-heterogeneity of $\alpha$-Actinin-Cross-Linked Actin Filament Networks, *Biophysical Journal*, **81**:1643 (2001)

[205] Tseng, Y. Schafer, B. W., Almo, S. C. and D. Wirtz, Functional Synergy of Actin Filament Cross-linking Proteins, *The Journal of Biological Chemistry*, **277**(28):25609 (2002)

[206] Ugural, A., Stresses in Plates and Shells, *The McGraw - Hill Companies, Inc.*, (Second Edition) (1999)

[207] Valberg, P. A. and D. F. Albertini, Cytoplasmic Motions, Rheology, and Structure Probed by a Novel Magnetic Particle Method, *The Journal of Cell Biology*, **101**:130 (1985)

[208] Wachsstock, D. H., Schwarz, W. H. and T. D. Pollard, Affinity of $\alpha$-Actinin for Actin Determines the Structure and Mechanical Properties of Actin Filament Gels, *Biophysical Journal*, **65**:205 (1993)

[209] Wachsstock, D. H., Schwarz, W. H. and T. D. Pollard, Cross-linker dynamics determine the mechanical properties of actin gels, *Biophysical Journal*, **66**(3 Pt 1):801 (1994)

[210] Wagner, O., Zinke, J., Dancker, P., Grill, W. and J. Bereiter-Hahn, Viscoelastic Properties of f-actin, Microtubules, f-actin$\alpha$-actinin, and f-actin/Hexokinase Determined in Microliter Volumes with a Nondestructive Method, *Biophysical Journal*, **76**:2784 (1999)

[211] Wagner, O., Schuler, H., Hofmann, P., Langer, D., Dancker, P. and J. Bereiter-Hahn, Sound attenuation of polymerizing actin reflects supramolecular struc-

tures: viscoelastic properties of actin gels modified by cytochalasin D, profilin and $\alpha$-actinin, *Biochem. Journal*, **355**:771 (2001)

[212] Wang, N., Butler, J. P. and D. E. Ingber, Mechanotransduction Across the Cell Surface and Through the Cytoskeleton, *Science* **260**:1124 (1993)

[213] Wang, N., Mechanical Interactions Among Cytoskeletal Filaments, *Hypertension*, **32**:162 (1998)

[214] Wang, N. and D. Stamenovic, Contribution of intermediate filaments to cell stiffness, stiffening and growth, *American Journal of Physiology and Cell Physiology*, **279**:C188 (2000)

[215] Wang, N., Mechanical behavior in living cells consistent with the tensegrity model, *Proceedings of the National Academy of Sciences, USA*, **98**(14):7765 (2001)

[216] Ward, K. A., Li, W., Zimmer, S. and T. David, Viscoelastic properties of transformed cells: role in tumor cell progression and metastasis formation, *Biorheology*, **28**:301 (1991)

[217] Waugh, R. E. and E. A. Evans, Thermoelasticity of red blood cell membrane, *Biophysical Journal*, **26**(1):115 (1979)

[218] Wei, C., Lintihac, P. M., and J. J. Tanguay, An Insight into Cell Elasticity and Load-Bearing Ability- Measurement and Theory, *Plant Physiology*, **126**:1129 (2001)

[219] Wilhelm, J. and E. Frey, Radial Distribution Function of Semiflexible Polymers, *Physical Review Letters*, **77**(12):2581 (1996)

[220] Witke, W., Sharpe, A. H., Hartwig, J. H., Azuma, T., Stossel, T. P. and D. J. Kwiatkowski, Hemostatic, inflammatory, and fibroblast responses are blunted in mice lacking gelsolin, *Cell*, **81**(1):41 (1995)

[221] Wottawah, F., Determining Viscoelastic Properties of Fibrobasts Using the Optical Stretcher, *MA Thesis*, UT Austin (2002)

[222] Wu, H. W., Kuhn, T. and V. T. Moy, Mechanical Properties of L929 Cells Measured by Atomic force Microscopy: Effects of Anticytoskeletal Drugs and Membrane Crosslinking, *Scanning*, **20**:389 (1998)

[223] Wu, Z., Zhang, G., Long, M., Wang, H., Song, G. and S. Cai, Comparison of the viscoelastic properties of normal hepatocytes and hepatocellular carcinoma cells under cytoskeletal perturbation, *Biorheology*, **37**:279 (2000)

[224] Xu, J., Schwarz, W. H., Kas, J. A., Stossel, T. P., Janmey, P. A. and T. D. Pollard, Mechanical properties of actin filament networks depend on preparation, polymerization conditions, and storage of actin monomers, *Biophysical Journal*, **74**(5):2731 (1998)

[225] Xu, J., Wirtz, D. and T. D. Pollard, Dynamic Cross-linking by $\alpha$-Actinin Determines the Mechanical Properties of Actin Filament Networks, *Journal of Biological Chemistry*, **273**(16):9570 (1998)

[226] Xu, J., Viasnoff, V. and D. Wirtz, Compliance of actin filament networks measured by particle-tracking microrheology and diffusing wave spectroscopy, *Rheologica Acta*, **37**:387 (1998)

[227] Xu, J., Palmer, A. and D. Wirtz, Rheology and Microrheology of Semiflexible Polymer Solutions: Actin Filament Networks, *Macromolecules*, **31**:6486 (1998)

[228] Xu, J., Casella, J. F. and T. D. Pollard, Effect of Capping Protein, CapZ, on the Length of Actin Filaments and Mechanical Properties of Actin Filament Networks, *Cell Motility and the Cytoskeleton*, **42**:73-81 (1999)

[229] Xu, J., Tseng, Y. and D. Wirtz, Strain Hardening of Actin Filament Networks: Regulation by the dynamic crosslinking protein alpha-actinin, *The Journal of Biological Chemistry*, **275**(46):35886 (2000)

[230] Yamada, S., Wirtz, D. and S. C. Kuo, Mechanics of Living Cells Measured by Laser Tracking Microrheology, *Biophysical Journal*, **78**:1736 (2000)

[231] Yoshimura, K., Terashima, M., Hozan, D., Ebato, T., Nomura, Y., Ishii, Y., and K. Shirai, Physical properties of shark gelatin compared with pig gelatin, *Journal of Agriculture and Food Chemistry*, **48**(6):2023 (2000)

[232] Zahalak, G. I., McConnaughey, W. B. and E. L. Elson, Determination of cellular mechanical properties by cell poking, with an application to leukocytes, *Journal of Biomechanical Engineering*, **112**(3):283 (1990)

[233] Zaner, K. S., The Effect of the 540-Kilodalton Actin Cross-Linking Protein Actin-Binding Protein on the Mechanical Properties of F-Actin, *Journal of Biological Chemistry*, **261**(17):7615 (1986)

[234] Zaner, K. S. and P. A. Valberg, Viscoelasticity of F-Actin Measured with Magnetic Microparticles, *The Journal of Cell Biology*, **109**:2233 (1989)

[235] Zaner, K. S., Physics of Actin. 1. Rheology of Semi-Dilute F-Actin, *Biophysical Journal*, **68**:1019 (1995)

193

[236] Ziemann, F., Radler, J. and E. Sackmann, Local measurements of viscoelastic moduli of entangled actin networks using an oscillating magnetic bead micro-rheometer, *Biophysical Journal*, **66**(6):2210 (1994)

[237] Zigmond, S. H., Recent quantitative studies of actin filament turnover during locomotion, *Cell Motility and the Cytoskeleton*, **25**:309 (1993)

[238] Zilker, A., Ziegler, M. and E. Sackmann, Spectral analysis of erythrocyte flickering in the 0.3-4 $(\mu m)^{-1}$ regime by microinterferometry combined with fast image processing, *Physical Review A*, **46**(12):7998 (1992)

# Vita

Revathi Ananthakrishnan was born in Nagercoil, India, on 16th February 1975, the daughter of Subramaniam Ananthakrishnan and Sudha Ananthakrishnan. She completed her high school at Fairview High School, Boulder, CO, where her parents spent a year and a half due to her father's sabbatical. After returning to India, she joined the University of Pune in 1993 and completed her Bachelor of Physics degree in 1996. She then entered the Indian Institute of Technology, Powai, where she obtained a Master of Physics degree in 1998. She was accepted to the Graduate School in Physics at the University of Texas at Austin in Fall 1998. She spent a year of her graduate studies at the Institute of Soft Matter Physics, Germany when one of her advisors took up a Professorship there in May 2002.

Permanent address: E-5, TIFR Colony,
Pune Univ. Campus,
Pune - 411007, India.

This dissertation was typeset with LaTeX[†] by The Author.

---

[†]LaTeX is a document preparation system developed by Leslie Lamport as a special version of Donald Knuth's TeX Program.